CR-137828

Calspan

Technical Report

(NASA-CR-137828) EVAIUATION OF XV-15 TILT ROTOR AIRCRAFT FOR FLYING QUALITIES RESEARCH APPLICATION Final Report, Jun. - Dec. 1975 (Calspan Corp., Buffalo, N.Y.) 132 p HC $6.00 CSCL 01C G3/05

N76-24208

Unclas 41220

Calspan Corporation
Buffalo, New York 14221

NASA CR 137828

Calspan

EVALUATION OF XV-15 TILT ROTOR AIRCRAFT FOR FLYING QUALITIES RESEARCH APPLICATION

Robert C. Radford, Arno E. Schelhorn,
Ralph J. Siracuse, Robert D. Till & Richard Wasserman

AK-5752-F-1

Prepared For:

NATIONAL AERONAUTICS AND SPACE ADMINISTRATION
Ames Research Center
Moffett Field, CA 94035

Tech. Monitor, D. L. Key

April 1976
Contract No. NAS2-8855
Final Report

Calspan Corporation
Buffalo, New York 14221

Unclassified

SECURITY CLASSIFICATION OF THIS PAGE (When Data Entered)

REPORT DOCUMENTATION PAGE		READ INSTRUCTIONS BEFORE COMPLETING FORM
1. REPORT NUMBER NASA CR-137828	2. GOVT ACCESSION NO.	3. RECIPIENT'S CATALOG NUMBER
4. TITLE (and Subtitle) Evaluation of XV-15 Tilt Rotor Aircraft For Flying Qualities Research Application		5. TYPE OF REPORT & PERIOD COVERED Final June to Dec. 1975 6. PERFORMING ORG. REPORT NUMBER AK-5752-F-1
7. AUTHOR(s) Robert C. Radford, Arno E. Schelhorn, Ralph J. Siracuse, Robert D. Till and Richard Wasserman		8. CONTRACT OR GRANT NUMBER(s) NAS 2-8855
9. PERFORMING ORGANIZATION NAME AND ADDRESS Calspan Corporation P.O. Box 235 Buffalo, New York 14221		10. PROGRAM ELEMENT, PROJECT, TASK AREA & WORK UNIT NUMBERS
11. CONTROLLING OFFICE NAME AND ADDRESS National Aeronautical & Space Administration Ames Research Center & USAAMRDL Moffett Field, CA 94035		12. REPORT DATE April 1976 13. NUMBER OF PAGES 120
14. MONITORING AGENCY NAME & ADDRESS (if different from Controlling Office) United States Army Air Mobility Research and Development Laboratory Moffett Field, CA 94035		15. SECURITY CLASS. (of this report) Unclassified 15a. DECLASSIFICATION DOWNGRADING SCHEDULE

16. DISTRIBUTION STATEMENT (of this Report)

Distribution of this report is provided in the interest of information exchange. Responsibility for the contents resides in the author or organization that prepared it.

17. DISTRIBUTION STATEMENT (of the abstract entered in Block 20, if different from Report)

18. SUPPLEMENTARY NOTES

19. KEY WORDS (Continue on reverse side if necessary and identify by block number)

XV-15
Flying Qualities Research
V/STOLAND
Flight Director
Stability and Control Augmentation

20. ABSTRACT (Continue on reverse side if necessary and identify by block number)

This report documents the results of a design review study and evaluation of the XV-15 Tilt Rotor Research Aircraft for flying qualities research application. The objectives of this study program were to determine the capability of the XV-15 aircraft and the V/STOLAND system as a safe, in-flight facility to provide meaningful research data on flying qualities, flight control systems and information display systems.

DD FORM 1 JAN 73 1473 EDITION OF 1 NOV 65 IS OBSOLETE

Unclassified

SECURITY CLASSIFICATION OF THIS PAGE (When Data Entered)

The study indicates that the flying qualities research capability of the XV-15 aircraft (including V/STOLAND) could be considerably expanded by suitable systems modifications. SCAS authority is insufficient for many control system investigations and independent control of all feel system characteristics is not possible with the existing system mechanization. The aircraft sensors do not provide the three components of airspeed in hover and low speed flight. The electronic and electromechanical displays of the XV-15 could be modified through software changes to provide sufficient flexibility for generalized flying qualities control/display research. The existing RPM governor mechanization can introduce undesirable higher-order system dynamics when collective feedback is used. For flying qualities research applications, the level of the control system "lost motion," and the lags introduced by the digital computer system in the research mode require further definition and analysis.

FOREWORD

This study program was sponsored by the United States Army Air Mobility Research and Development Laboratory (USAAMRDL), and NASA Ames Research Center. It was conducted by the Flight Research Department of Calspan Corporation, Buffalo, New York under Contract No. NAS2-8855. The sponsor technical monitor was Mr. D.L. Key while the Calspan project engineer was Mr. Richard Wasserman. Additional technical supervision was provided by Messrs. A. E. Schelhorn and Mr. C. R. Chalk.

The authors wish to express their appreciation to several members of the Flight Research Department of Calspan for their contributions. Special thanks are due to Ms. F. Scribner and P. Ford for the preparation of this report, and to Mr. J. Lyons for his contributions to the development of the XV-15 derivatives and the analysis of the XV-15 characteristics.

ABSTRACT

This report documents the results of a design review study and evaluation of the XV-15 Tilt Rotor Research Aircraft for flying qualities research application. The objectives of this study program were to determine the capability of the XV-15 aircraft and the V/STOLAND system as a safe, in-flight facility to provide meaningful research data on flying qualities, flight control systems and information display systems.

The study indicates that the flying qualities research capability of the XV-15 aircraft (including V/STOLAND) could be considerably expanded by suitable systems modifications. SCAS authority is insufficient for many control system investigations and independent control of all feel system characteristics is not possible with the existing system mechanization. The aircraft sensors do not provide the three components of airspeed in hover and low speed flight. The electronic and electromechanical displays of the XV-15 could be modified through software changes to provide sufficient flexibility for generalized flying qualities control/display research. The existing RPM governor mechanization can introduce undesirable higher-order system dynamics when collective feedback is used. For flying qualities research applications, the level of the control system "lost motion," and the lags introduced by the digital computer system in the research mode require further definition and analysis.

Cost estimates for Force Feel System and Stability and Control Augmentation System modifications to increase the present capability of the XV-15 aircraft have been prepared. Suggestions for system improvement and recommendations for additional system analysis are presented in the report.

TABLE OF CONTENTS

TABLE OF CONTENTS (cont.)

LIST OF ILLUSTRATIONS

LIST OF ILLUSTRATIONS (cont.)

LIST OF ILLUSTRATIONS (cont.)

LIST OF SYMBOLS

a_o	rotor coning coefficient, rad
a_1	rotor longitudinal cyclic flapping coefficient, positive for tip path plane inclined rearward, rad
B	system damping, Newtons/meter/sec
B_{1s}	longitudinal component of cyclic pitch in shaft axis system (longitudinal inclination of control axis system with respect to shaft axis system), rad
b_1	rotor lateral cyclic flapping coefficient, positive for tip path plane inclined downward on advancing blade side, rad
C_T	thrust coefficient, $T/\rho\pi R^2(\Omega_o R)^2$
C_Q	torque coefficient, $Q/\rho\pi R^3(\Omega_o R)^2$
F	stick force, Newtons
H_s	rotor horizontal force in shaft axis system (perpendicular to shaft and positive rearward), Newtons (lb)
K	spring stiffness, Newtons/meter
K_1	governor time constant, sec
K_F	force gain, meters/Newton
K_G	governor gain, deg-sec
K_P	position feedback gain, meters/meter
K_Q	rotor nondimensionalization coefficient, $\rho\pi R^4$, Kg-m (slug-ft)
K_β	rotor longitudinal flapping spring restraint, n-m-deg^{-1} (ft-lb-deg^{-1})
K_δ	control feedforward gain coefficient
L, M, N	total moments exerted on fuselage in aircraft body axis system, Newtons-meter (ft-lb)

LIST OF SYMBOLS CONT.

$$\left.\begin{aligned} L_j &= \frac{1}{I_{xx}} \frac{\partial L}{\partial j} \\ M_j &= \frac{1}{I_{yy}} \frac{\partial M}{\partial j} \\ N_j &= \frac{1}{I_{zz}} \frac{\partial N}{\partial j} \end{aligned}\right\} \text{rate of change } L, N, M \text{ with respect to } j, \text{ rad-sec}^{-2}\text{-(units of } j)^{-1}$$

$$\begin{bmatrix} L_j' \\ N_j' \end{bmatrix} = \frac{1}{1 - \frac{I_{xz}^2}{I_{xx} I_{zz}}} \begin{bmatrix} 1.0 & \frac{I_{xz}}{I_{xx}} \\ \frac{I_{xz}}{I_{zz}} & 1.0 \end{bmatrix} \begin{bmatrix} L_j \\ N_j \end{bmatrix}$$

M	mass, kilogram
$\dot{p}$	rate of change of roll rate
$\dot{q}$	rate of change of pitch rate
$\bar{q}_c$	dynamic pressure, Newtons/square meter
r	rate of change of yaw rate
R	rotor radius, m(ft)
S	Laplace operator
T_s	rotor thrust in shaft axis system (parallel to shaft and positive vertical), N(lb)
$\bar{u}$	rotor advance ratio in control axis system, $u_R/\Omega_o R$
$\dot{u}$	rate of change of longitudinal airspeed
V	free stream velocity, m/sec (ft/sec)
$\dot{v}$	rate of change of lateral/airspeed
$\bar{w}$	rotor vertical velocity ratio in control axis system, $w_R/\Omega_o R$
$\dot{w}$	rate of change of vertical airspeed
X	displacement, meters
X_a	actuator displacement, meters

X Y Z	total forces exerted on fuselage at c.g. in aircraft body axis system, N(lb)
$X_j = \frac{1}{m}\frac{\partial X}{\partial j}$ $Y_j = \frac{1}{m}\frac{\partial Y}{\partial j}$ $Z_j = \frac{1}{m}\frac{\partial Z}{\partial j}$	rate of change of X, Y, Z with respect to j, m-sec^{-2}-(units of j)$^{-1}$ (ft-sec^{-2}-(units of j)$^{-1}$)
α	angle of attack in aircraft body axis system, rad (deg)
β_m	rotor shaft inclination with respect to vertical (aircraft z-axis), deg(rad)
Δ	SCAS actuator command overshoot parameter
δ	blade section drag coefficient
ζ	damping ratio
ζ_A	actual damping ratio
θ	pitch attitude, rad (deg)
θ_c	rotor blade root collective pitch setting, rad (deg)
θ_G	governor collective pitch, rad (deg)
θ_t	total rotor blade (linear) twist, root collective pitch minus tip collective pitch, rad (deg)
λ	total inflow ratio
ρ	air density, K_g/m^3 (slugs/ft^3)
σ	rotor solidity ratio
Ω	rotor angular velocity perturbation, rad/sec
Ω_o	trim or reference rotor angular velocity, rad/sec
ω_n	undamped natural frequency, rad/sec
ω_{NA}	actual undamped natural frequency, rad/sec

1. INTRODUCTION

The United States Army Air Mobility Research and Development Laboratory (USAAMRDL) and NASA Ames Research Center contracted in 1973 with the Bell Helicopter Company to design and manufacture two XV-15 tilt-rotor research aircraft. These vehicles are designed to explore, in a series of proof-of-concept tests, the technical value/potential of the tilt rotor concept in civil and military missions.

Following proof of concept tests, NASA plans to install an avionics system referred to as V/STOLAND to perform research into autopilot design and terminal area navigation and guidance. Both USAAMRDL and NASA are also interested in the use of the XV-15 for stability and control, and flying qualities research. This report presents the results of a design review and evaluation study program, performed by Calspan, on this potential research application of the XV-15 aircraft and the V/STOLAND system. The objective of this program was to determine the capability of the overall XV-15 system as a workable facility, that would be safe for inflight operation and have adequate system performance to produce meaningful research data. To accomplish this objective, the program effort was directed toward the accomplishment of the following tasks:

(1) Review and evaluate the flight control and feel system to determine their adequacy for flying qualities and flight control research. Propose design changes (with associated cost estimates to incorporate these changes) necessary to produce generally applicable research data.

(2) Review and evaluate the capability and adequacy of the XV-15 V/STOLAND system for flight research application. Analyze the V/STOLAND system for potential interface problems with the XV-15. Determine whether or not the sensors, computer capability, displays and data recording capability are adequate for flying qualities, flight control and display system research. Evaluate the overall system safety-of-flight as a research facility.

(3) Review and analyze the aerodynamic, stability and control characteristics of the XV-15 aircraft to estimate ranges of flying qualities parameters that can be explored. Estimate operating limits of the XV-15 as an in-flight research vehicle.

This report is organized as follows: Section's 2, 3 and 4 respectively present the results of the tasks indicated above. Conclusions and recommendations for system modifications or additional analysis efforts are presented in Section 5.

2. FLIGHT CONTROL SYSTEM

The objective of this task was to perform a design review and evaluation of the XV-15 Flight Control System (FCS) to determine if the system would have adequate performance to operate as a research augmentation vehicle. The study was directed at the Force Feel System (FFS) and the Stability and Control Augmentation System (SCAS) portions of the FCS. An examination of the impact of lost motion in the linkage system was also made.

Section 2.1 contains a description of the existing XV-15 FFS. Design modifications to expand the FFS capability for flight research applications and estimated costs for these modifications are presented in Section 2.2. The SCAS capabilities, limitations, proposed modifications and cost estimates are presented in Section 2.3. Impact of the predicted lost motion of the control system linkages on research system was estimated. Potential solutions based on Calspan's flight control system experience are discussed in Section 2.4.

2.1 Force Feel System Description and Modification

The XV-15 force feel system (FFS) is a three-axis electrohydraulic system that produces forces proportional to the pilot's longitudinal and lateral cyclic stick and directional control displacement. The FFS functions as a pilot-assist actuator to overcome control system inertia, friction forces, and isolates the pilot controls from SCAS actuator feedback forces. The pitch axis force gradient is increased with airspeed to maintain relatively constant stick force per normal acceleration characteristics. Control harmony is maintained by proportionally increasing the lateral and directional force gradients.

The longitudinal and lateral cyclic control systems also incorporate mechanical springs which provide control forces when the electrohydraulic system is disengaged. Longitudinal trim is achieved by positioning the reference point of the spring by means of a hydraulic trim actuator. For the lateral cyclic stick, which does not have a trim actuator, the spring is connected to a fixed point on the aircraft structure. The pedal control has neither a spring capsule or a trim actuator. Lateral stick and pedal trim is achieved by electrically summing the trim inputs into the electrohydraulic servo.

The FFS was designed for safe, effective control of the XV-15 throughout its operational flight envelope. No special considerations were given to the potential use of this vehicle for handling qualities and control system investigations. Consequently, the flexibility normally designed into a research FFS was omitted. Independent control of the static or dynamic characteristics was not provided. Simplicity and integrity were paramount in the design.

The FFS role can be expanded to include flying qualities and control system research by various degrees of system modification. The extent of any modifications is dependent upon the nature of research intended by the user. Research in certain areas such as V/STOL display for automatic landing systems may be conducted with the present configuration while flying qualities research or control system studies would necessitate system modifications.

Sections 2.1.1 through 2.1.5 summarize the XV-15 Force Feel System characteristics developed by Calspan under Bell Contract 60707 and discusses potential system modifications of varying complexity. Advantages of each of the modifications are presented and recommendations made based upon projected system utilization.

2.1.1 FFS Conceptual Design

The XV-15 FFS is an electrohydraulic analog of a spring-mass damper system where both the dynamic and the static characteristics are controlled by a single variable, $\bar{q}_c$ (dynamic pressure). The primary input to the FFS is the pilot applied force which generates a hydraulic fluid flow and moves the actuator until the position feedback balances the applied force. Thus, a gradient is developed analogous to the compression or extension of a spring. The gradient (N/m) can be increased by either a decrease in the force gain or an increase in the position feedback gain.

The theoretical force vs. position feel characteristics are defined by the differential equation that relates force to position for a spring, mass and dampler. This equation in Laplace form is:

$$x = \frac{F}{K}\left[\frac{1}{\frac{MS^2}{K} + \frac{BS}{K} + 1}\right] \qquad (1)$$

where M = system mass
B = system damping
K = system spring stiffness

The corresponding equation in terms of natural frequency, ω and damping ratio, ζ is:

$$x = \frac{F}{K}\left[\frac{1}{\frac{S^2}{\omega_n^2} + 2\zeta\frac{S}{\omega_n} + 1}\right] \qquad (2)$$

where

$$\omega_n = \sqrt{\frac{M}{K}} \; ; \quad \zeta = \frac{B}{2\sqrt{KM}}$$

For the FFS, the position servo contained in Figure 1 simulates the second order transfer function desired with control over the natural frequency, damping ratio, and gradient.

With the position gain, K_p, held constant, the gradient can be controlled by the gain of the force signal ($1/K_F$), independent of the natural frequency. The $1/K_F$ adjustment can only be used over a small range before variations must be made in the natural frequency gains (ω) if harmonious dynamic and static feel characteristics are to be preserved.

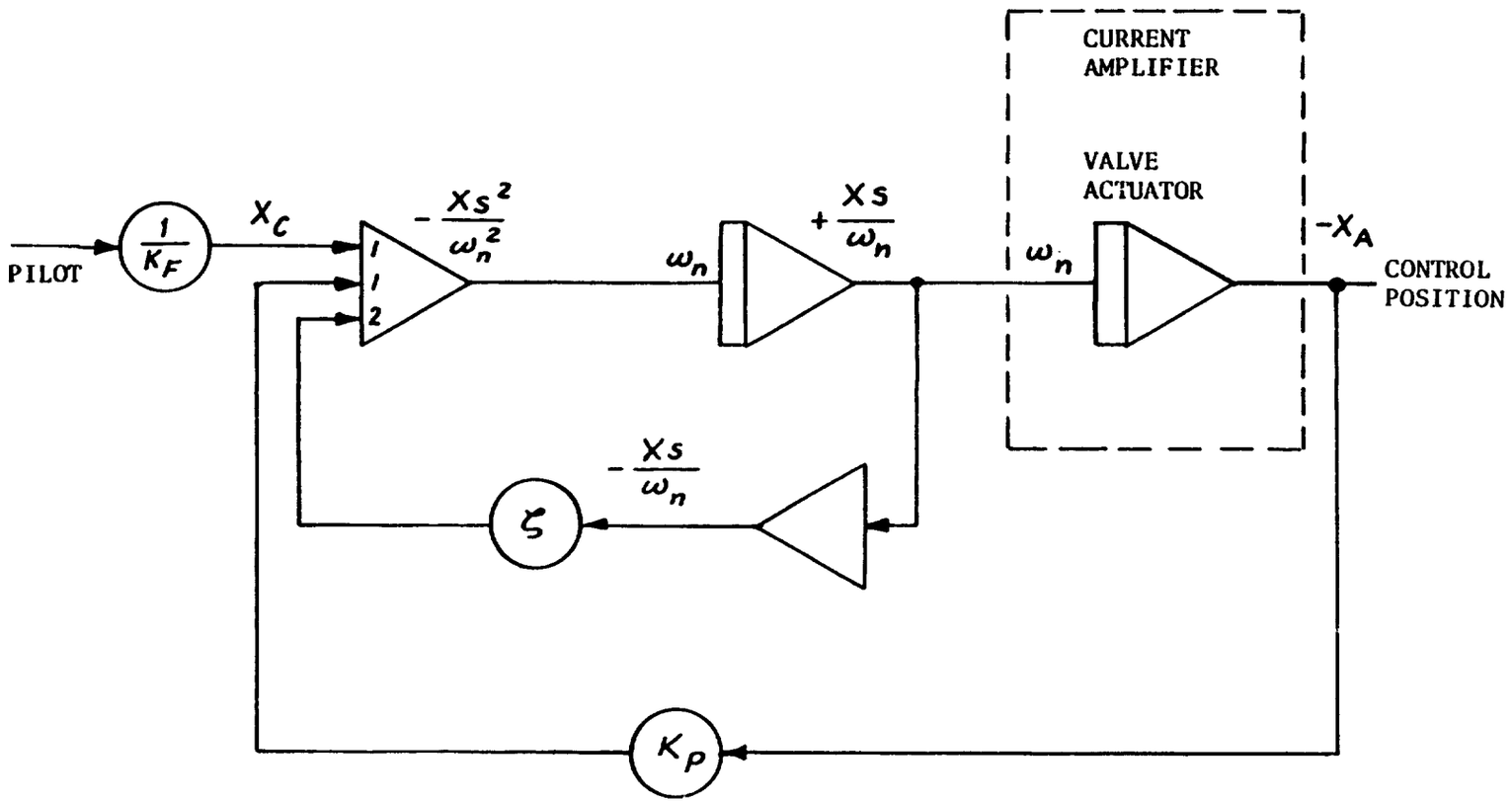

Figure 1 ANALOG DIAGRAM OF FEEL SYSTEM POSITION SERVO

A variation in gradient can also be achieved by the position feedback gain, K_p . Variation of K_p changes the frequency of the position loop consistently with the change in the gradient. However, a change in damping ratio also occurs. Additional gain variation circuitry in the rate feedback eliminates this effect.

2.1.2 FFS Operation

The XV-15 FFS has a ten to one variation in the longitudinal stick force gradient as the airspeed varies from 0 m/sec (0.0 knots) to 153 m/sec (300 knots). To obtain this wide variation in gradient and yet maintain harmonious dynamic characteristics, gradient control is achieved by scheduling the position feedback gain K_p . The force gain, $1/K_F$, is not variable in the present design. An additional circuit maintains a constant damping ratio.

A representation of the existing FFS mechanization is presented in Figure 2. The force to position transfer function of this mechanization is the following:

$$\frac{X_A}{F_p} = \frac{\frac{1}{K_F K_p}}{\frac{s^2}{K_p \omega_n^2} + \frac{2\zeta s}{K_p \omega_n} + 1} \qquad (3)$$

The actual natural frequency ω_{n_A} and damping ratio ζ_A of the position loop are the following:

$$\omega_{n_A} = \omega_n \sqrt{K_p}$$

$$\zeta_A = \zeta$$

The frequency, ω_n , and a damping ratio, ζ , are determined exclusively by electrical gains of the loop. The actual frequency (ω_{n_A}) is directly proportional to K_p , while the damping ratio is constant for all K_p . The force gain, K_F , is fixed. Independent changes of gradient, frequency and damping are not possible.

The functional schematic for the longitudinal FFS is presented in Figure 3. The total force signal is generated by summing the outputs of the pilot and co-pilot force transducers. The total signal is compensated and is the primary command input to the position loop. As previously discussed, the position servo is configured as a second-order system with the position feedback gain scheduled with dynamic pressure. The gain scheduling is accomplished by biasing the output of the dynamic pressure transducer and using this function to modify the position feedback signal. The square root of the dynamic pressure signal is also used to modify the rate term of the system to keep the damping ratio constant as the force gradient is changed with airspeed. Modification of the loop gain in this manner not only varies the force gradient but also alters the dynamic response as discussed previously.

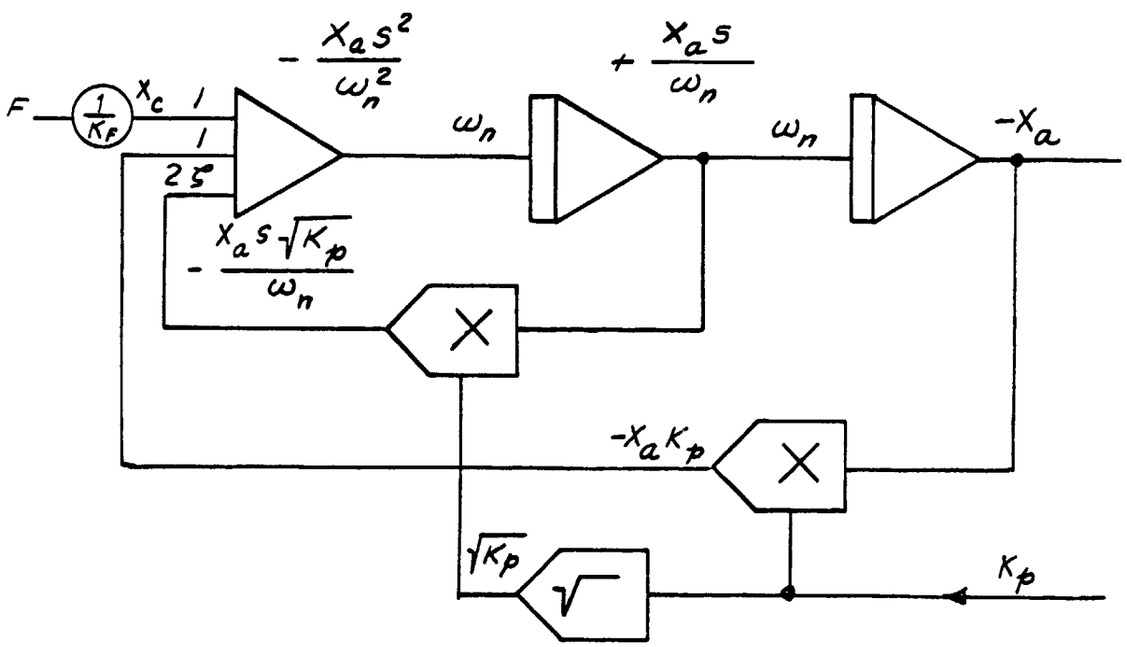

$$\frac{X_a}{X_c} = \frac{\frac{1}{K_p}}{\frac{s^2}{K_p \omega_n^2} + \frac{2\zeta s}{\sqrt{K_p}\,\omega_n} + 1}$$

where:

$$\omega_{n_A} = \sqrt{K_p}\,\omega_n$$

$$\zeta_A = \zeta$$

Figure 2 FFS POSITION LOOP MECHANIZATION

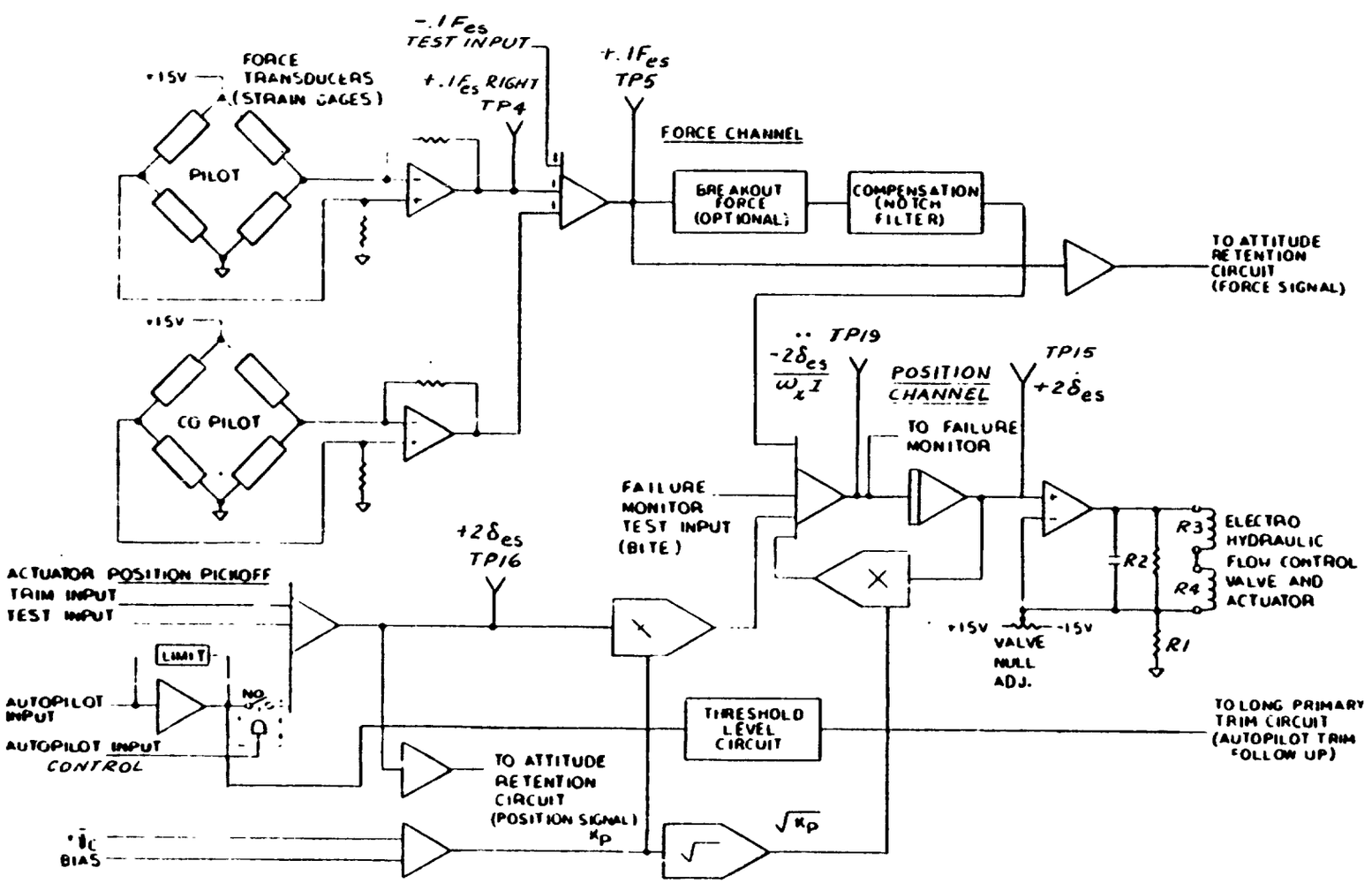

Figure 3 LONGITUDINAL FFS FUNCTIONAL SCHEMATIC DIAGRAM

Provisions presently exist in the force channel to incorporate breakout force by the addition of two resistors. The practical limit on a minimum value (other than zero) is dependent on the drift of the force transducers. A typical minimum value of breakout force that can be achieved is ±2.2 N (±0.5 lbs) in each of the three axes. Compensation networks (lead circuits) are included in the force channel of each axis to improve the system stability.

The XV-15 stability and control system (SCAS) has an attitude retention system designed to aid the pilot during steady state flight. The system when selected, updates the attitude reference automatically whenever a pilot control is made. Both force and position signals are available for this function with the force currently being used. This force signal originates in the FFS electronics and is scaled specifically for this function. It is the only direct electrical connection between the FFS and the SCAS.

A test input is shown on the functional schematic. This input provides step type inputs of sufficient amplitude to test operation of the failure monitor circuits. Provisions are also made for autopilot signal inputs and control.

The longitudinal trim channel of the FFS has an automatic trim follow up circuit. When the longitudinal FFS position servo is used for autopilot inputs, the autopilot system can automatically compensate for any changes in trim. Upon autopilot disengage, this trim signal is removed. Without the automatic trim capability, the stick would revert to the position it had prior to autopilot engage and introduce an undesirable pitch transient. The auto trim circuit detects steady state autopilot command and repositions the trim actuator. This circuit could perform the same function during research augmentation. Auto trim capability is not provided for either the lateral or directional axes.

Figures 4 and 5 are the functional schematics for the lateral and pedal axes. Operation of these two axes is similar to that of the longitudinal axis with the following exceptions:

- A force transducer is installed on both the pilot's and co-pilot's stick for longitudinal and lateral control. The force measurement for the directional axis is obtained from a single transducer on a common linkage between the two sets of rudder pedals.
- The directional axis does not have an output for attitude retention.
- Neither the lateral nor directional axes have outputs for automatic trim follow-up.

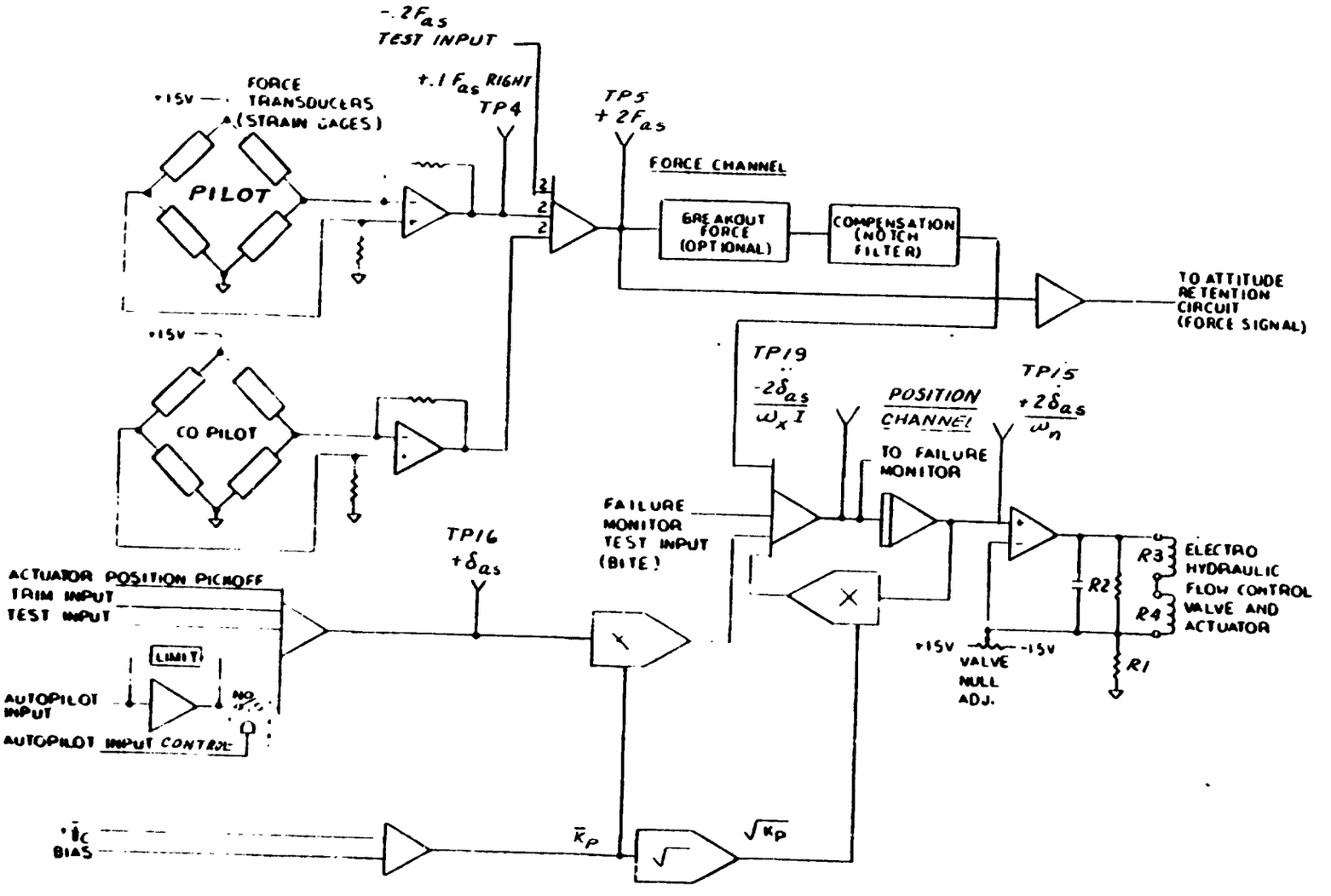

Figure 4 LATERAL FFS FUNCTIONAL SCHEMATIC DIAGRAM

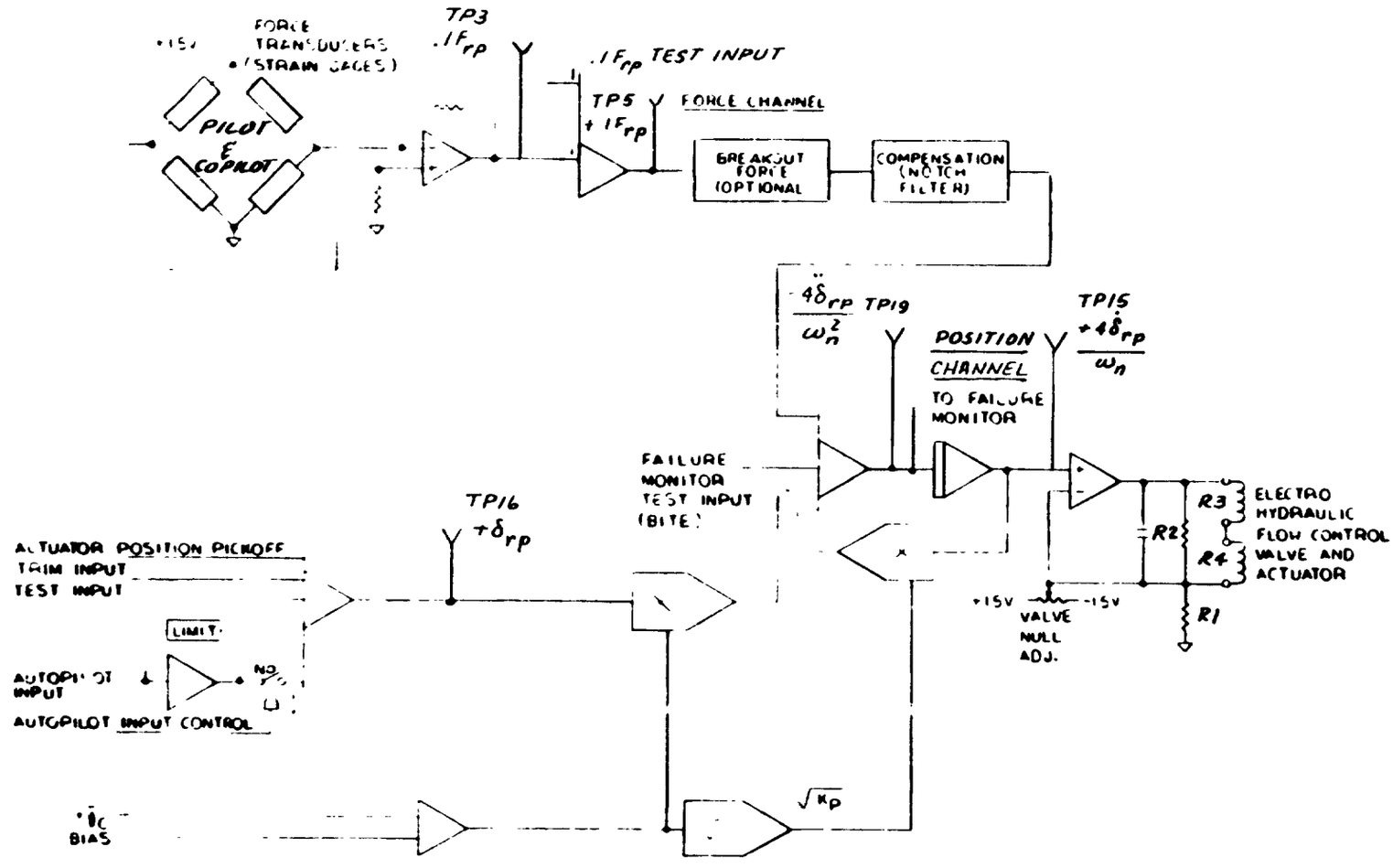

Figure 5 PEDAL FFS FUNCTIONAL SCHEMATIC DIAGRAM

2.1.3 FFS Characteristics

The force feel system electrohydraulic gradients as a function of airspeed for the longitudinal, lateral and directional axes are presented in Figures 6 through 8. The variation, for the longitudinal and lateral axes, can be less than, equal to, or greater than their respective mechanical spring gradients depending on the airspeed. The maximum force capability of each FFS actuator is limited by load relief valves across the servo piston. The pilot's forces are determined by the electrohydraulic gradient when the FFS is engaged if the sum of pilot applied force and the spring force does no exceed the relief valve setting. When the combined forces exceed this level, the gradient changes from that determined by the electrohydraulic FFS to that of the mechanical spring. These characteristics, and the gradient plots that indicate the hysteresis effect of the mechanical system when the relief valve settings are exceeded, are illustrated in Reference 1, pages 14 through 20.

The springs are included in the system design primarily as a back-up for the electrohydraulic FFS. They provide the gradient when the FFS is disengaged. In the event of an FFS malfunction not detected by the safety system the mechanical spring forces generate a differential pressure across the actuator. This pressure opens the relief valves and limits deflections to the level determined by the combination of mechanical gradient and valve setting. This system configuration restricts longitudinal and lateral control deflections for autopilot inputs to the hardover values, approximately ±0.036 m (±1.4 in.).

The pedal system does not contain a mechanical spring, thus with the FFS disengaged there is no pedal gradient (except for friction forces). With the pedal force feel system engaged, the pedal actuator relief valves open if the rudder boost actuator ever reaches its force limit and the combination of pilot applied force and the reflected surface load exceed the valve setting. The autopilot authority in pedal control is limited electrically.

2.1.4 FFS Dynamic Performance

The FFS servos are second-order systems which have the natural frequency programmed as a function of airspeed. The servo damping ratios remain essentially constant over the range of zero to 153 m/sec (300 knots). The three servos all have a natural frequency of 25 rad/sec at 153 m/sec (300 knots) that decreases with airspeed. The relationship between frequency and is described by the following expression:

$$\omega_{n_A} = \omega_n \sqrt{K_p}$$

where ω_{n_A} = actual natural frequency of servo

ω_n = frequency of servo at 153 m/sec (300 knots)

K_p = position feedback gain.

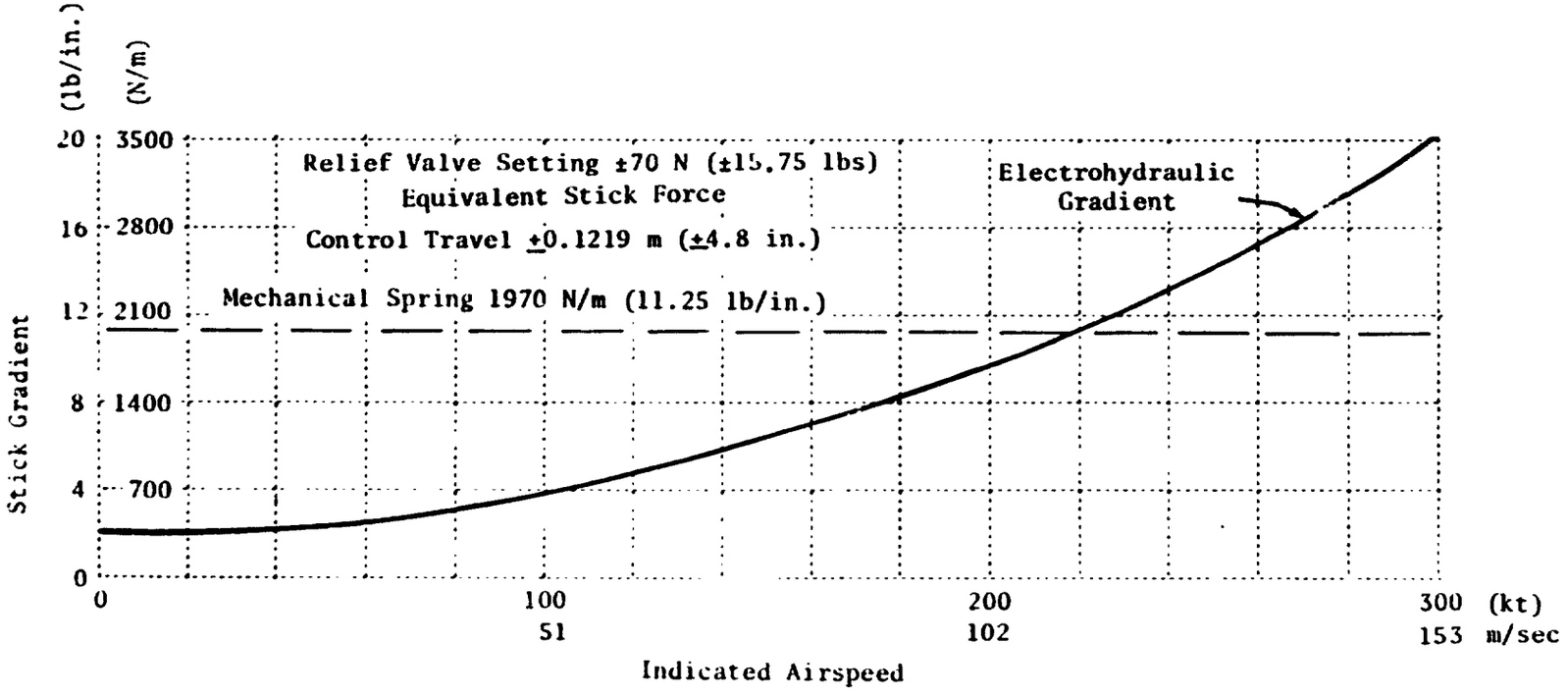

Figure 6 LONGITUDINAL FORCE FEEL SYSTEM CHARACTERISTICS
STICK GRADIENT VS. AIRSPEED

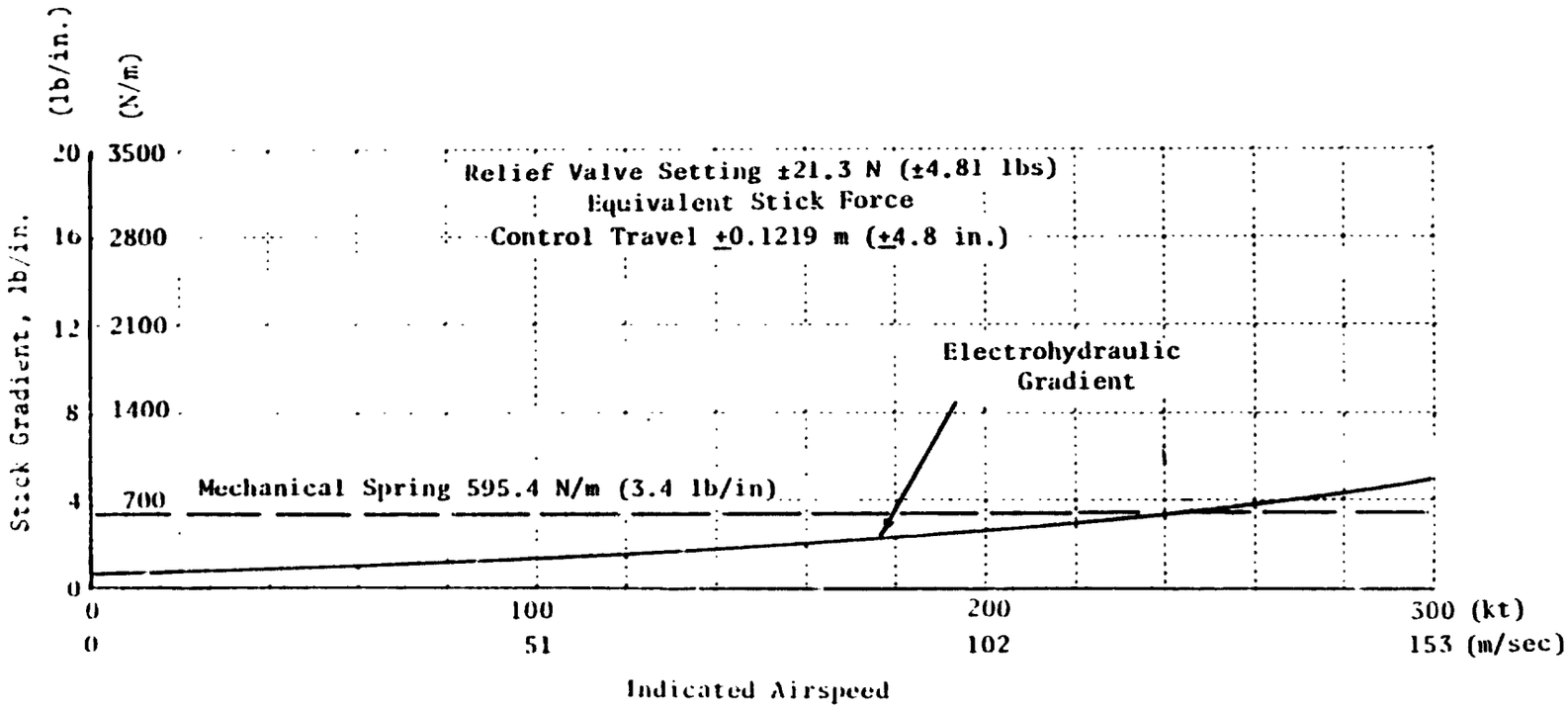

Figure 7 LATERAL FORCE FEEL SYSTEM CHARACTERISTICS
STICK GRADIENT VS. AIRSPEED

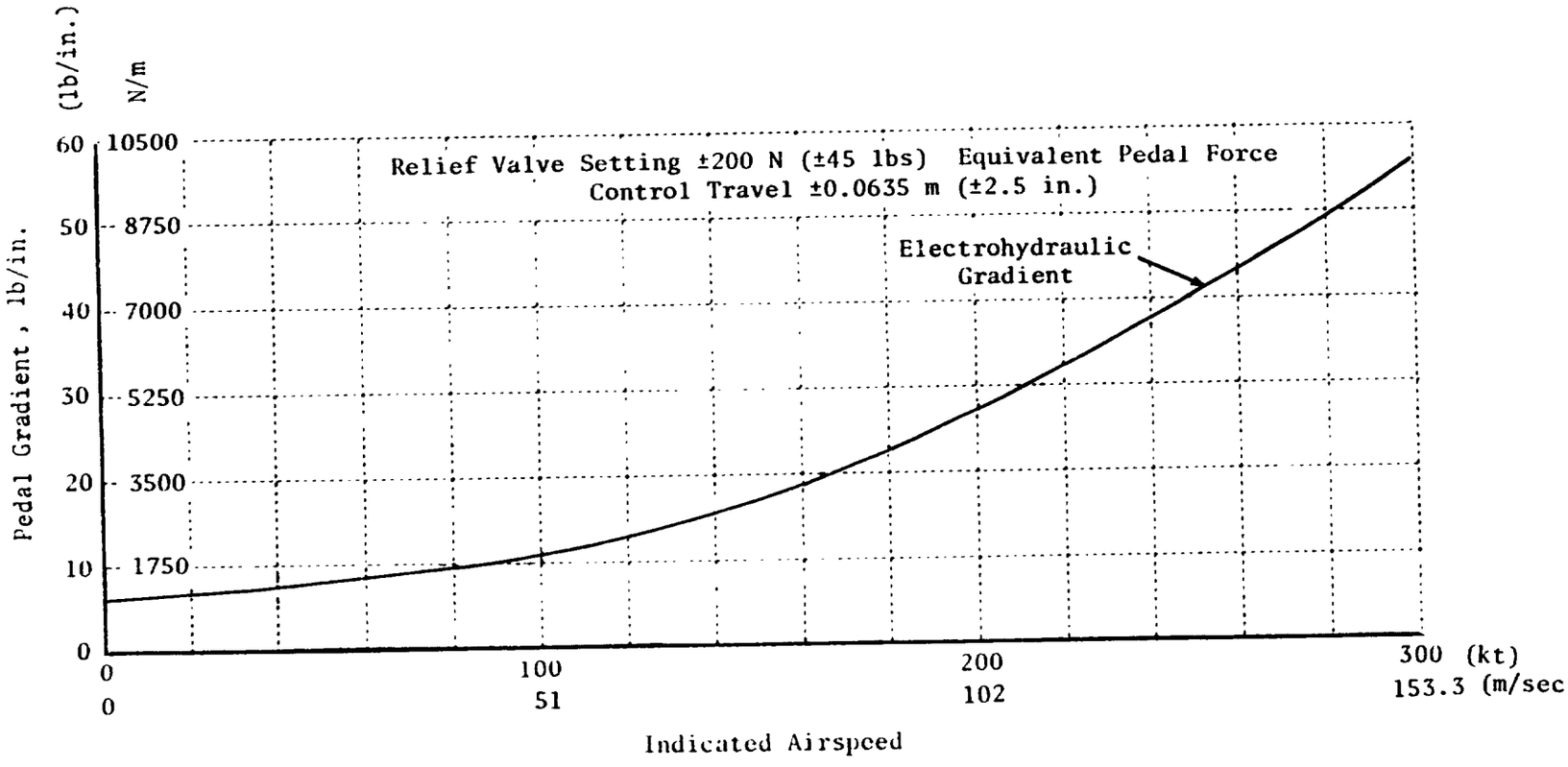

Figure 8 DIRECTIONAL FORCE FEEL SYSTEM CHARACTERISTICS
PEDAL GRADIENT VS. AIRSPEED

The position gain (K_p), natural frequency (ω_{n_A}), and damping ratio (ζ) are given in Table 1 for various airspeeds. Test stand frequency response data for each of the three position servos are contained in Reference 1.

TABLE 1

FORCE FEEL SYSTEM DYNAMIC CHARACTERISTICS VS. AIRSPEED

Airspeed m/sec	Airspeed (knots)	Axis	K_p	ω_{n_A} rad/sec	ζ_A
		Longitudinal			
0	0		.1	7.0	0.85
51	100		.20	11.05	0.85
102	200		.49	17.5	0.85
153	300		1.0	25	0.85
		Lateral			
0	0		.2	11.1	0.85
51	100		.29	13.4	0.85
102	200		.55	18.5	0.85
153	300		1.0	25	0.85
		Pedal			
0	0		.125	8.8	0.85
51	100		.20	11.0	0.85
102	200		.50	17.6	0.85
153	300		1.0	25	0.85

2.1.5 FFS Trim System

An independent hydraulic actuator is used for the FFS longitudinal trim. There are two operational modes for the longitudinal trim. The primary system operates only when the FFS is engaged, making the trim rate a function of airspeed. The secondary longitudinal trim system operates when rate trim capability is desired with the FFS engaged. The secondary trim rate does not vary with airspeed. In either case, the trim actuator repositions the reference point of the longitudinal feel spring and the authority is limited by the actuator's mechanical stop.

The lateral and pedal axes do not have trim actuators. Rate trim is provided by positioning the lateral and pedal FFS actuators. Trim is only possible in these axes with the FFS engaged. The trim rates vary with airspeed and the authority is electrically limited.

The trim rate and authority for the three axes is summarized in Table 2. Figure 9 is a functional schematic for the longitudinal trim channels. The primary and secondary channels operate from independent sources. Each channel is a closed loop position servo controlled by the output of an integrator. The integrator is controlled by operation of the trim switches. The primary channel trim rate is varied by the gain of the $\bar{q}_c$ divider. An initial condition circuit on each integrator allows transition between channels without transients.

During autopilot operation if the stick is displaced beyond a +0.0127 m (+0.5 in.) threshold, the trim actuator will move at 0.00127 m/sec (0.05 in./sec) to take out any static spring displacement. This minimizes a longitudinal transient when the autopilot is disengaged as previously discussed.

TABLE 2

FFS TRIM RATE AND AUTHORITY LIMITS

Trim Rate

Airspeed	Longitudinal		Lateral	Pedal
	Primary	Secondary		
m/sec (knots)	mm/sec (in./sec)	mm/sec (in./sec)	mm/sec (in./sec)	mm/sec (in./sec)
0	12.7	6.35	12.7	12.7
(0)	(0.5)	(0.25)	(0.5)	(0.5)
153	2.54	6.35	2.54	2.54
(300)	(0.1)	(0.25)	(0.1)	(0.1)

Trim Authority

Longitudinal	Lateral	Pedal
meters (in.)	meters (in.)	meters (in.)
±0.1	±0.038	±0.019
(±3.84)	(±1.5)	(±0.75)

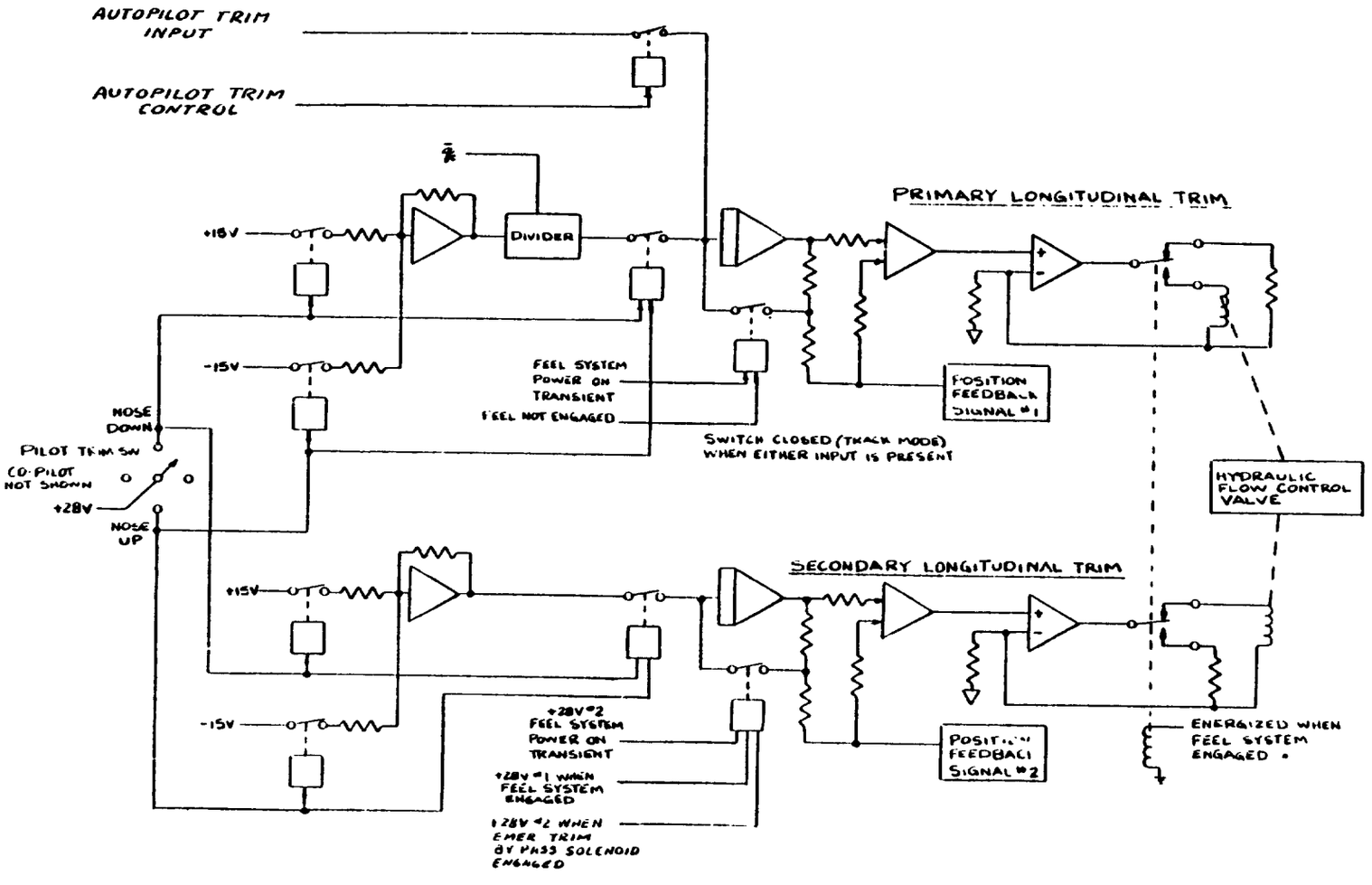

Figure 9 LONGITUDINAL PRIMARY AND SECONDARY TRIM CHANNELS (HYDRAULIC TRIM ACTUATOR)

The lateral and pedal trim circuits are the same as the longitudinal circuits. In these two axes, the integrator outputs position of the FFS actuators directly.

For complete details of the FFS and trim circuit operation, refer to the Operations and Maintenance Instructions, XV-15 Tilt Rotor Aircraft Automatic Flight Control (Reference 2).

2.2 FFS Configurations For Flight Research Applications

The primary function of the XV-15 FFS during a flight research operation is the simulation of various feel characteristics. Separation of the pilot's controls from the co-pilot's controls would make it possible to expand the role of the feel system to include research augmentation. The necessity for this additional capability is dependent on the SCAS actuator performance. If the SCAS does not have the authority or cannot be increased in authority to accommodate the requirements of the augmentation system, the feel actuators will have to be used for augmentation during flight research operations. If a SCAS actuator output linkage modification can increase the authority sufficiently, this additional augmentation may be unnecessary. A discussion of the analysis performed to ascertain the authority required of the SCAS and FFS actuators for research augmentation is contained in Section 4.4.

In the existing XV-15 flight control system, provisions exist for autopilot command inputs through either SCAS actuators, the FFS actuators, or both. It is through these autopilot lines that the research augmentation may be implemented. When the SCAS servos are used, the normal SCAS servo commands can be removed by external control of the SCAS input control line. The SCAS actuator position can then be controlled solely by an external computer into the autopilot line. The mechanization is illustrated in Figure 10. When the research augmentation system is disengaged, SCAS actuator control reverts back to the normal SCAS inputs.

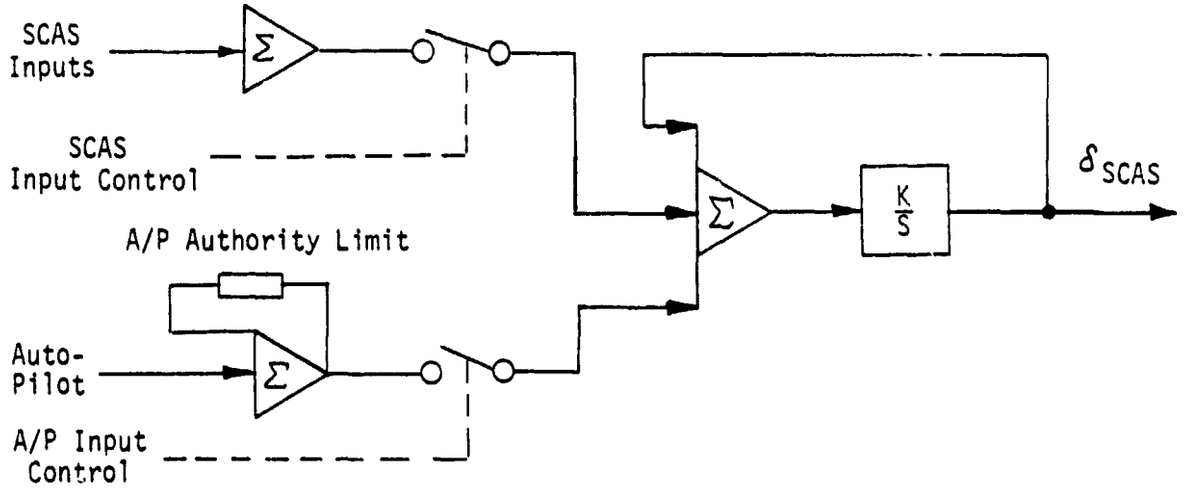

Figure 10 RESEARCH AUGMENTATION MECHANIZATION

Thrust augmentation can be implemented to control the fourth degree of freedom. This can be achieved through the collective actuator supplied by Calspan. For this control it is mandatory that the pilot and co-pilot controls be mechanically separated. When separated, the evaluation pilot's collective control becomes a command to the collective servo which is closed around the aircraft through the research computer.

The force feel system can be implemented in various configurations for use during flight research operations. Four possible configurations are the following:

- Configuration 1
  No FFS modifications, all augmentation would be made through the existing SCAS actuators with the control laws generated on an auxiliary computer.

- Configuration 2
  Modify the existing FFS to allow gradient control from an auxiliary computer. Vehicle augmentation would be the same as in Configuration 1.

- Configuration 3
  Revise the existing FFS electronics to allow independent control of gradient, frequency and damping from an auxiliary computer. Vehicle augmentation would be the same as in Configuration 1.

- Configuration 4
  Separation of longitudinal and lateral cyclic controls and pedals and installation of a second, independent FFS for research purposes. Augmentation signals can control the aircraft through both the existing FFS servos and the SCAS servos.

Configuration 1

If the system is used as presently configured, all research augmentation will be performed through the existing SCAS actuators. The aircraft's stability characteristics would be modified by an external computer used to generate servo commands from measured aircraft responses. The gear ratio of the existing mechanical system could be modified by adding or subtracting pilot control positions to the SCAS actuator commands.

This approach allows the research augmentation system to be evaluated from either seat, maintains the integrity of the existing FFS and SCAS, and when the research system is disengaged the SCAS actuators revert back to normal operation.

Limitations are due primarily to the lack of independent control of the gradient and dynamic characteristics of the feel system and the limited authority of the SCAS. The existing SCAS authority limits for the pitch, roll and yaw axes are detailed in paragraph 2.3.1. As presently configured the

autopilot authority is electrically limited to 50% of the total SCAS authority. The impact of this limited authority is discussed in Section 4.4. Methods for increasing the SCAS authority are discussed in Section 2.3.

Since no FFS modifications are required, the cost impact is negligible except for the possible changes required to increase the SCAS authority. Disadvantage is that the SCAS control activity is not reflected in safety pilot's controls. This reduces his ability to anticipate need to take control.

Configuration 2

Modifications to the existing FFS could be made that allow gradient and dynamic parameter control by the pilot or an auxiliary computer. As in the existing system independent control of the gradient, frequency and damping would not be possible but harmony between the gradient and bandwidth would be preserved throughout the range of control.

In the existing system the position loop has the feedback gain scheduled as a function of dynamic pressure. This is illustrated in Figure 3. Here the gain schedule would be switched from dynamic pressure to a pilot control or a computer output during research flying. At all other times the normal XV-15 capability would be preserved. Figure 11 is a functional diagram of this modification. The reference voltage, +V, on the pilot's gain control could either be a constant or a computed function of flight condition originating in the V/STOLAND research computer.

The same technique could be used to change the control of trim rate from dynamic pressure to another parameter as dictated by the requirements of the research program. SCAS operation is identical to that discussed in Configuration 1.

The modifications required for this alternative results in a system similar to the existing system. In this case however, the FFS gradient could be controlled externally. The dynamic characteristics, however, would not be independent of the gradient. The modification could be implemented in the existing chassis with no modification of the FFS circuit cards. The integrity of the existing FFS is maintained and as in Configuration 1, the research augmentation system can be flown from either seat. The FFS and SCAS revert back to normal when research augmentation system is disengaged. Since no mechanical modifications are required and the only electrical changes require chassis wiring the cost is small and would not be a factor if this approach is used.

The same SCAS authority limits of Configuration 1 exist and the SCAS control activity is not reflected to the safety pilot.

Configuration 3

The previous alternatives require negligible FFS changes and substantial research could be performed within the systems capability. If

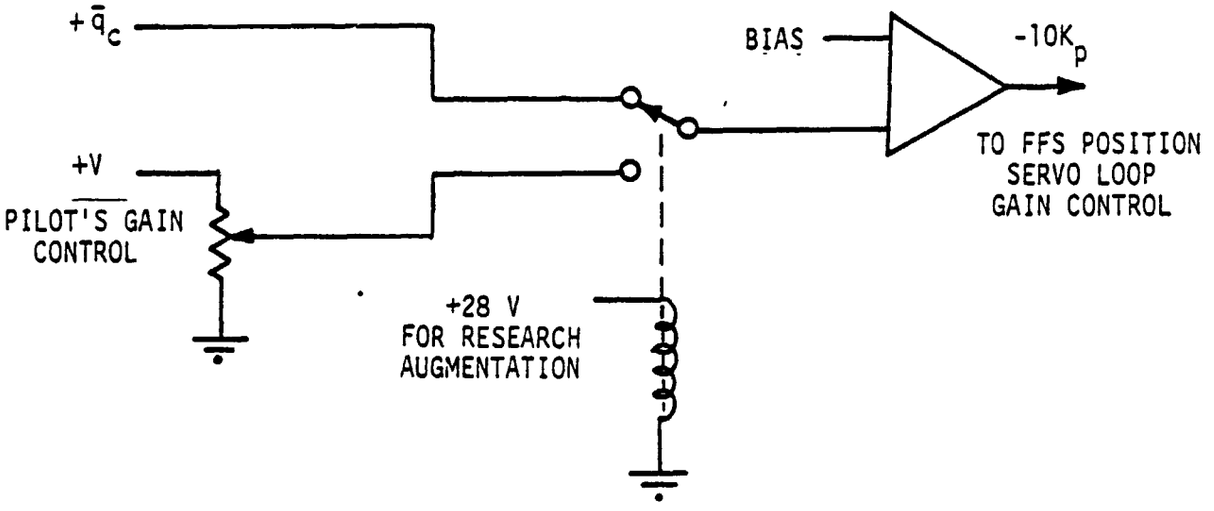

Figure 11 PROPOSED SYSTEM MODIFICATION - CONFIGURATION 2

independent gradient, frequency and damping control are required or extensive non-linear system capability is desired, modifications in addition to the FFS electronics become mandatory. The system can be configured so a completely different set of circuits are used to control the FFS during research operation. When the research augmentation system is disengaged, control would revert back to the normal XV-15 system. The research system would exhibit independent control of gradient, frequency and damping, have the capability of adding variable nonlinear characteristics, such as deadband breakout force, hysteresis, nonlinear gearing, etc.

The system would make use of the existing force transducer and feel actuators. During research operation, FFS servo control would be transferred from the normal FFS electronics to the research electronics. The pilot and co-pilot's controls would still be mechanically connected so control of the airplane could be possible from either seat in both normal and research operation.

Since the controls would not be separated, augmentation would be performed through the SCAS actuators as in the two previous configurations. Costs involved here would include design, fabrication, checkout and testing of the circuit cards and the required chassis. Wiring changes would be required in the airplane and existing FFS control unit to accommodate the research control logic and switching functions. The force feel system capability would be increased for research flying, however, the increase in complexity would reduce the integrity of the primary FFS.

The mechanical spring-relief valve combination would function during both modes of force feel system operation. This nonlinear characteristic would have to be considered when the research mode is engaged.

The same SCAS authority limits of Configuration 1 exist and the SCAS control activity is not reflected to the safety pilot.

Configuration 4

Extensive capability can be achieved by the separation of the pilot's controls and installing an independent feel system for the evaluation pilot. This requires removal of control rods, re-design of the longitudinal cyclic torque tube and installation of additional electrohydraulic actuators. A conceptual mechanical design for the split controls is presented in Figures 12 through 14. Figure 13 includes the conceptual design for the pilot's collective controller. The research pilot's controls uses a typical helicopter collective lever instrumented with a position transducer to generate a signal for use in the research computer. The servoed collective handle controls the thrust during research augmentation. Provisions could be made in the design to connect the controls for normal dual operation.

This mechanization also requires a new feel system electronic unit. The electronics would provide independent control of gradient, frequency,

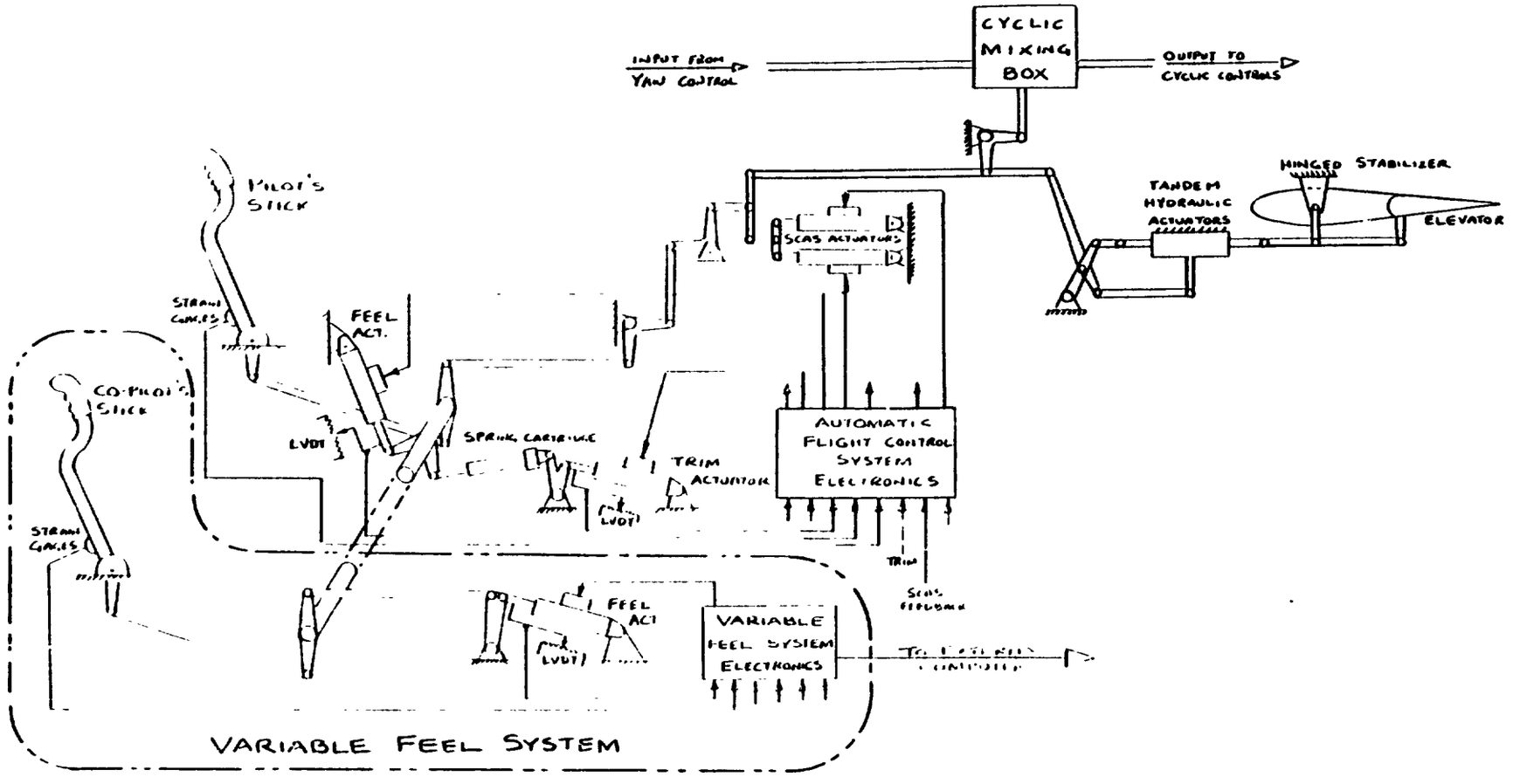

Figure 12 LONGITUDINAL CONTROL

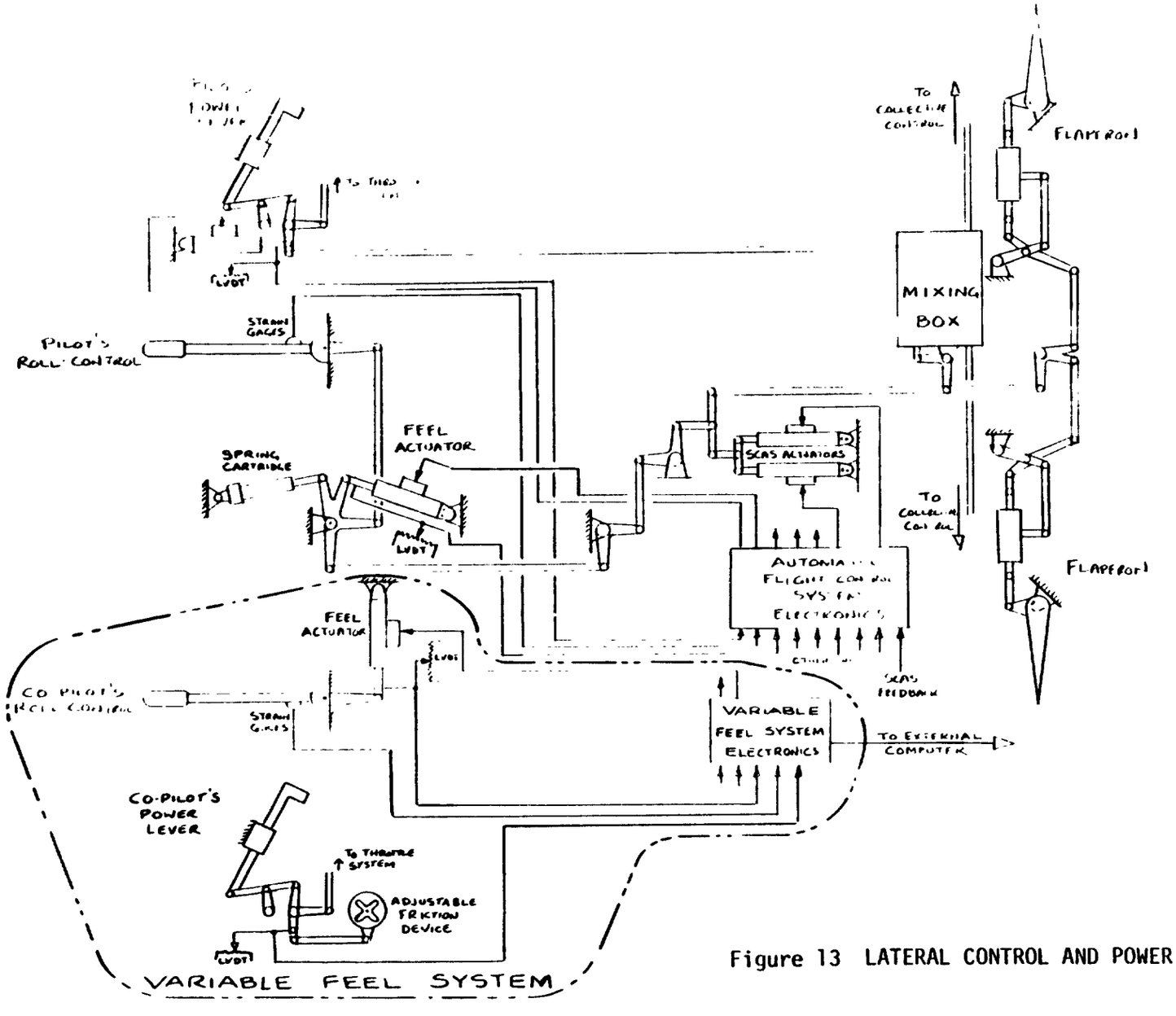

Figure 13 LATERAL CONTROL AND POWER LEVER

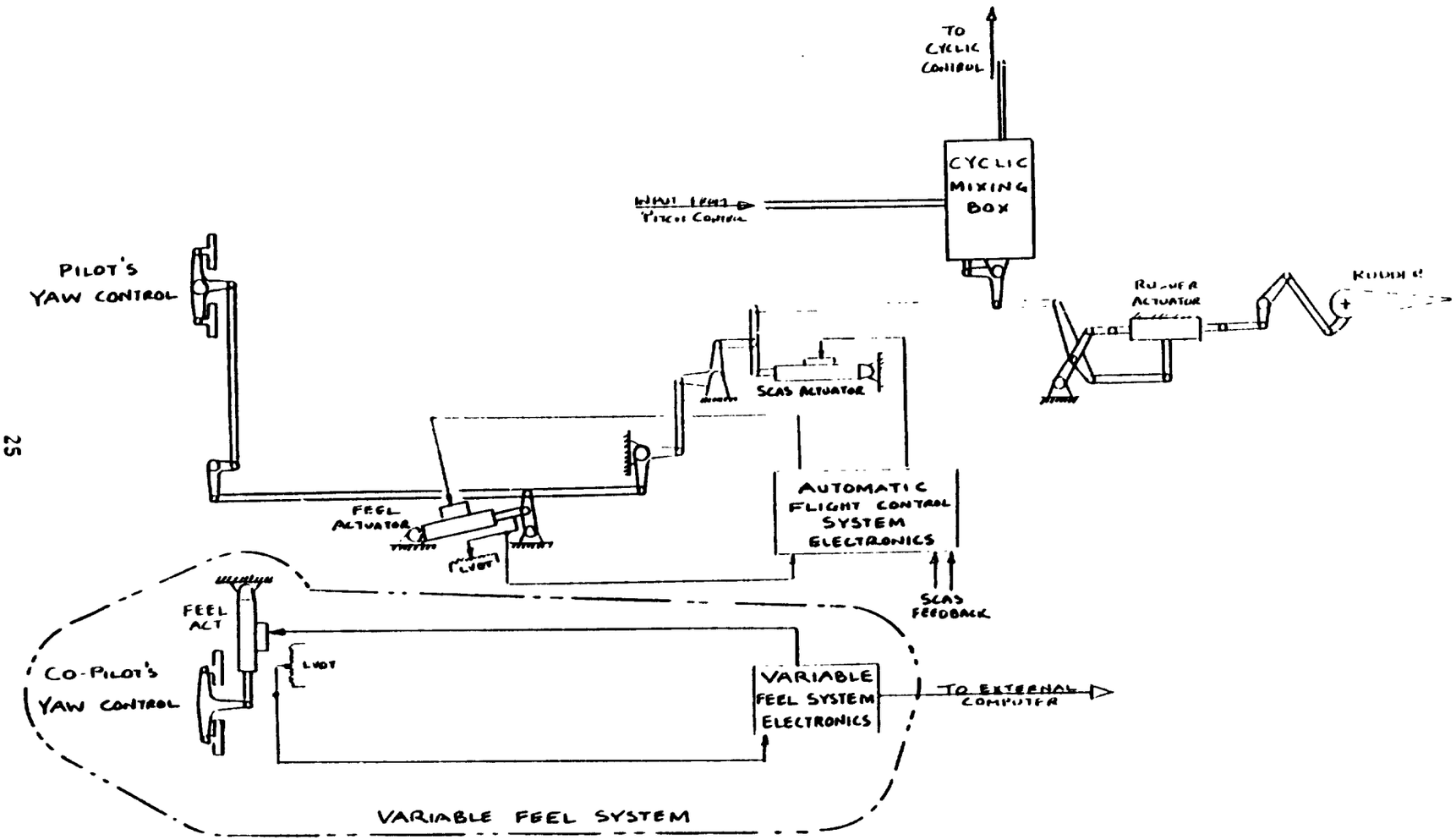

Figure 14 DIRECTIONAL CONTROL

'amping and trim. In addition adjustable nonlinearities such as hysteresis and breakout force can be included.

The research augmentation could be performed through the FFS actuators as well as the existing SCAS actuators. The augmentation inputs to the SCAS would be the same as in the previous configurations. Augmentation inputs to the existing FFS actuator would be through its autopilot input line in a manner similar to that used in the SCAS.

There are two severe limitations to this concept. The first is the authority limit imposed on the FFS cyclic actuators when used as position servos. The limit is a result of the mechanical spring-relief valve combination of the existing system. The second limitation is the low bandwidth of the FFS position servos at low airspeeds. This limits their capability as augmentation servos. One way to circumvent these limits is by changing the authority and increasing the bandwidth of the FFS servos when the research augmentation system is engaged. The authority and bandwidth of the research augmentation system could be increased by one or more of the following modifications:

- decrease the mechanical spring gradient, relief valve ratio
- disconnect the mechanical spring when the research augmentation system is engaged
- reconfigure the FFS actuators so that a higher relief valve setting occurs when the research augmentation system is engaged
- reconfigure the existing FFS electronics so that the position servo bandwidth is increased during research augmentation system operation
- effective use of complementary filters where the high frequency component of the augmentation signal commands the SCAS servos and the low frequency component commands the existing force feel actuators.

A variation of this configuration is where the research augmentation signals command the force feel position servo only. The force feel position servo would have to be modified to achieve a full authority and high bandwidth. All augmentation signals to the SCAS servos would be disabled. This variation has the advantage of reflecting full control activity to the safety pilot during research augmentation.

For any of these modifications it is necessary for the FFS and SCAS to revert back to normal operation whenever the research augmentation system is disengaged. Some of these modifications will compromise the integrity of the existing FFS because of the envisioned system complexity.

The cost factor associated with this configuration is the highest of the four alternatives discussed. The cost includes design, fabrication, installation and checkout of the research FFS and the associated actuators, hardware and electronic components. The system flexibility would be higher than any of the previous configurations.

2.2.1 Summary of Modified FFS Capabilities and Cost

The FFS configurations discussed in this report represent diverse levels of system modification. From an operational standpoint, the first two configurations offer the least amount of flexibility but minimum system modification. However, the integrity of the existing system is maintained. Configuration 3 offers complete FFS flexibility, but the additional control switching compromises the overall integrity of the system. For each of these three configurations, the research augmentation will be performed through autopilot control inputs to the SCAS servos. The SCAS servo authority is electrically limited by limiters on the autopilot control input line and mechancially limited by the configuration of the output linkages. The authority of the external inputs can be increased by removing the limiters from the autopilot line in the SCAS electronics. In addition, the SCAS actuator output linkages can be reconfigured to increase SCAS actuator authority. Possible SCAS modifications are discussed in Section 2.3. Control of the XV-15 is possible by both pilots in each of these three configurations during both research and normal operation.

If the feel servos are required to supplement the research augmentation performed by the SCAS servos, the pilot's controls must be split and the fourth configuration implemented. This modification requires both mechanical and electronic reconfiguration and will result in the highest costs. When the research system is disengaged, the associated feel system would be inoperative. Consequently, XV-15 control could only be maintained through the safety pilot's controls. Augmentation would be performed through either SCAS actuators, feel actuators or both.

In all configurations, it is possible to feed back additional variables (e.g. rate and acceleration terms) to FFS position loop to simulate bobweights, etc. The autopilot input line would be used for this purpose in configuration one or two. The signal would be generated on the external computer. For configuration three or four, this function would be performed as part of the new FFS electronics with inputs from the external computer. Table 3 summarizes the advantages, complexity and relative cost for each of the four configurations discussed.

A preliminary estimate of the cost required, less fee, to modify the FFS to configurations three or four is contained in Table 4. The estimate contains parts costs and professional and technical labor for each of the three phases; design, fabrication, installation and checkout. Both manhours and labor dollars are included.

2.3 Stability and Control Augmentation System Description and Modification

The stability and control augmentation system (SCAS) is that portion of the automatic flight control system (AFCS) design to enhance the handling qualities of the XV-15. Full control of the air vehicle is provided throughout the entire flight envelope including helicopter, conversion and con-

TABLE 3

SUMMARY OF FFS CONFIGURATION CAPABILITY

CONFIGURATION	FFS MODIFICATION REQUIRED	ESTIMATED COST	SAFETY IMPACT	FFS FLEXIBILITY
No. 1	None	None	Integrity of existing system maintained. SCAS actuator motion not reflected.	FFS characteristics determined as a function of dynamic pressure. Augmentation through SCAS.
No. 2	Convert gain schedule from $\bar{q}_c$ to external control.	$10,000	Integrity of existing system maintained. SCAS actuator motions not reflected.	FFS characteristics externally controlled. No independent control of gradient frequency, damping. Augmentation through SCAS.
No. 3	Install separate electronics for the research system and to control the transition between normal and research system.	$123,000	Switching compromises FFS integrity. SCAS actuator motions not reflected.	Independent control of gradient frequency damping and nonlinear characteristics. Augmentation through SCAS.
No. 4	Install additional FFS for the research system. The normal XV-15 FFS may require modification.	$256,000 plus $120,000 additional if modifications to existing electronics are made.	Normal XV-15 FFS operational during research operation. Loss of two-seat capability.	Independent control of gradient frequency damping and nonlinear characteristics. Augmentation through FFS servos or SCAS or both.

TABLE 4

COST ESTIMATE FOR FFS MODIFICATIONS

	Configuration 3		Configuration 4	
	Hours	Dollars	Hours	Dollars
Design				
Professional	1100	38,000	2200	76,000
Technical	800	16,000	1600	32,000
Fabrication				
Professional	400	13,000	800	26,000
Technical	700	14,000	1400	28,000
Installation & Checkout				
Professional	600	20,000	1200	40,000
Technical	600	12,000	1200	24,000
Parts	----	10,000	----	30,000
Total	4200	123,000	8400	256,000

ventional flight modes. It is a three-axis system (pitch, roll, yaw) with two operational channels in the pitch and roll axes. The dual pitch and roll channels comprise completely redundant components up to and including all sensors, electronic components and SCAS actuators. The SCAS servo outputs are mechanically summed on a walking beam linkage prior to driving the power actuator. This redundancy allows continued SCAS operation in the pitch and/or roll axes following a single failure. Failures are detected by a comparison type failure warning system which monitors the actuator positions of the dual pitch and roll axes. A passive yaw channel provides this function in the yaw axis. The system does not provide automatic disconnect following a malfunction but allows the pilot to disengage the complete SCAS, or turn off the failed axis, or select single channel operation in one or more axes. Single channel operation reduces the SCAS authority and system gains to 50% of normal operation.

A pitch and roll attitude retention system reduces pilot workload during steady state flight conditions when selected. The attitude retention system provides limited control authority (50% of each SCAS actuator authority) when engaged. The attitude system may be engaged at any time provided:

1. the FFS is engaged
2. one or more of the pitch or roll channels are engaged
3. the attitude gyro is on and working properly.

The reference attitudes (pitch attitude or roll attitude) automatically update whenever the pilot cyclic stick forces, longitudinal or lateral, exceed their respective thresholds. Yaw attitude retention is not available.

The SCAS actuators are first order positions servos with a corner frequency of 50 rad/sec and can be controlled by external commands as indicated by Figure 15. Independent control of each axis allows research augmentation to replace the normal SCAS commands or supplement them. An electronic limit on the command signal limits the external signal authority to 50% of maximum SCAS capability. This limit was included in the present design to prevent the autopilot signal from saturating the normal augmentation system. For use as a research augmentation system, this imposes a limitation to the system capability and should be removed when the XV-15 is used in this capacity.

The SCAS consists of aircraft motion sensors, stick position transducers, signal conditioning and servo system electronics and electrohydraulic actuators for each of the three axes. The primary SCAS inputs are the pilot commands (control position) and the aircraft responses (angular rates). The cyclic stick (lateral and longitudinal) and pedal positions are measured by DC-DC LVDT's, an integral part of the three FFS actuators. Two transducers are provided on each FFS actuator one for each of the redundant SCAS channels. Two three-axis rate gyro assemblies provide the required rate feedback signals.

Control of a fourth degree of freedom will be through an FFS-type hydraulic actuator configured as a rate limited position servo which drives the XV-15 cockpit power lever. This servo is to be installed for operation

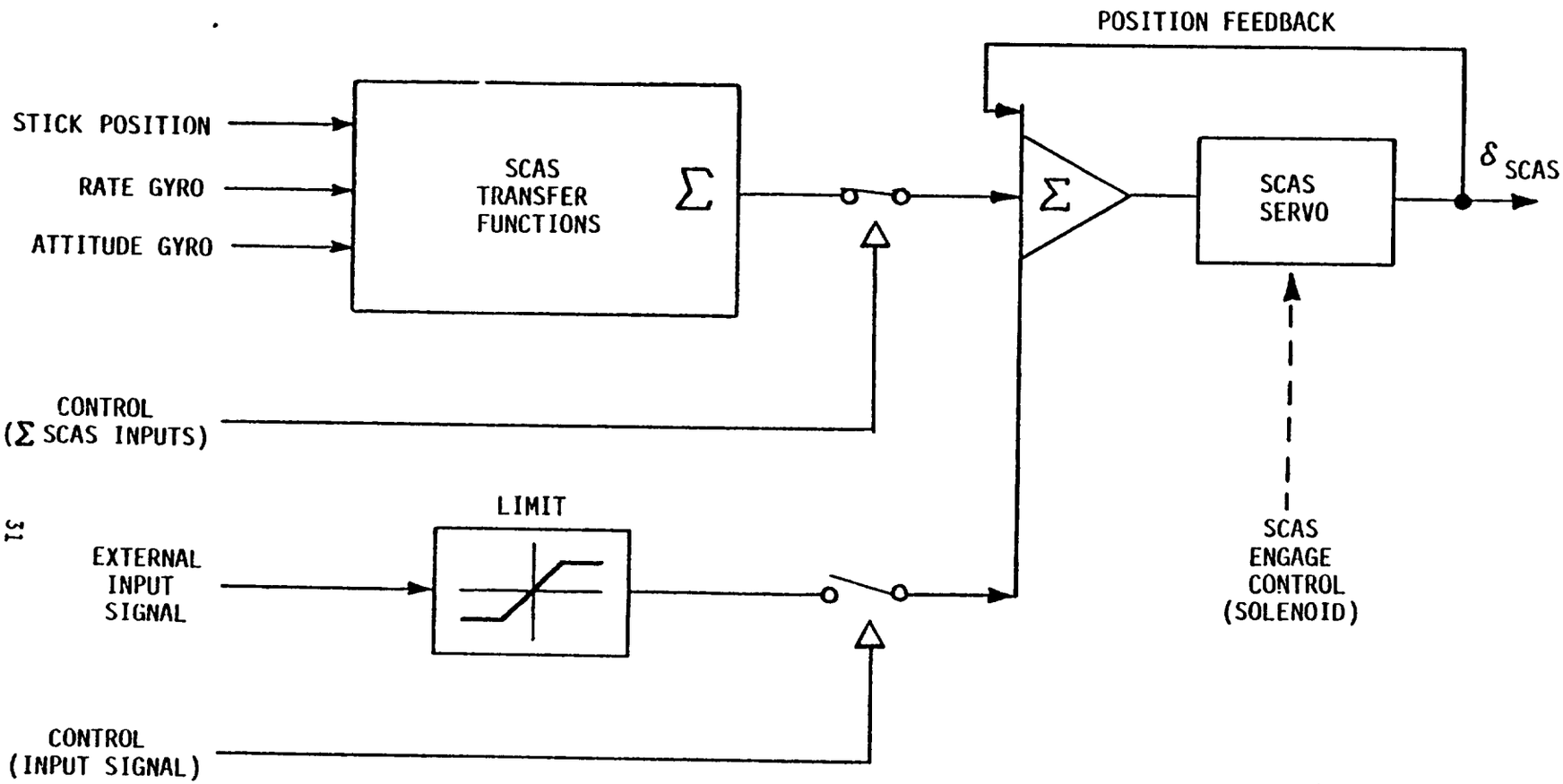

Figure 15 BLOCK DIAGRAM, SCAS INPUTS AND CONTROL

with the V/STOLAND system and can be incorporated for research augmentation through the collective path. When used in this manner, it is mandatory that the pilots collective controls be separated to provide the capability for the evaluation pilot to apply collective inputs. The evaluation pilots collective inputs would then be used together with augmentation signals through the research computer to drive the power lever servo.

A system block diagram is contained in Figure 16. This diagram only depicts one of the two channels for the longitudinal and lateral axis. The directional axis contains a single operational channel and a model. During normal operation the autopilot control lines are both disengaged. The summing amplifier outputs command their respective servos through the normally closed (NC) switched while the autopilot input signals are disabled by the normally open switched (NO).

For operation in the research mode, the SCAS must be engaged and the autopilot logic under computer control. Independent operation of the control logic allows modification of characteristics of the augmented vehicle or the open loop XV-15. The control law for the research augmentation will be generated on the external computer. Control reverts back to normal when the research system is disengaged.

2.3.1 Research Augmentation System Authority Limits and Proposed Modification

The SCAS authority is defined in terms of equivalent meters of pilot control. The existing XV-15 control authority for SCAS and autopilot inputs is:

	Pilot Control Travel		SCAS Actuator Authority		Autopilot Authority	
	meters	in.	meters	in.	meters	in.
Pitch Axis	± 0.1219	± 4.8	± 0.0254	± 1.0	± 0.0127	± 0.5
Roll Axis	± 0.1219	± 4.8	± 0.0391	± 1.54	± 0.02	± 0.77
Pedal Axis	± 0.0635	± 2.5	± 0.020	± 0.8	± 0.012	± 0.4

For research augmentation, the autopilot limit restricts the system capability and should be removed. This modification can easily be made on the SCAS circuit cards for each axis.

The mechanical limit is dictated by the control linkage gearing and the SCAS actuator mechanical stops. The SCAS control authority can be increased by either an increase in actuator travel or a modification of the SCAS linkages. The latter is desirable from both cost and practicality.

The rocking lever arrangement at the Yaw SCAS control is shown in Figure 17. The pitch and roll SCAS controls are similar in concept except that twin actuators working on an equalizing beam are used at the bottom end of each output lever.

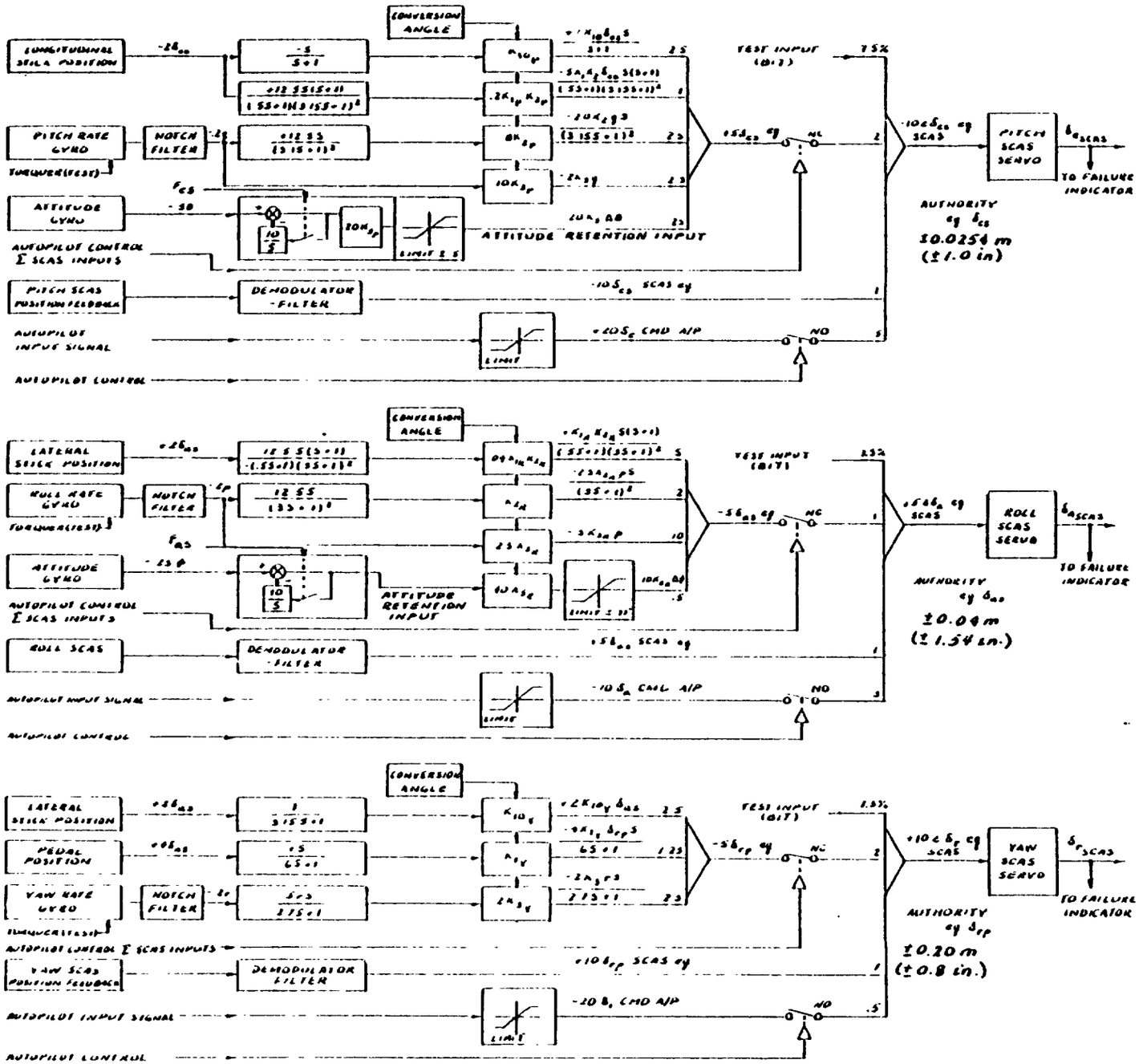

Figure 16 SCAS BLOCK DIAGRAM, SINGLE CHANNEL

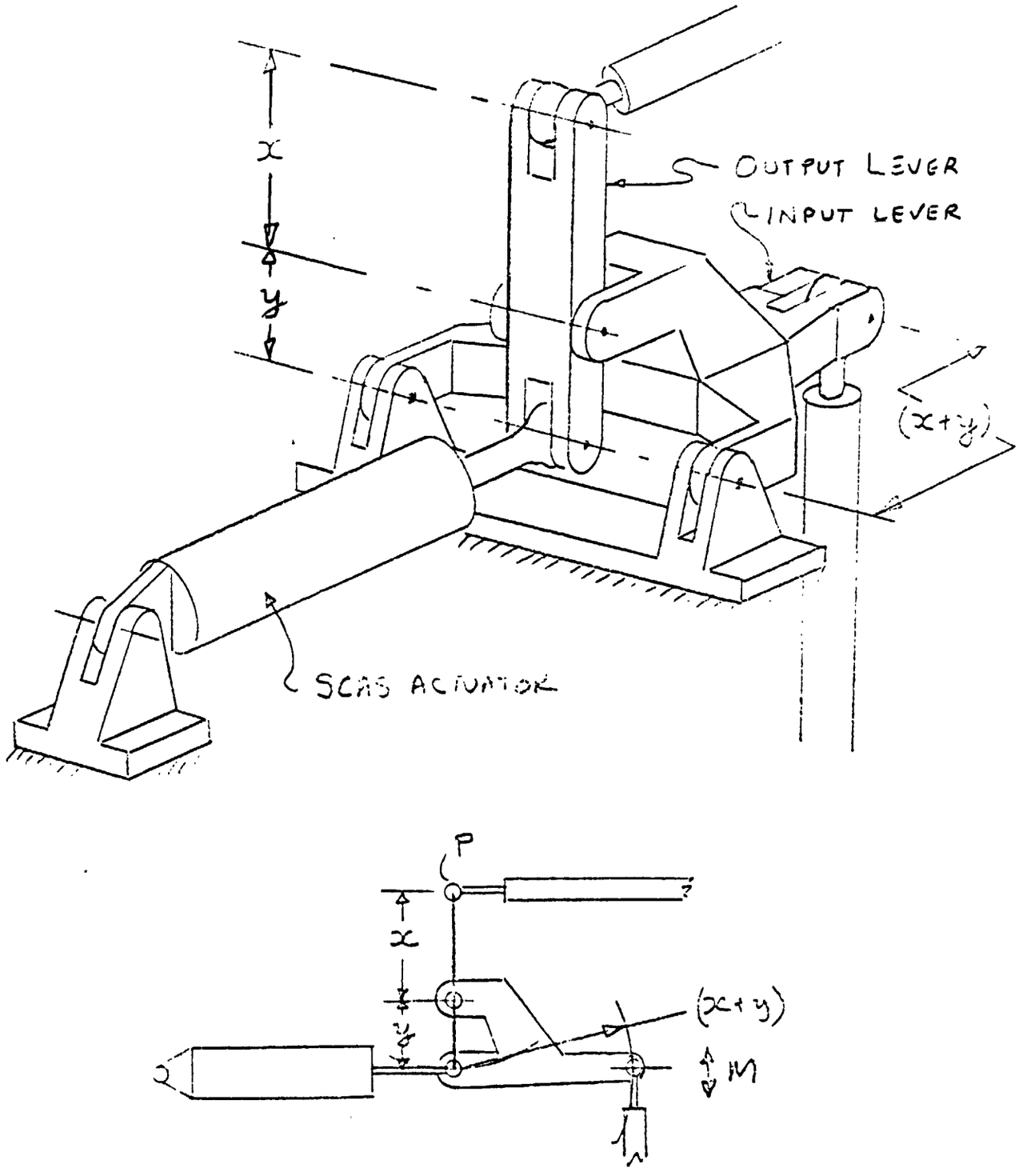

Figure 17 SCAS LINKAGE ARRANGEMENT

In order to use the same actuators, which have a stroke of ±0.085m (±0.336 in.), the same control geometry and the push-pull rod movements that are presently used in the XV-15 airplane, it is necessary to change the ratio of x to y without changing (x + y). Physically, this involves bringing the pivot points closer together and is limited by the minimum distance which can be attained between bearings when they are mounted on the same lever. With this restriction as a criteria, two linkage modifications were considered: One used the present bearings at minimum center distance; the second replaced the present ball type bearings with smaller diameter plain type Faflon bearings used at minimum center distance. Details of this proposal revision are contained in Ref. 3 and 4.

The two linkage modifications considered result in the maximum change which can be made to the SCAS authority while retaining the existing linkage geometry. If greater authority than that indicated is required, it would be necessary to either increase (x + y) (which might entail problems in changing the routes of push-pull rods through frame structure) or change the simple type of output lever to a more elaborate, forked type which would permit bearing diameters to overlap. This is not an attractive concept, however.

The combined effect of eliminating the electrical limit add modifying the SCAS linkage can increase the authority to external commands a substantial amount in each of the three axes. The net increases are listed in Table 5 for the two conditions discussed and in combination with removal of the electrical limit.

A preliminary estimate of the cost required to modify the SCAS putput linkages is summarized in Table 6. The estimate contains parts cost and the professional and technical labor for the design, fabrication, installation and checkout of the modified linkage system. Both man hours and labor dollars are included in the table. The effort is the same for either mechanical modification hence the estimate is valid for both of the configurations discussed.

TABLE 5

RESEARCH AUGMENTATION SYSTEM AUTHORITY

LIMIT MODIFICATION EFFECTS

	Existing System	Condition 1	Condition 2	Condition 3
Longitudinal	±0.0127 (±0.5)	±0.0254 (±1.0)	±0.033 (±1.728)	±0.073 (±2.88)
Lateral	±0.02 (±0.77)	±0.039 (±1.54)	±0.069 (±2.72)	±0.107 (±4.22)
Directional	±0.0102 (±0.4)	±0.020 (±0.8)	±0.023 (±0.91)	±0.039 (±1.54)

The above figures indicate the autopilot signal command authority in equivalent meters (in.)

Cond. 1 - after removal of electrical limit only.

Cond. 2 - after removal of electrical limit and linkage modification using existing bearing.

Cond. 3 - after removal of electrical limit and linkage modification using Faflon bearings.

TABLE 6

COST ESTIMATE FOR SCAS LINKAGE MODIFICATION

	Man Hours Required				Dollars
	Pitch Axis	Roll Axis	Yaw Axis	Total	
Design					
Professional	60	60	60	180	6300
Technical	60	60	60	180	3600
Fabrication					
Professional	20	20	20	60	2100
Technical	180	160	160	500	10000
Installation and Checkout					
Professional	20	51	15	50	1750
Technical	80	60	60	200	4000
Parts	-	-	-	-	250
Total					28000

2.4 Implications of FCS Lost Motion

The existence of excessive lost motion in the XV-15 flight control system can result in poor system performance or possible instabilities when used as a closed loop augmentation system. An XV-15 linkage control study was performed by Systems Technology Inc. (STI) to determine the impact of these nonlinearities on the basic aircraft flight control system. The amount of hysteresis, deadband, friction, etc. was predicted using the BHC development specifications, BHC drawings and Calspan reports. From this analysis STI concluded a possible lack of precise control during hover and a tendency toward lateral PIO (Reference 5).

The XV-15 FFS and SCAS servo actuators control the surfaces through various linkages, belcranks and mixing boxes which all contribute to these nonlinearities. This mechanical control system configuration is similar to the original variable stability system that was installed in the X-22A during the early phase of its development program and found to be unacceptable for variable stability research. When confronted with this problem on the X-22A it was necessary to install a feedforward system to eliminate the effect of the lost motion on the closed loop system performance. The output of the feedforward actuators is summed with the output of the control linkage at the input to the main surface boost servos. Their motion is gain scheduled with flight condition, duct angle, etc. to allow precise control. Their sole function is to provide an incremental input to the boost to compensate for the motion lost in the linkage system. The authority of the feedforward actuators is limited to prevent an unsafe condition in the event of failure.

The feedforward system used in the X-22A was developed in a series of simulator studies (References 6, 7, and 8) to determine:

- The amount of lost motion that could be tolerated.
- The gain schedule required for each axis.
- If the feedforward system made the system acceptable.

Preliminary indications are that the amount of lost motion predicted by STI could make the closed loop performance unacceptable as an augmentation system for flying qualities research. The actual lost motion will not be known until data is obtained from the aircraft, consequently recommendations for improvement are somewhat subjective. A study should be made, using the STI predictions as a base, to determine the level of improvement that can be achieved with various configurations. The feedforward technique used in the X-22A can be evaluated. If adequate compensation for the lost motion in the existing linkage system can not be achieved a fly-by-wire system with a mechanical back up should be considered. The fly-by-wire actuators would be located at the control surfaces similar to the feedforward actuators, bypassing the linkage nonlinearities. The FBW actuators authority, however, would not have to be limited as in the feedforward system due to the mechanical back-up. A FBW system would eliminate the SCAS modifications required for research augmentation discussed in Section 2.3 since all augmentation could be performed through the FBW computer and the associated full authority actuators.

The introduction of a FBW system would also have impact on the suggested force feel system modification (Configuration 4) presented in Section 2.2. A separate research force feel system would still be required, however modifications to the basic feel system would be eliminated. In a fly-by-wire mode, the basic feel system would be disengaged and control surface motion would be reflected at the safety pilot's controls through the mechanical back up system.

A cost estimate for flight control system modifications was not determined because of the uncertainty in the amount of lost motion of each control linkage. A realistic cost estimate can only be made after the amount of lost motion in each control linkage has been measured, and the effect on system performance assessed. Since the extent of modifications could vary from relatively simple mechanical improvements to the addition of a FBW system, it is not feasible to accurately predict the level of required system modifications at this time.

3. XV-15 V/STOLAND SYSTEM EVALUATION

The basic terms of this evaluation task is to examine the capability of the V/STOLAND system for specific application towards flying qualities and flight control research.

The primary documents used for this evaluation, were the XV-15 V/STOLAND Specification, Reference 9, and the V/STOLAND Tilt Rotor Interface Document, Reference 10, supplied by USAAMRDL and the NASA XV-15 V/STOLAND Project Office. Additional information was obtained from the UH1-H V/STOLAND documentation, and sensor manufacturers' technical specifications.

The subtasks of this evaluation were directed toward the examination of the adequacy of the sensors (Section 3.1), the 1819B computers (Section 3.2), recording system (Section 3.3), and the display system (Section 3.4) for flying qualities research. Safety-of-flight aspects are discussed in Section 3.5. Additional detailed information on the above subjects is documented in Reference 11.

3.1 Sensor System

The V/STOLAND system incorporates or interfaces with sensors that measure the aircraft motion, control deflections, air data and NAVAID information. These sensors consist of attitude and heading gyros, rate gyros, linear accelerometers, air data (pitot pressure, static pressure, temperature and J-TEC true airspeed), angle of attack and sideslip. Sensors which measure pilot forces, pilot cockpit control positions, flap, conversion angle, and SCAS motions are interfaced to the V/STOLAND system. In addition, information from NAVAIDS (inertial navigation system, TACAN, DME, ILS, radar altitude, Doppler radar and microwave landing system) is supplied to the V/STOLAND system. A detailed analysis of the characteristics and suitability of each sensor was made and is presented in Reference 11. Specific sensor inadequacies and limitations are summarized in this section.

Information was unavailable to evaluate in detail sensors or NAVAIDS for suitability to provide adequate information for the research mode. Those sensors or NAVAIDS are:

- Doppler radar
- Rate gyros
- Angle of attack sensor
- Angle of sideslip sensor
- Microwave landing system

In general, the sensors are suitable to provide the range, resolution, accuracy and dynamics response required for the intended research application. A major deficiency however, is the lack of a sensor or sensors with the capability to measure the longitudinal, lateral and vertical components of airspeed at or near hover. The V/STOLAND system incorporates a J-TEC true airspeed sensor. As installed, the device measures only the forward component of airspeed. The sensor counts vortices to determine airspeed. Rotor down-

wash effects, flow recirculation and other disturbed air flow patterns around the aircraft could appear to the sensor as vortices and be directly counted. This device, therefore, could be extremely position sensitive and may require extensive testing to obtain a suitable location especially for those research applications that require velocity feedback signals for augmentation.

Other inadequacies and limitations of the XV-15 V/STOLAND sensors for this research application are the following:

- Surface control motions are not directly measured as part of the V/STOLAND system. This information is required for research applications.
- Lead variables such as $\dot{u}$, $\dot{v}$, $\dot{w}$, $\dot{p}$, $\dot{q}$ and $\dot{r}$ which may be required in the control law mechanization and for recording/analysis are not provided in the present V/STOLAND hardware. All signals excepting $\dot{V}$ and $\dot{\omega}$ could be synthesized using software. Additional sensors would be required to obtain $\dot{V}$ and $\dot{\omega}$.
- The ability to provide gust and turbulence measurements for this research application is uncertain. Specific characteristics of the angle of attack and sideslip sensors were unavailable to determine their capability for gust measurements at moderate to high airspeeds. At low airspeeds, lateral and vertical components of airspeed are not measured.

3.2 V/STOLAND Computers

The V/STOLAND system incorporates two general purpose 1819B digital computers. One computer is designated as the basic computer while the other is designated as the research computer. In the present V/STOLAND mechanization, all data is processed through the basic computer for flight control, display, recording and safety of flight monitoring. The computation link represented by the input/output architecture and basic computer is assumed to be satisfactory for the V/STOLAND role. The research computer primarily performs the preflight diagnostics for the V/STOLAND system. In the research role however, the two computers are configured to operate in a serial fashion between the pilot's control inputs, response variables, servo and display commands and recording system. The research computer does not directly interact with the input/output equipment. All research computer data is processed through the basic computer which results in processing lags which may be unacceptable for specific handling qualities and flight control system research. Thus, in the research role where minimization of time lag and phase shift is of paramount importance, the existing structure produces a significant time lag.*

*Prior to publication of this final report, changes have been incorporated so that the system will operate at a 25 ms cycle time in the research mode. To stay within the 25 ms cycle time, research computation is limited to 9 ms. If longer research computations are required, the extended cycle time of 50 ms must be used.

The major inadequacies and limitations of the V/STOLAND computers in the research mode are the following:

- Excessive overall system time lag which consists of the sampling process and transport lags from input and sensor data to servo and display commands.

- Memory and computation time of the research computer will be required for: the preflight diagnostics (approximately 4000 words) research executive routine (approximately 300 words), I^2S interface and input/output interface. This allows approximately 12,000 words for the research load. If additional capacity is required, the preflight diagnostics can be overwritten, but this does not allow the new program to be preflighted.

3.2.1 Input/Output

The "basic" 1819B computer has eight I/O channels numbered 0 through 7. Not all channels are specifically used for V/STOLAND. Those channels pertient to the operation of the V/STOLAND system are listed in Table 7 with an I/O timing diagram depicted in Figure 18. All I/O's are referenced with respect to the basic computer. The cyle time is divided into two, twenty-five millisecond periods, an odd and even period as shown in Figure 18.

The I/O arrangement of the V/STOLAND system introduces two time lags on the data processed by the computers. One source of lag is due to the sampling/desampling process. The second lag is a transport delay introduced on the data measured from the onset of the sampling process to the time computed data is transmitted as an update to the servo command.

In the basic V/STOLAND mode the sensor data processed by the basic computer that is used to generate servo commands is sampled every fifty milliseconds and has a total servo command transport lag of twenty-one milliseconds. In the research mode of operation, the sensor data is sampled every twenty-five milliseconds, however, the servo command transport lag is approximately forty milliseconds. In the V/STOLAND mode of operation, the ratio of transport lag to the sampling interval is 0.42, while in the research mode this ratio is increased to approximately 1.6 with the present system structure.*

*Prior to publication of this final report, changes have been incorporated so that the system will operate at a 25 ms cycle time in the research mode. To stay within the 25 ms cycle time, research computation is limited to 9 ms. If longer research computations are required, the extended cycle time of 50 ms must be used.

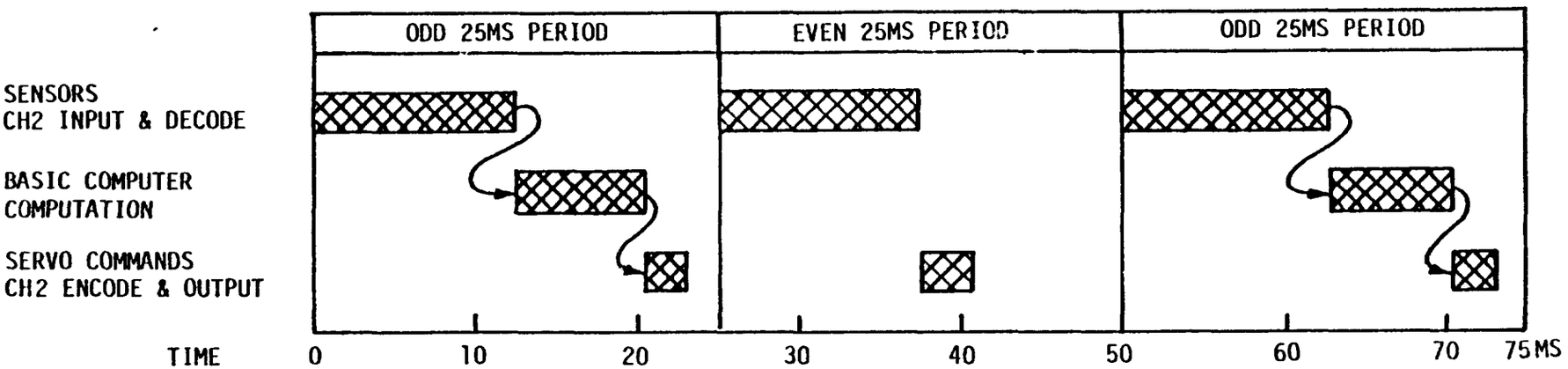

(a) BASIC COMPUTER MODE

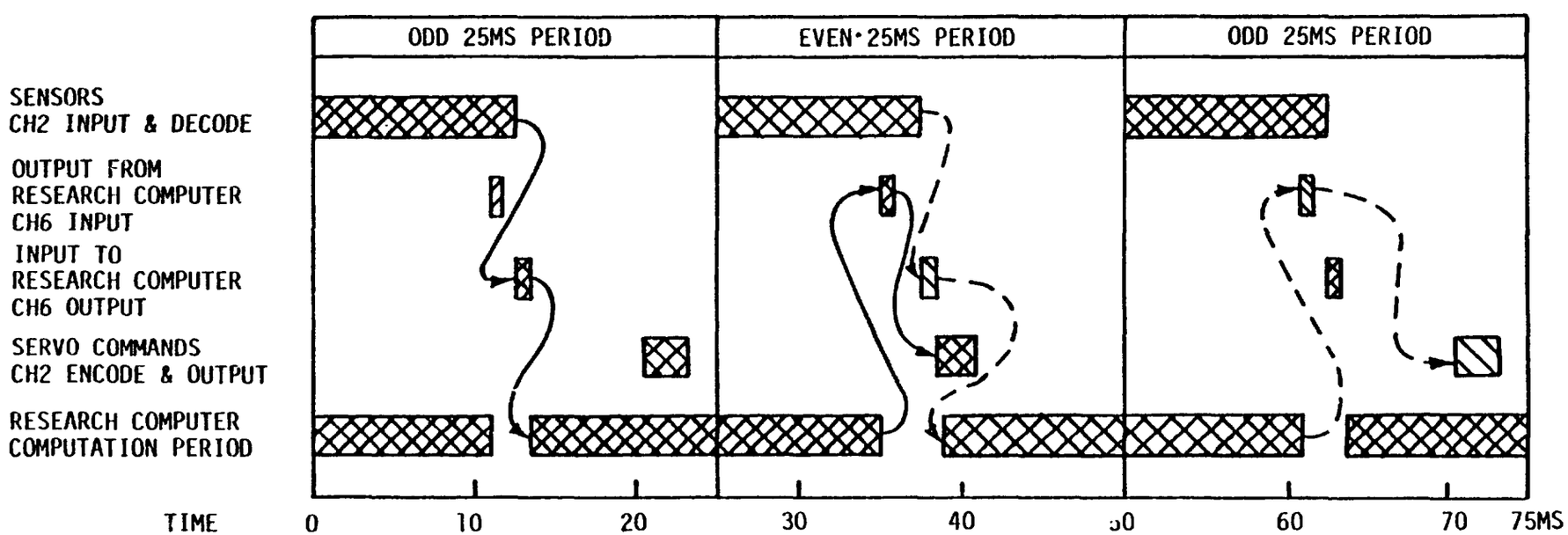

(b) RESEARCH COMPUTER MODE

Figure 18 V/STOLAND SENSOR TO SERVO COMMAND TIMING DIAGRAM

A study performed by Montgomery of NASA Langley Research Center (Reference 12), which considered the effect of sampling time and transport lags on a closed loop digital flight control system indicates that a system instability results when the transport lag exceeds one-half the sampling time. Although this study was performed using a specific control law and may not be directly applicable to the V/STOLAND system, it does indicate a potential problem. Further study is necessary to determine if this problem exists in the XV-15 V/STOLAND system when operated in the research mode.

Individual I/O deficiencies for Channels 1, 2, 6 and 7 are discussed in the following paragraphs.

Channel 1

The asynchronous nature of the input interface results in a time skew ambiguity of the sensor data. The random sampling of these signals inhibits the accuracy of data analysis. The data analysis ambiguity could be ameliorated by encoding a portion of the time code or other timing information along with each data word.

Channel 2

The basic interface arrangement and computation cycle creates transport lags. A significant lag is created by the conversion process from analog to digital and an additional lag from digital to analog between the sensor inputs and the servo command outputs. The total transport lag is almost doubled when the research computer is involved in computations. The transport lag can be decreased by a hardware modification (e.g. restructuring the I/O to provide a faster I/O data transfer utilizing multiple analog to digital converters). In addition, it is possible to use software techniques to compensate for transport lag (e.g. Appendix A).

Channel 6

A primary deficincy of the V/STOLAND system for research application is the significant transport lag Introduced by the I/O timing sequence and the allocated computation time of the research computer. A rearrangement of the research and basic computer I/O timing sequence and the research computer computation time period could be employed to reduce the transport lag from approximately 40 ms to 21 ms. The effect of this reduction should be evaluated.

Channel 7

Various time skews are induced in the recorded data. Specific details are discussed in Section 3.3.

TABLE 7

V/STOLAND I/O CHANNELS

CHANNEL NUMBER	DATA	DATA FORMAT	DATA ADAPTER SAMPLING RATE
I Input	NAVAIDS, Time Code INS, Static Pressure	36 bit serial digital	20/sec
I Output	Mode Select Panel	36 bit serial digital	10/sec, 20/sec
2 Input	Sensors	Analog, Discretes	40/sec
2 Output	Servos, Instruments	Analog and discrete	40/sec
4 Input/Output	Gnd. Simulation Computer		-----
5 (Input to Res. Computer)	I^2S	Digital	40/sec
5 Output	Multi-Function Display	36 bit serial digital	20,3,1/sec
6 Input	Research Computer	18 bit parallel "	40/sec
7 Output	DDAS (Recording System)	16 bit parallel	20/sec

3.3 Recording System

Data analysis for both the V/STOLAND and research mode requires an accurate recording system. V/STOLAND data for recording is processed by the computers and transmitted through channel 7 of the basic computer to the recording system. The input/output structure of the computers introduces time delays to all recorded data processed through the computer. Of all the lags discussed in this section the most insidious are those of a random nature. Unless known they cannot be accounted for or calibrated out of the data. It is mandatory that these random lags be eliminated if meaningful flying qualities analysis is to be performed using the recorded data. In addition, the sampling process and input/output structure introduce a fixed lag. This known lag is different for each data word, but can be compensated for in processing.

A deficiency imposed by the V/STOLAND system and the digital data acquisition system are the random and fixed lags which are described in the following subsection and diagrammed on Figure 19.*

3.3.1 Random Lags

- Asynchronous interrupt from the Digital Data Acquisition System (DDAS). Responsibility for this lag is attributed to permitting the DDAS to request data independent of the computer timing. Synchronizing both the computer timing interval and the DDAS clock could eliminate this delay.

  Data processed through 1/O channel 1 (NAVAIDS) is received asynchronously. All channel 1 data is not received every 50 milliseconds. Generally this is slowly changing data as used in the V/STOLAND computations. However, some velocity information from the Inertial Navigation System is processed through this channel. One possible solution to eliminate the time ambiguity would be to encode timing information with each word received from channel 1.

- Software Lags

  Data is encoded for recording in channel 7 every 50 milliseconds (in the odd time period) as shown in Figure 2. Data output of the research computer is available in every odd and even 25 millisecond period. It is not clear from the V/STOLAND recording system specification whether odd or even time period research computer output data is recorded. Also it is not clear whether it is possible to record a combination of odd and even data. If the software allows the recording of a combination of odd and even data, random lags will occur.

*Prior to publication of this final report, changes have been made so that DDAS recording will be achieved thru use of a double buffer. Thus, recording will be at 40 samples/sec. with no greater than a 25 milliseconds deterministic skew. The random skew will be at most a few milliseconds.

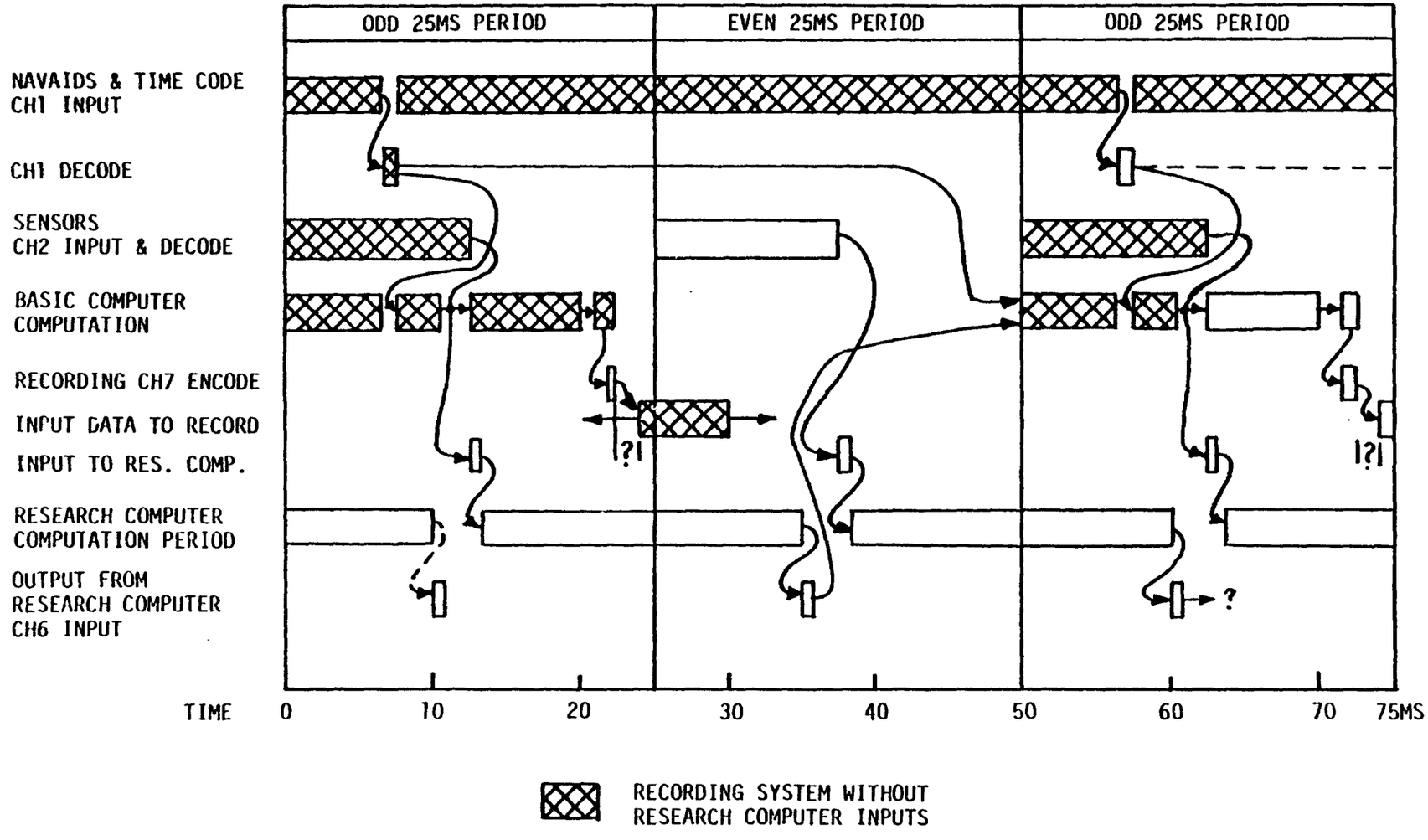

Figure 19 V/STOLAND RECORDING SYSTEM - TIMING DIAGRAM

3.3.2 Fixed Lags

For data analysis the fixed time delays become cumbersome and awkward to accommodate. Time correlation is required not only between each data word processed through the V/STOLAND computer but also between data recorded external to the V/STOLAND system. It is not specified in the V/STOLAND Technical Specification, Reference 9, that all control surface motions will be processed for recording through the V/STOLAND system. The XV-15 V/STOLAND project office has indicated that some surface motion will not be recorded through the V/STOLAND computer but will be recorded directly. Thus time correlation between all data recorded by the DDAS is difficult. A real time, post flight, quick look capability will be severely hampered by these limitations.

3.4 Display System

The primary elements of the XV-15 display system are the electromechanical attitude director and horizontal situation indicators and the programmable electronic multifunction display (MFD) unit. The attitude director indicator is situated on the instrument panel directly in front of the evaluation indicator with the horizontal situation indicator mounted directly below. The multifunction display is located about six inches to the right of these instruments. At present, the multifunction display is programmed to present navigation information (aircraft position and orientation). The attitude director indicator has three flight director steering elements, a vertical bar, horizontal bar and vertical tab which can be utilized to provide lateral and longitudinal stick and collective lever control commands respectively.

A variety of flying qualities experiments can be performed without changing the present display system configuration or format. For simple tasks, such as constant speed or decelerating IFR approaches with constant nacelle angle, evaluations of conventional electromechanical flight director presentation can be conducted with the present system by modifying the control laws used to drive the three steering elements. For more complex tasks, such as decelerating landing approaches with varying nacelle angle, the flare or decision height indicators located on the attitude director indicator could be used as a fourth cue to explore the possibility of supplying transition commands.

Beyond some minimum level of task complexity it is likely that the attitude director indicator will be incapable of providing sufficient information to the pilot. For example, in an IFR precision hover task described in Reference 13, an integrated display format combining status information and command cues was found to be necessary. In the XV-15, this requirement for increased display sophistication could easily be satisfied by reprogramming the multifunction display to serve as the flight director indicator. Since in this mode, the MFD will be the primary display element, its location should be evaluated to determine if it is ergonomically acceptable to pilots.

Some tasks envisioned for the XV-15, specifically oriented to Army missions, may require additional displays or modified MFD formats. For example, low altitude, nap of the earth maneuvering tasks may require the addition of either a head-up display or a head-down display with a raster scan format that mixes flight director symbology with a TV image of the outside environment. Mechanical interface constraints dictated by the shape of the windshield, ejection seat envelope and visual accessibility to the evaluation pilot must be considered when contemplating the installation of a head-up display.

3.5 Safety of Flight

Safety of flight requires additional considerations when the aircraft is operated in the research mode. In general, increased authority and high bandwidth control servos are required in this mode. Thus, a control system malfunction may allow an unsafe flight condition to develop very rapidly. This imposes a stringent requirement on the failure detection and automatic V/STOLAND disengagement system. The V/STOLAND disengagement system is oriented towards a low authority system for the navigation and guidance role. Delays are designed into the system to prevent nuisance trips. For use in the research role the monitoring system design philosophy must be reviewed. Calspan's experience with operating variable stability aircraft established a criteria that it is necessary to detect a fault within 8 to 10 milliseconds and disengage the control servos within 40 milliseconds.

A data valid is generated in hardware or software for all V/STOLAND control servos and critical V/STOLAND system elements. The data valids are monitored by a diagnostic software routine located within the basic computer. Detection of a failure is evidenced by absence of a data valid. The diagnostic routine prescribes the specific resultant action dependent upon the weighted criticality of the failed element to the operation of the V/STOLAND system. Any mode, dependent upon the failed element, will result in the disengagement of that mode and a "fail" message will be displayed on the Flight Mode Annunciator panel. The monitor, and diagnostic software is executed once every 50 millisecond compute cycle. A hardware monitor failure indication such as a failure of a servo may be intentionally delayed several compute cycles before an appropriate action is initiated. The UH-1 V/STOLAND failure mode analysis (reference 14) indicates that a failure of a series servo with a servo amplifier hardover will result in the actuators being driven to their full authority position because the proposed monitoring scheme could require as long as 2 seconds to detect, disconnect the V/STOLAND system and warn the pilot of the failure.*

*The latest failure monitoring XV-15 document (Sperry Flight Systems Report No. 5720-0888-P106) indicates a maximum of one second for a non-critical failure and from 0.2 to 0.5 seconds for more critical failure. This information was received prior to the publication of this report.

The existing XV-15 feel force system includes a hardware monitor and disconnect system which disengages the feel system automatically when a large input is commanded. The SCAS system only detects a tracking error between the two SCAS channels but does not automatically disengage. In the case of the yaw axis, an error is detected between the SCAS actuator and a yaw model.

A separate hardware monitor and disconnect system completely independent of the 1819'B' computer control should be included for all servos and aircraft states that could cause a dangerous condition to develop if not promptly detected and the system disengaged. This isolates the failure detection and disengagement system from insidious computer malfunctions.

Another aspect that must be considered for safe flight operation is the extent of XV-15 flight test qualification prior to the beginning of flying qualities evaluations. Only two vehicles are scheduled for construction; therefore, insufficient data may be accumulated pertaining to the overall integrity and reliability of systems and subsystems of the XV-15 basic airframe. Thus, close monitoring of structural and subsystem operating limitations throughout the aircraft's role as a flying qualities research vehicle may be necessary. It is anticipated that additional instrumentation and possibly in-flight computations will be required to fulfill this monitoring task. In addition, the in-flight monitoring of the operational limits of the vehicle should not impose additional burdens upon the pilots nor detract from the research experiment. Either an airborne computer or a telemetry system could be used to perform this monitoring task. The telemetry system has other advantages besides safety of flight monitoring. Progress of the flight test can be monitored. This allows in-flight data analysis which introduces the capability to modify the flight plan. In addition a telemetry link permits ground installation of the monitoring computer and recording system. Ground recording equipment and computers are less costly than their airborne counterparts and do not effect aircraft payload.

4. ANALYSIS OF XV-15 FLYING QUALITIES RESEARCH CAPABILITY

4.1 Synopsis

The purpose of this section is to document the results of the final phase of this study program, that is, the evaluation of the flying qualities research capabilities and limitations of the XV-15 when integrated with the V/STOLAND avionics system.

Fundamental to in-flight investigations of flying qualities is the capability to vary the research aircraft's stability and control characteristics over a wide range. Further, because many of the characteristics of the man-machine interface are indistinguishable to the pilot from inherent vehicle dynamics, it is also desirable that the parameters of the force feel system (frequency, damping, gradient, etc.) can be independently varied. The goal of this program was to determine a scheme for integration of V/STOLAND with the force feel system, the flight control system and sensors of the XV-15 to realize these capabilities in the most cost-effective manner.

Physical constraints, imposed by the configuration of the basic aircraft and its associated systems can limit its research capability and flexibility, especially when the aircraft was not designed from the start for flying qualities research. The initial phases of this study program were directed to an examination of the key elements which will comprise the XV-15 research aircraft. The results and recommendations arising from these studies are documented in Sections 2 and 3 as follows:

Section 2.1 - Force Feel System
Section 2.3 - SCAS Actuator Authority Limits
Section 2.4 - Mechanical Control System Freeplay
Section 3. - V/STOLAND Computers, Recording System, XV-15 Sensors

In the final phase of the study, the limitations imposed on the flying qualities research capability of the XV-15 by the most critical of these systems and the characteristics of the basic XV-15 were examined. This evaluation was performed by

1. Proposing tentative schemes for integration of V/STOLAND with the XV-15.

2. Determining V/STOLAND computer configurations (i.e. either response feedback or model following gains) for realization of a range of vehicle dynamic characteristics.

3. Assessing limits imposed by system constraints.

Preliminary to these activities, however, it was necessary to develop equations of motion for the bare airframe XV-15. As a result of this effort, a characteristic of the XV-15 not anticipated at the initiation of the study was discovered.

It was found that the mechanization of the XV-15 rotor speed governor system is such that the dynamics of rotor angular speed are coupled with the conventional longitudinal rigid body responses of the aircraft. The characteristic frequency associated with the RPM mode is low enough that a conventional 4th order linearized model of the longitudinal dynamics of the aircraft may be inadequate. In addition, governor modulation of rotor collective pitch in response to pilot collective commands effectively determines the character of the long term rotor force and moment response. The dynamics of the rotor thrust response may limit the usefulness of the collective as an independent controller in either response feedback or model following mechanizations of research dynamic configurations.

In the following section, the interaction of the governor with the rotor angular speed degree of freedom and the rotor thrust response to collective control commands is illustrated with a restrained rotor model. In Section 4.3 , the effect of the governor on the longitudinal vehicle dynamics is illustrated by comparison to the dynamics exhibited by a conventional 4th order dynamic model. Finally, in Section 4.4 , the implications of various force-feel system configurations and SCAS actuator authority limits on XV-15 flying qualities research capability are presented.

4.2 XV-15 Governor Dynamics

In order that a systematic investigation of various V/STOLAND and flight control system integrations could be conducted, an analytical model, describing the rigid body state responses of the XV-15 to control inputs, was required. Consistent with the available data base and the scope of the program, linearized equations valid for small perturbation motions about a fixed operating point (trimmed flight) condition with constant mast angle were selected as the basis for subsequent analysis. It is recognized that for rotary wing aircraft, the variation of stability and control derivatives with airspeed and angle of attack can limit the validity of linearized models for large amplitude maneuvering. However, it was felt that cost effectiveness considerations and ease of interpretation of results justified this choice. In addition, the implementation of the linear models would be greatly facilitated since References 15 to 17 contained sets of conventional stability and control coefficients, appropriate to 4th order longitudinal and lateral directional models for the XV-15 over a wide range of operating conditions (airspeed and rotor mast angle).

During initial project meetings, attended by representatives of the Army, NASA and Calspan, the possibility of the rotor speed governor system causing coupling of the rotor RPM degree of freedom with the vehicle's conventional rigid body dynamics was discussed. After a review of the

governor implementation by Calspan it was decided to undertake a brief analysis to ascertain whether it was necessary to incorporate the RPM degree of freedom in the vehicle's equations of motion.

The XV-15 governor system regulates rotor angular speed (R.P.M.) by maintaining the power required by the rotors equal to the power output of the engines. The regulation of power required is accomplished by modulating rotor collective pitch as a function of R.P.M. error with respect to a reference speed.

Movement of the cockpit collective lever commands engine power through a lever/cam arrangement connected to the throttles and rotor collective pitch through the mechanical summing junction with the governor actuator collective input. The governor mechanization is illustrated schematically below.

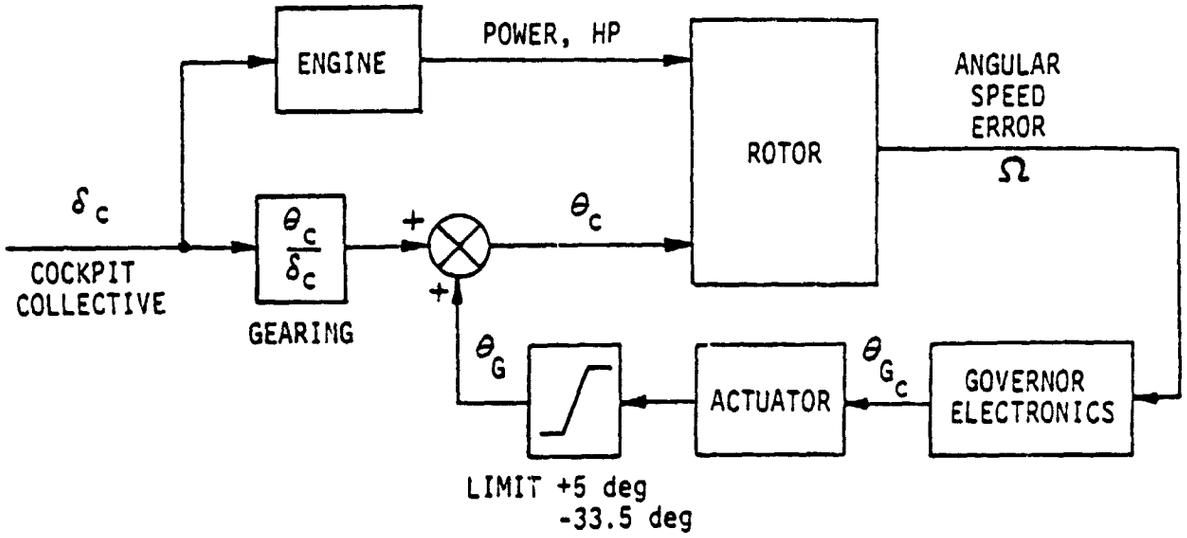

If, for simplicity, it is assumed that the rotor is restrained ($u = w = q = 0$), then the angular acceleration is a function only of collective pitch (θ_c), the angular speed perturbation (Ω), and the incremental engine torque at the rotor shaft (Q_E).

$$\dot{\Omega} = Q_\Omega \Omega + Q_{\theta_c} \theta_c + Q_E \qquad (4)$$

The governor actuator commands an actuator displacement θ_{G_c} proportional to a weighted sum of speed error and integral of speed error.

$$\theta_{G_c} = K_G \left(K_1 + \frac{1}{s} \right) \Omega , \qquad K = 0.955 \frac{\text{deg}}{\text{rad}} \tag{5}$$

For small displacements, the governor actuator is essentially a 9.5 radian first order filter with unity gain. For the purpose of this example, it will be assumed that the actuator dynamics are negligible. Thus,

$$\dot{\theta}_s = \dot{\theta}_{G_c} = K_G K_1 \dot{\Omega} + K_G \Omega \tag{6}$$

and

$$\theta_c = \left(\frac{\theta_c}{\delta_c} \right) \delta_c + \theta_G \tag{7}$$

Since horsepower developed at the rotor shaft is proportional to the product of rotor angular speed and torque, to the first order, a perturbation in horsepower is related to the incremental torque and speed error by the relationship

$$HP = \left[\frac{Q_{E_o}}{550} \Omega + \frac{\Omega_o}{550} Q_E \right] I_R \tag{8}$$

where torque is expressed in radians/second^2, I_R is the moment of inertia of the rotor system, and the subscript o denotes the initial value.

Therefore,

$$Q_E = \frac{550}{\Omega_o I_R} HP - \frac{Q_{E_o}}{\Omega_o} \Omega \tag{9}$$

If it is assumed, for the moment, that the engine can develop power instantaneously in response to power commands then

$$HP = HP_{\delta_c} \delta_c \tag{10}$$

The state equations for the system are

$$\begin{bmatrix} \dot{\Omega} \\ \dot{\theta}_G \end{bmatrix} = \begin{bmatrix} Q'_\Omega & Q_{\theta_c} \\ K_G(1 + K_1 Q'_\Omega) & K_G K_1 Q_{\theta_c} \end{bmatrix} \begin{bmatrix} \Omega \\ \theta_G \end{bmatrix} + Q'_{\delta_c} \begin{bmatrix} 1 \\ K_G K_1 \end{bmatrix} \begin{bmatrix} \delta_c \end{bmatrix} \tag{11}$$

where $$Q'_\Omega = Q_\Omega - \frac{Q_{EQ}}{\Omega_o}$$

and $$Q'_{\delta_c} = \frac{550}{\Omega_o I_R} HP_{\delta_c} + \left(\frac{\theta_c}{\delta_c}\right) Q_{\theta_c}$$

The transfer functions relating speed error and governor collective to collective command are,

$$\left.\begin{aligned} \frac{\Omega}{\delta_c} &= \frac{sQ'_{\delta_c}}{s^2 - (Q'_\Omega + K_G K_1 Q_{\theta_c})s - K_G Q_{\theta_c}} \\ \frac{\theta_G}{\delta_c} &= \frac{K_G K_1 \left(s + \frac{1}{K_1}\right)}{s^2 - (Q'_\Omega + K_G K_1 Q_{\theta_c})s - K_G Q_{\theta_c}} \end{aligned}\right\} \tag{12}$$

It can be seen from these relations that the governor/RPM dynamics are second order with a natural frequency of $\sqrt{-K_G Q_{\theta_c}}$ and damping of $-(Q'_\Omega + K_G K_1 Q_{\theta_c})$. Since the rotor torque derivatives Q'_Ω and Q_{θ_c} vary with rotor forward velocity and angle of attack, the frequency and damping of the rotor RPM mode will likewise tend to vary.

In addition, RPM damping will vary with mast angle through the linear scheduling of K_1 with β_m.

$\beta_m = 0 \quad K_1 = 0.5$ (Helicopter Mode)

$\beta_m = 90 \quad K_1 = 0$ (Airplane Mode)

Since the data base provided for this study did not include rotor torque derivatives, it was necessary to calculate the requisite derivatives to permit a quantitative analysis of the rotor RPM dynamics. The equations employed are described in Appendix B.

Utilizing these estimated derivatives, the variation in governor frequency and damping ratio as a function of airspeed for the helicopter mode ($\beta_m = 0$) is as follows:

V m/sec	(knots)	ω_n rad/sec	ζ
0	(0)	1.40	0.69
21	(40)	1.24	0.59
41	(80)	1.33	0.47

It can be seen that over this airspeed range, the rotor RPM dynamics are of relatively low frequency and less than critically damped. Further, the damping ratio tends to reduce slightly with increasing airspeed.

As would be expected with integral feedback, in the steady state the RPM error is zero. In addition, from Equations (12) and (4), it can be seen that in the steady state, the governor collective pitch change is such that the final net torque applied to the rotor is zero.

It can also be seen from Equation (12) that if the cockpit collective to engine throttle gearing and collective to rotor gain (θ_c/δ_c) are such that the torque output of the engine exactly matches the increase in torque required by the rotor, no excitation of the RPM degree of freedom or the governor will result from discrete cockpit collective lever inputs. That is,

$$Q'_{\delta_c} = 0 = \frac{550}{\Omega_o I_R} HP_{\delta_c} + \left(\frac{\theta_c}{\delta_c}\right) Q_{\theta_c} \tag{13}$$

In practice, this relationship would be difficult to satisfy at all flight conditions since variations in the rotor torque derivative Q_{θ_c} with airspeed and angle of attack would require scheduling either the collective lever to throttle gearing or (θ_c/δ_c) as functions of these variables. Even with perfect gearing, the dynamics of engine power response to power commands will generate some excitation of RPM and governor response.

4.2.1 Effect of Governor on Thrust Response

In response to a collective control command, the incremental thrust of a restrained rotor will be given by

$$T = T_\Omega \Omega + T_{\theta_c} \theta_c + T_{\theta_c} \left(\frac{\theta_c}{\delta_c}\right) \delta_c \tag{14}$$

At $t = 0$, $\Omega = \theta_0 = 0$ and the initial thrust is proportional to the quasistatic thrust derivative T_{θ_c}

$$(T)_{t=0} = T_{\theta_c}\left(\frac{\theta_c}{\delta_c}\right)\delta_c \tag{15}$$

In the steady state, the thrust is

$$(T)_{ss} = -T_{\theta_c}\frac{Q'_{\delta_c}\delta_c}{Q_{\theta_c}} + T_{\theta_c}\left(\frac{\theta_c}{\delta_c}\right)\delta_c$$

$$= -\frac{550}{\Omega_0 I_R}\frac{HP_{\delta_c}}{Q_{\theta_c}} T_{\theta_c}\delta_c \tag{16}$$

Several observations are pertinent. First, the ratio of the final response to the initial response is proportional to the ratio $HP_{\delta_c}/Q_{\theta_c}$. In order that the final thrust response be equal to the initial thrust response, the collective to throttle gearing would have to be selected such that

$$-\frac{550}{\Omega_0 I_R}\frac{HP_{\delta_c}}{Q_{\theta_c}} = \left(\frac{\theta_c}{\delta_c}\right)$$

Satisfying this condition at all flight conditions would require a programmable interconnect since Q_{θ_c} is dependent on airspeed and angle of attack.

It is also observed that regardless of the collective lever to rotor collective pitch gearing, (θ_c/δ_c), in fact even with the mechanical path broken, the long term thrust response will be given by Equation (16).

The character of the thrust transient between initial and final response and the time to reach steady state is determined primarily by the governor dynamics, provided the engine response to power commands is rapid. To illustrate the effect of engine power response dynamics, Figures 20 to 22 present time histories of the rotor responses to a step collective command for several engine power response time constants. It can be seen that after the response time of the engine has been reduced below a certain level (i.e. nearly instantaneous power response), no significant reduction in the time to steady state thrust is realized. It is also observed that the ratio of the final thrust to the initial thrust is approximately 1.7 for these initial conditions. The assumed engine power response model has the form

$$HP = HP_{\delta_c}\frac{\lambda_E}{s+\lambda_E}\delta_c \tag{17}$$

Figure 23 is a similar time history for a restrained rotor at an airspeed of 41 meters/second (80 knots) with the mast nearly vertical. The transient response is similar to the previous examples except that, in this case, the ratio of final to initial thrust is approximately 2.7.

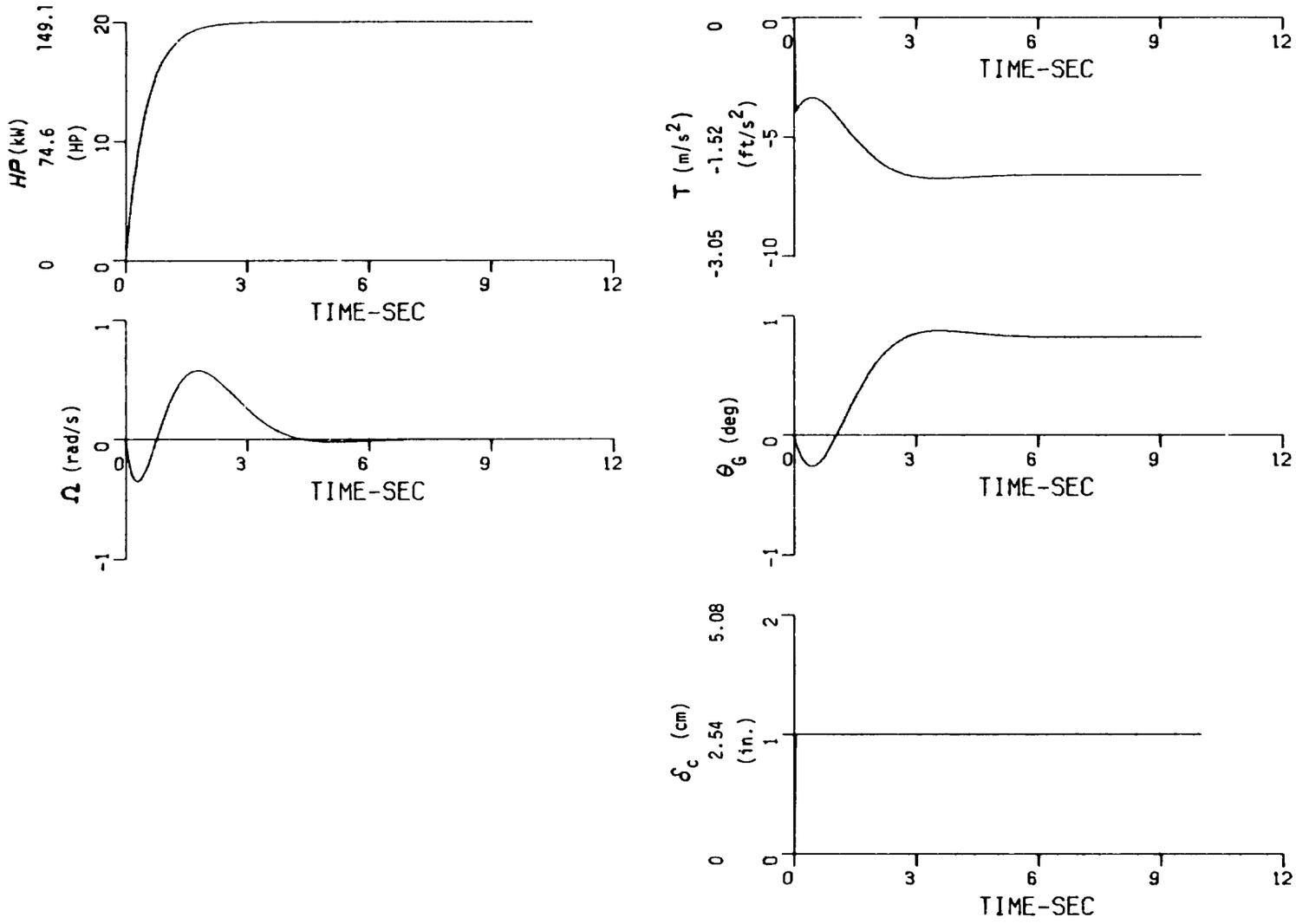

Figure 20 Rotor Response to Collective Command, Airspeed = 0, λ_E = 2 sec^{-1}

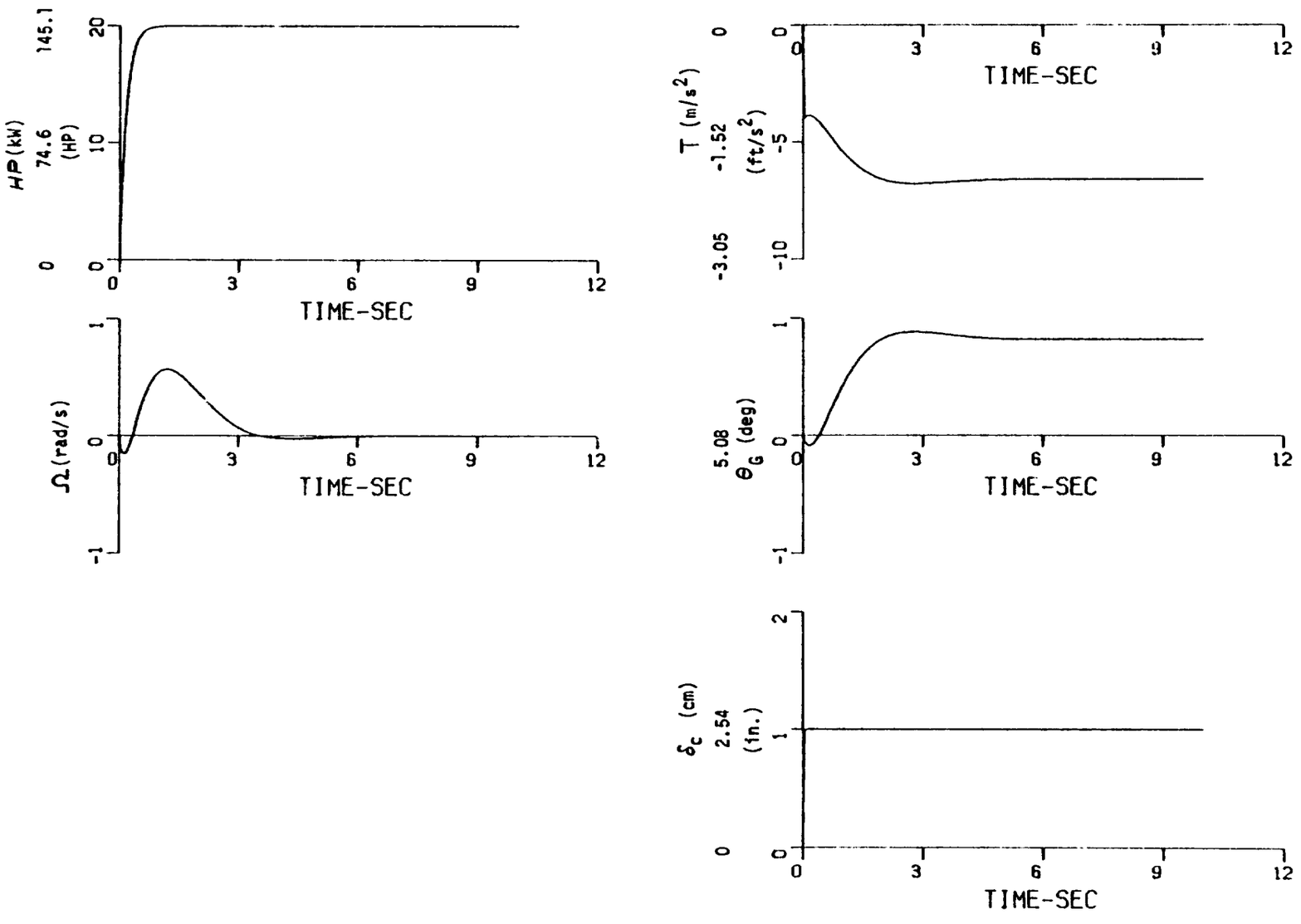

Figure 21 Rotor Response to Collective Command, Airspeed 0, λ_E = 6 sec^{-1}

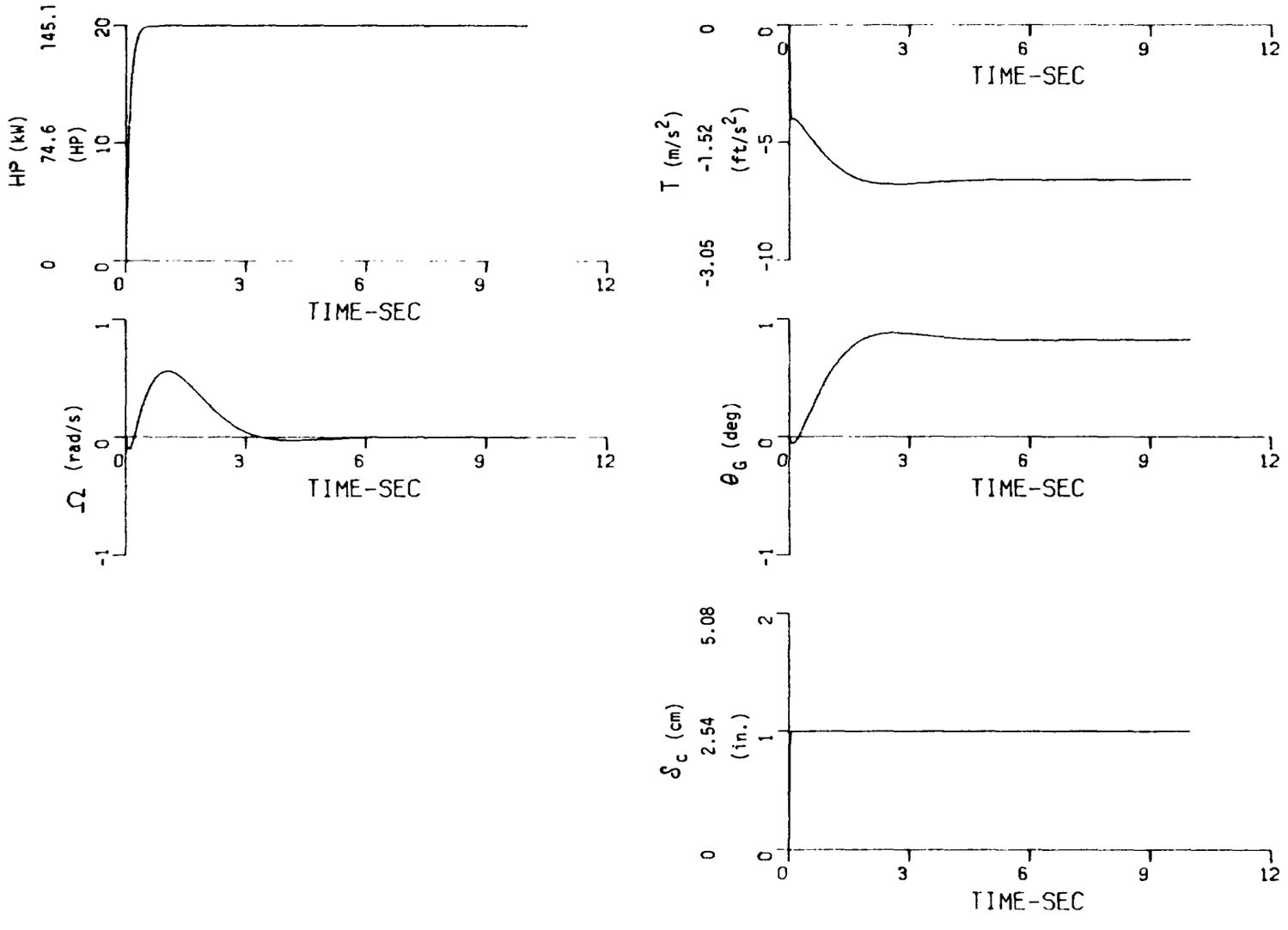

Figure 22 Rotor Response to Collective Command, Airspeed 0, $\lambda_E = 10\ sec^{-1}$

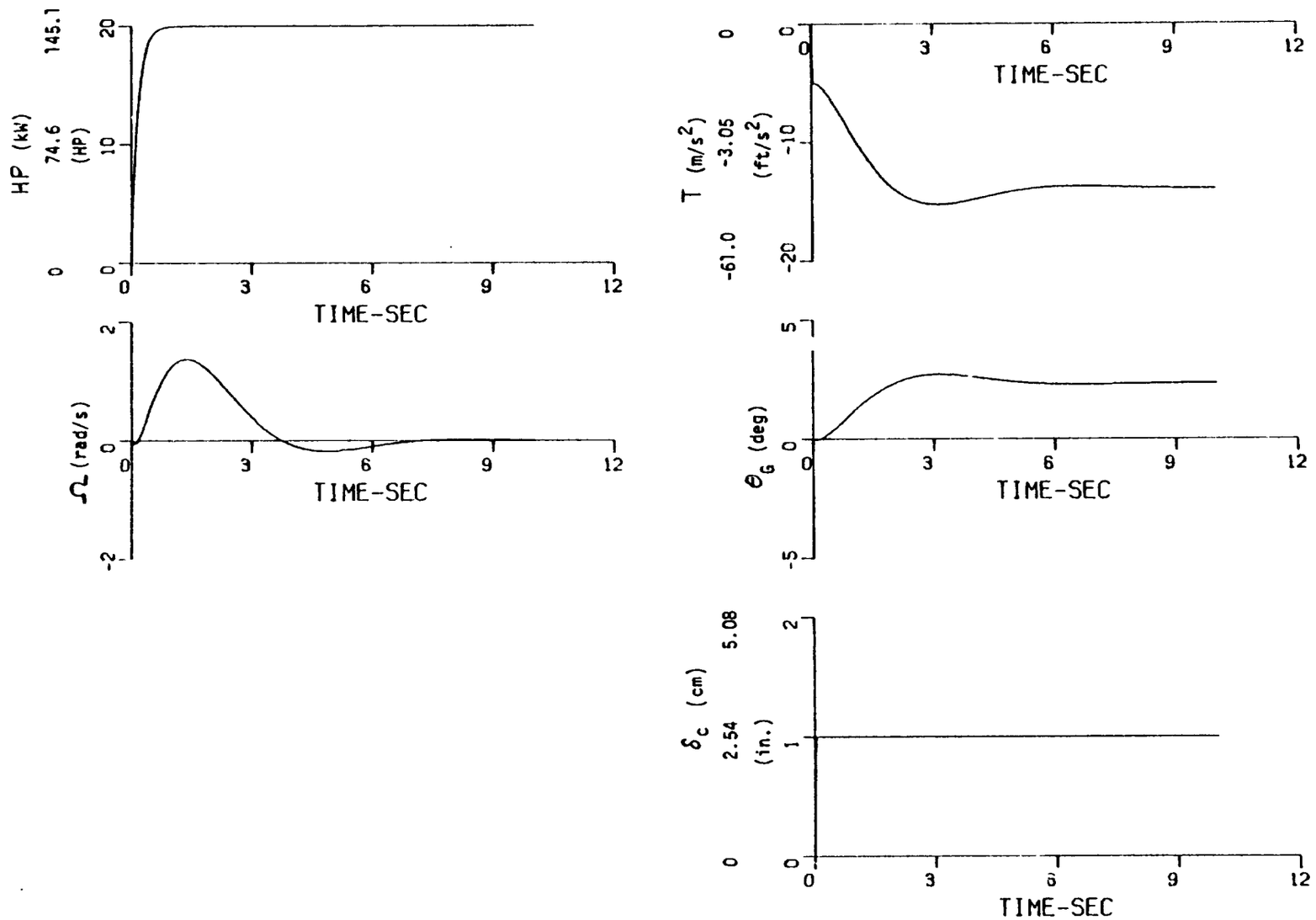

Figure 23 Rotor Response to Collective Command, Airspeed 41.2 m/s (80 knots), λ_E = 6 sec^{-1}

As a result of this analysis, it was concluded that the governor dynamics must be modelled, at least for the vehicle responses to collective commands, because the quasistatic derivative T_{δ_c} alone does not characterize the thrust transient or the steady state thrust magnitude. Further, the natural frequency of the RPM mode introduced by the governor is of the same order of magnitude as the frequencies of the rigid body modes typical of V/STOL aircraft.

In the following subsection, the interaction of the governor with the conventional rigid body dynamics of the XV-15 is examined and the implications for flight research applications are discussed.

4.3 Effect of Rotor Speed Governor on XV-15 Rigid Body Dynamics

By commanding the existing roll, yaw, and pitch SCAS actuators of the XV-15 flight control system in response to control laws programmed on the V/STOLAND computers, it will be possible to control 2 of the 3 lateral-directional but only 1 of the 3 longitudinal degrees of freedom. The inability to command rotor thrust automatically may be a serious limitation to flying qualities research applications of the XV-15 in that, without this capability, only the longitudinal characteristic roots can be varied. No control of the numerators of the pitch control transfer functions will be possible. In Section 2 , modifications to the flight control system, including the installation of a collective actuator are described which will provide thrust control capability. However, the analysis of the previous section indicates that the usefulness of the collective controller may be compromised by the dynamics of the rotor speed governor system.

For either response feedback or model following mechanizations, it is desirable that the force and moment responses to control commands exhibit little phase shift or amplitude attenuation. Realization of this characteristic requires that the natural frequencies of the controllers should be significantly higher than the bandwidth of the vehicle being simulated. Otherwise, compensation schemes may be required in the control law implementation to suppress the spurious dynamics introduced by the controller and to extend their effective bandwidth.

The analysis of a restrained rotor in the previous section indicates that the effect of the governor is to introduce a second order coupled collective pitch/RPM mode whose natural frequency is likely to be within the bandwidth of the vehicle's rigid body dynamics. Further, the rate at which rotor forces and moments are generated in response to collective control commands are effectively determined by the dynamics of the collective pitch/RPM mode.

From the standpoint of the capability to vary the dynamic characteristics of the XV-15 the significance of this collective/RPM mode is the manner in which it couples with the conventional rigid body dynamics of the vehicle. The nature of the coupling will be illustrated in this section with reference to key longitudinal transfer functions. The development of the

required longitudinal equations of motion is documented in Appendix C. As in the previous section, the governor actuator dynamics have been neglected and only the first order filtering of the RPM error signal has been modelled. Augmenting the conventional equations of motion with a first order model of the RPM degree of freedom and a first order governor model results in a 6th order controls fixed model for the longitudinal dynamics.

4.3.1 Pitch Attitude to Pitch Control Transfer Functions

Figures 24 to 26 illustrate the variation in the pitch attitude to pitch control (θ/δ_{ES}) transfer functions as airspeed is varied from 0 to 41 meters/second (0 to 80 knots) for the XV-15 in the helicopter configuration ($\beta_m = 0$). For comparison, the transfer characteristics for a conventional 4th order longitudinal model, neglecting the RPM degree of freedom are also presented. In Figure 24, it can be seen that the low frequency roots of the 6th order model assume a "classical" hovering cubic configuration and are essentially identical to those of the 4th order model. The complex poles associated with the governor are identically cancelled by a pair of zeros indicating this mode has no residue in the attitude response to pitch control in hover. This characteristic is attributable to the fact that the rotor power or torque required change with cyclic pitch ($Q_{B/S}$) is zero in hover.

At an airspeed of 80 knots, complex eigenvalues associated with the short period and phugoid modes can be identified together with an oscillatory governor/RPM mode whose frequency lies between that of the phugoid and the short period. At this flight condition, the associated complex zero pair has moved away from the governor poles, indicating that a small residue of the governor/RPM mode will be observed in the attitude response to pitch control inputs.

The residue of the RPM/governor mode in the attitude response to pitch command is a function of the derivative $Q_{B/S}$. Since $Q_{B/S}$ is sensitive to airspeed and rotor angle of attack, the separation of the RPM/governor pole-zero pair will vary with airspeed and rotor mast angle. Figures 27 and 28 illustrate the sensitivity of the residue of the RPM/governor modes at airspeeds of 80 and 120 knots for several rotor mast angles.

It is anticipated that control law mechanizations which tend to augment (i.e. increase) the basic aircraft short term or short period frequency and damping will likely tend to drive the RPM/governor mode poles toward their associated zeros thus further diminishing the residue of that mode in the pitch control responses. Conversely, deaugmenting the short term dynamics will likely tend to increase the pole zero separation and may result in large residues of this mode appearing in the responses, to the extent that the resulting vehicle dynamics become highly unconventional.

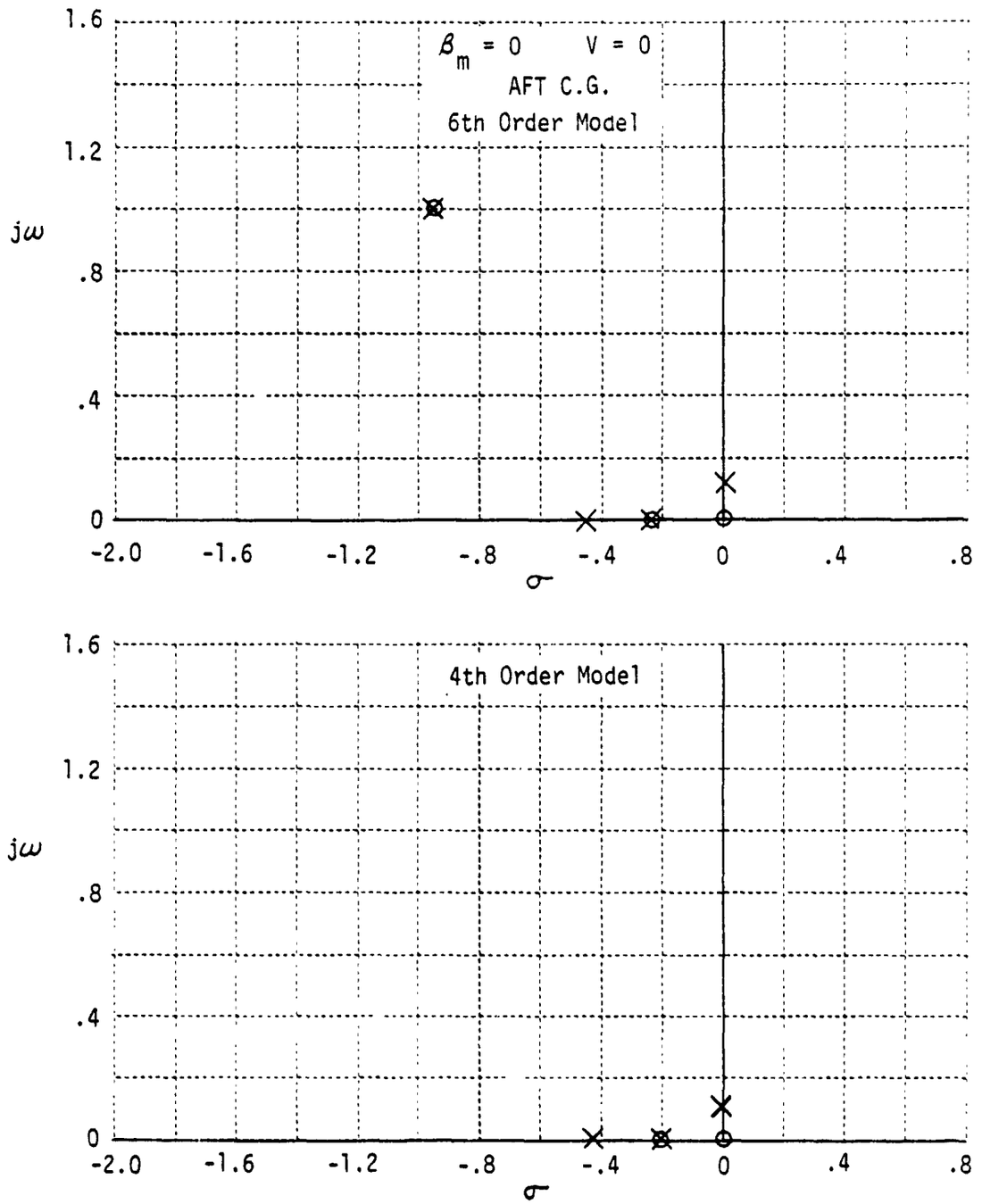

Figure 24 Pitch Attitude to Pitch Control Transfer Function - Comparison of 4th Order and 6th Order Models at 0 Velocity

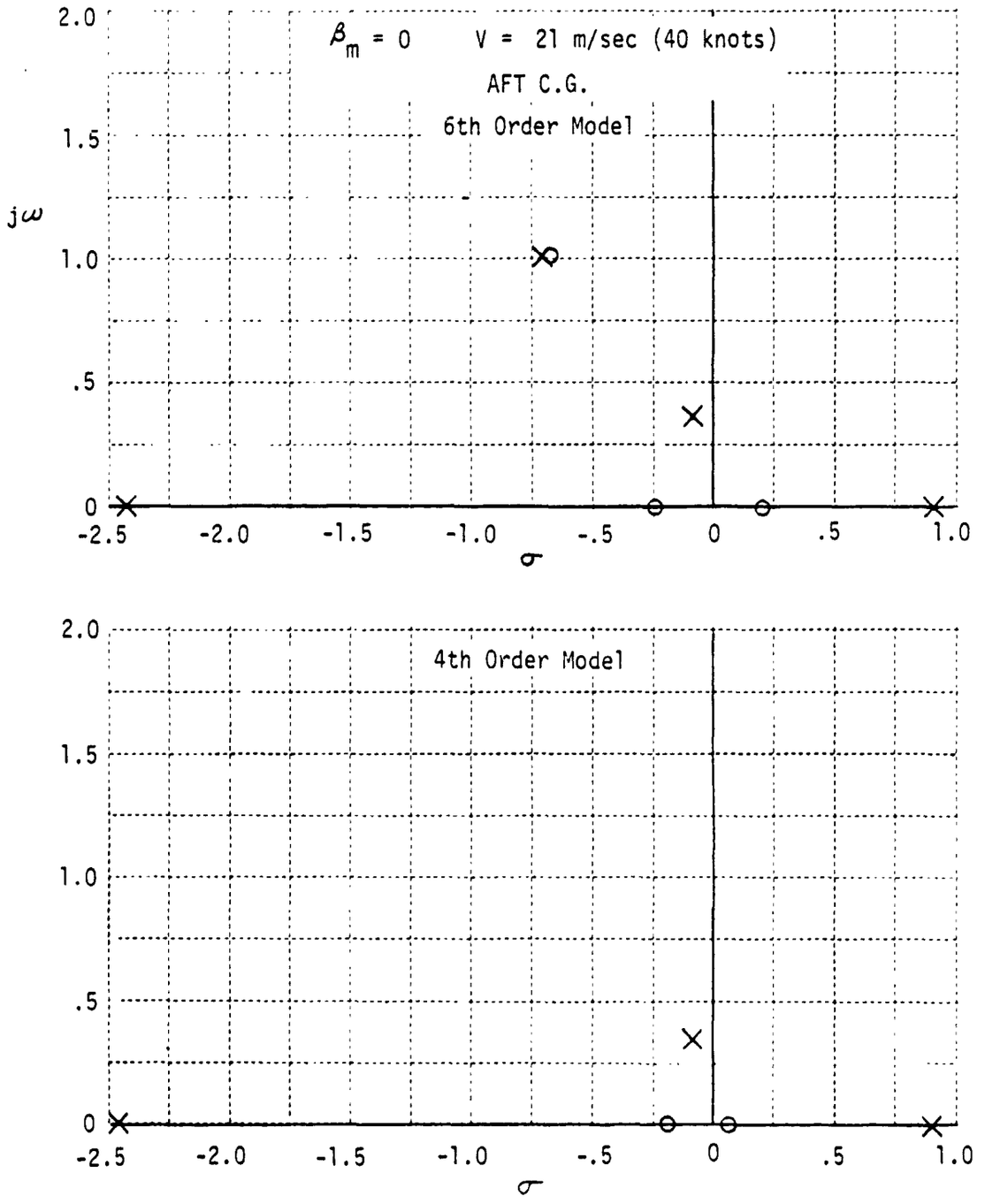

Figure 25 Pitch Attitude to Pitch Control Transfer Function - Comparison of 4th Order and 6th Order Model at 21 meters/sec (40 knots)

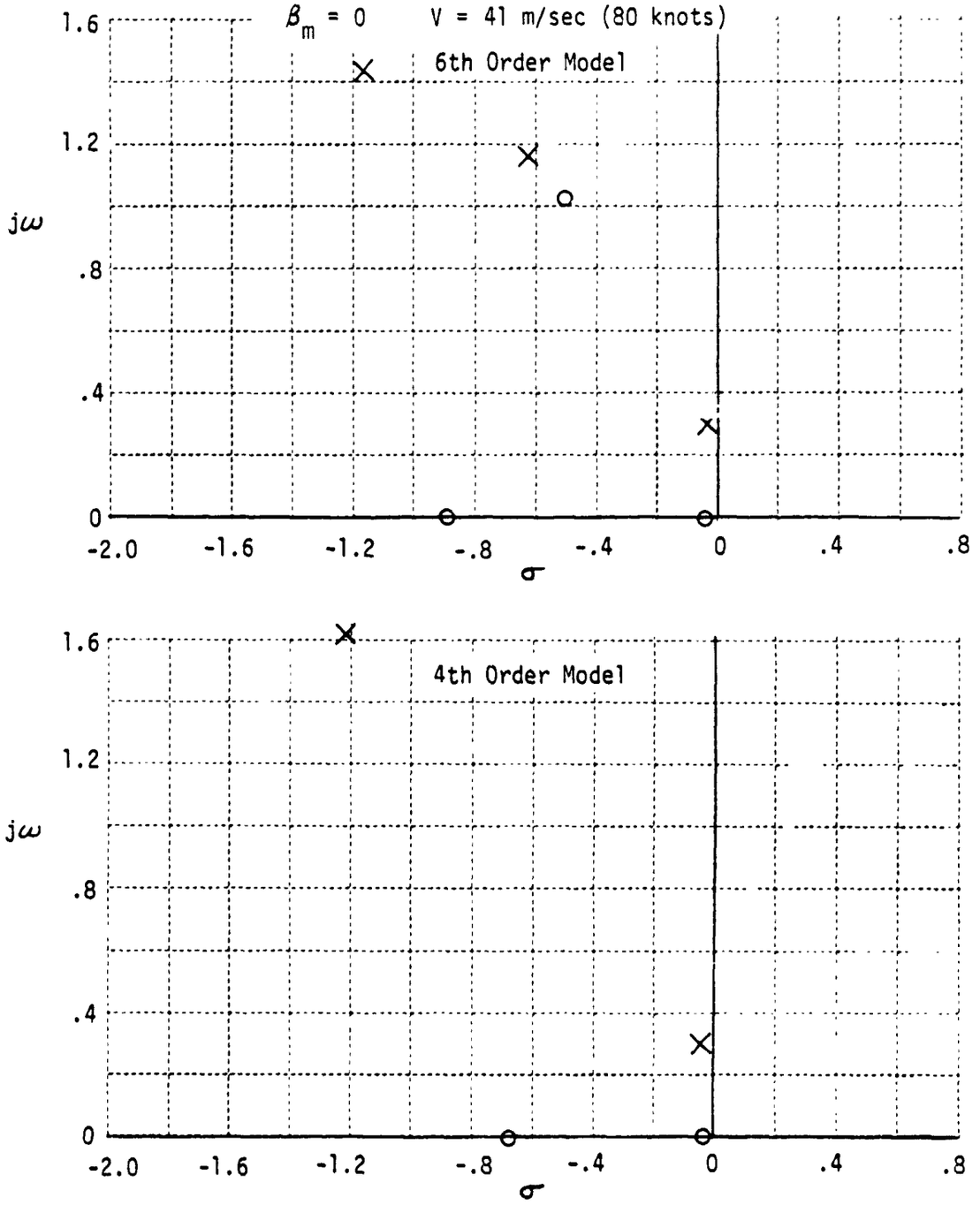

Figure 26 Pitch Attitude to Pitch Control Transfer Function - Comparison of 4th Order and 6th Order Models at 41 m/sec (80 knots)

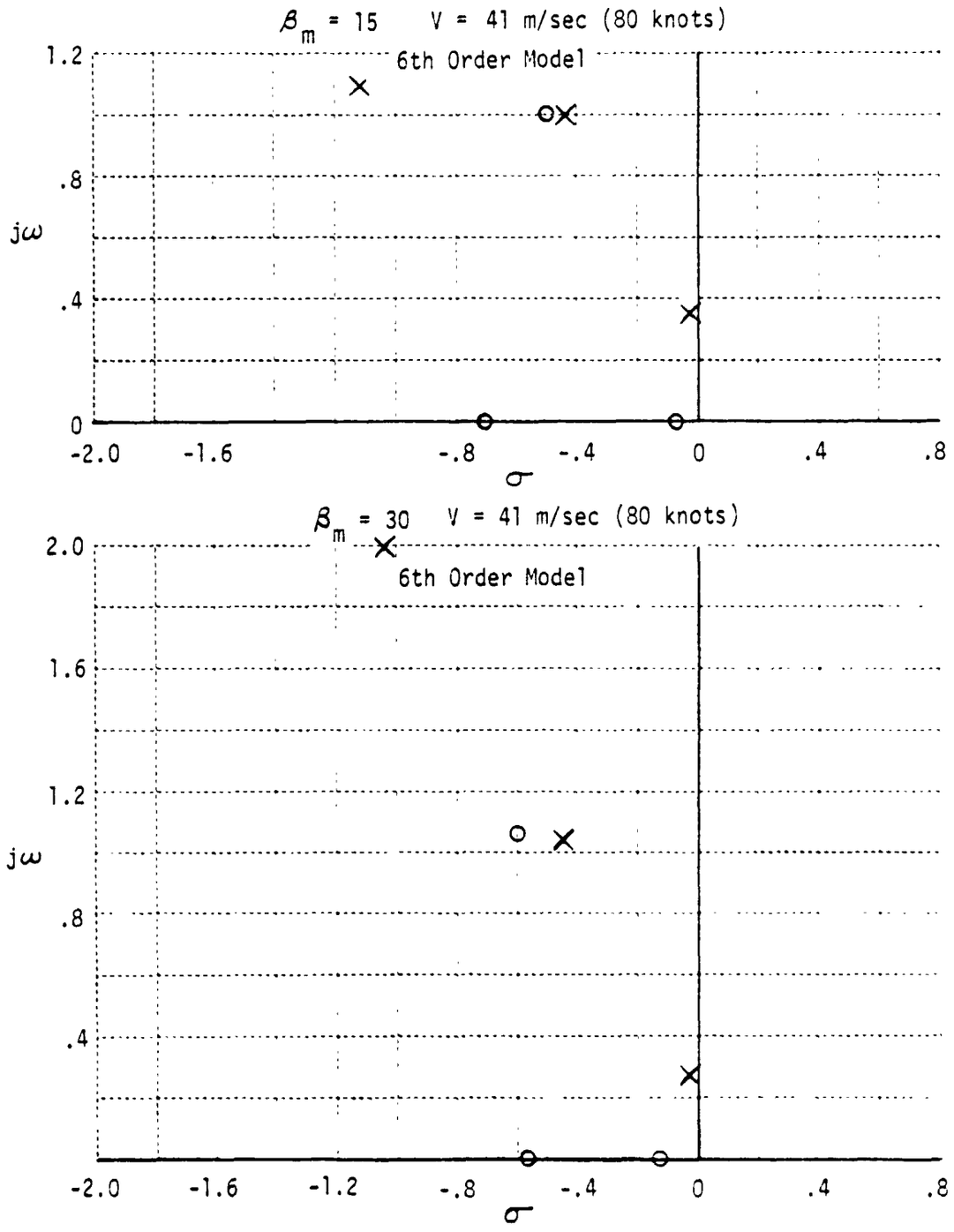

Figure 27 Pitch Attitude to Pitch Control Transfer Functions at 41 m/sec (90 knots) at Mast Angles 75 and 60 deg

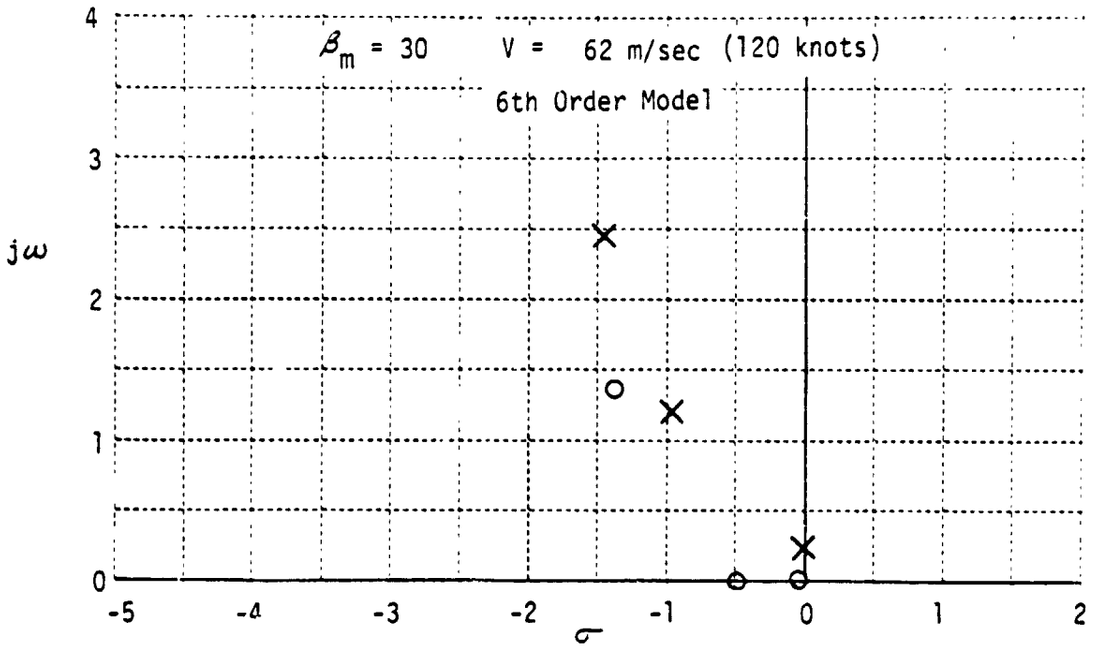

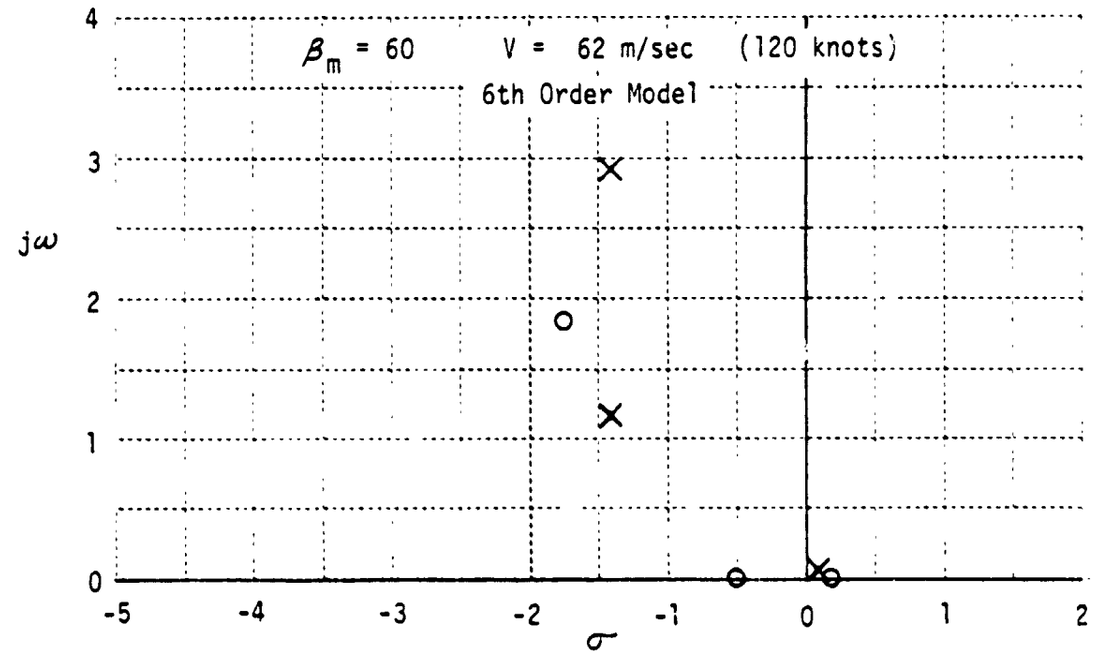

Figure 28 Pitch Attitude to Pitch Control Transfer Functions at 62 m/sec (120 knots) at Mast Angles 60 and 30 deg

4.3.2 Vertical Velocity to Cockpit Collective Transfer Functions (w/δ_c)

Cockpit collective inputs simultaneously command both rotor collective pitch and engine power output. Therefore, the development of transfer relations for vehicle responses to cockpit collective requires a linear model for engine power response to power commands.

In Appendix D, it is shown that the engine responds to small discrete power commands at a constant rate terminated by a short period of exponential capture of the commanded power. The rate of power increase is primarily a function of the initial or trim power setting of the engines. For a given trim power setting and power command magnitude, it is possible to approximate the response by a first or higher order linear filter. Because of the nonlinear (rate-limited) response of the engines, the characteristics of the linear model would have to be tailored specifically for each trim condition and power command magnitude. For a first order engine model, low initial power settings and large power commands would be approximated by large engine time constants.

It is also shown in Appendix D that for bandwidth and amplitude limited continuous power commands, it may be possible to neglect the effect of the engine response dynamics because the engine power rate limit will not be encountered. For a first order linear engine model, this limiting case would be approximated by an infinite filter break frequency

It is apparent then, that in the general case, a linear model of the vehicle responses to collective commands is only an approximation to the dynamic characteristics because of rate limiting of the engine power response. In the examples to follow, a linear first order engine model was employed to illustrate as simply as possible the major effects of engine power response characteristics on the cockpit collective transfer functions.

Because the cockpit collective excites the longitudinal dynamics through a direct path to the rotor collective pitch and through the first order engine dynamics, the collective transfer functions are 7th order. In Figures 29 to 31, s-plane plots of the poles and zeros of the vertical velocity to cockpit collective transfer functions for the 7th order and conventional 4th order longitudinal dynamic model are compared. For the limiting case of instantaneous power response to collective commands ($\lambda_E \rightarrow \infty$) it can be seen that the pole zero configurations of the 7th order model are similar to those of the 4th order model but with the addition of a complex pole-zero pair associated with the governor/RPM dynamics. As for the pitch control transfer functions, the separation of this pair of roots determines the residue of the RPM/governor mode appearing in the vertical velocity responses.

For the (w/δ_c) transfer functions, however, the residue will tend to be a minimum when the engine power commanded per unit collective is equal to the rotor power required increase per unit collective.

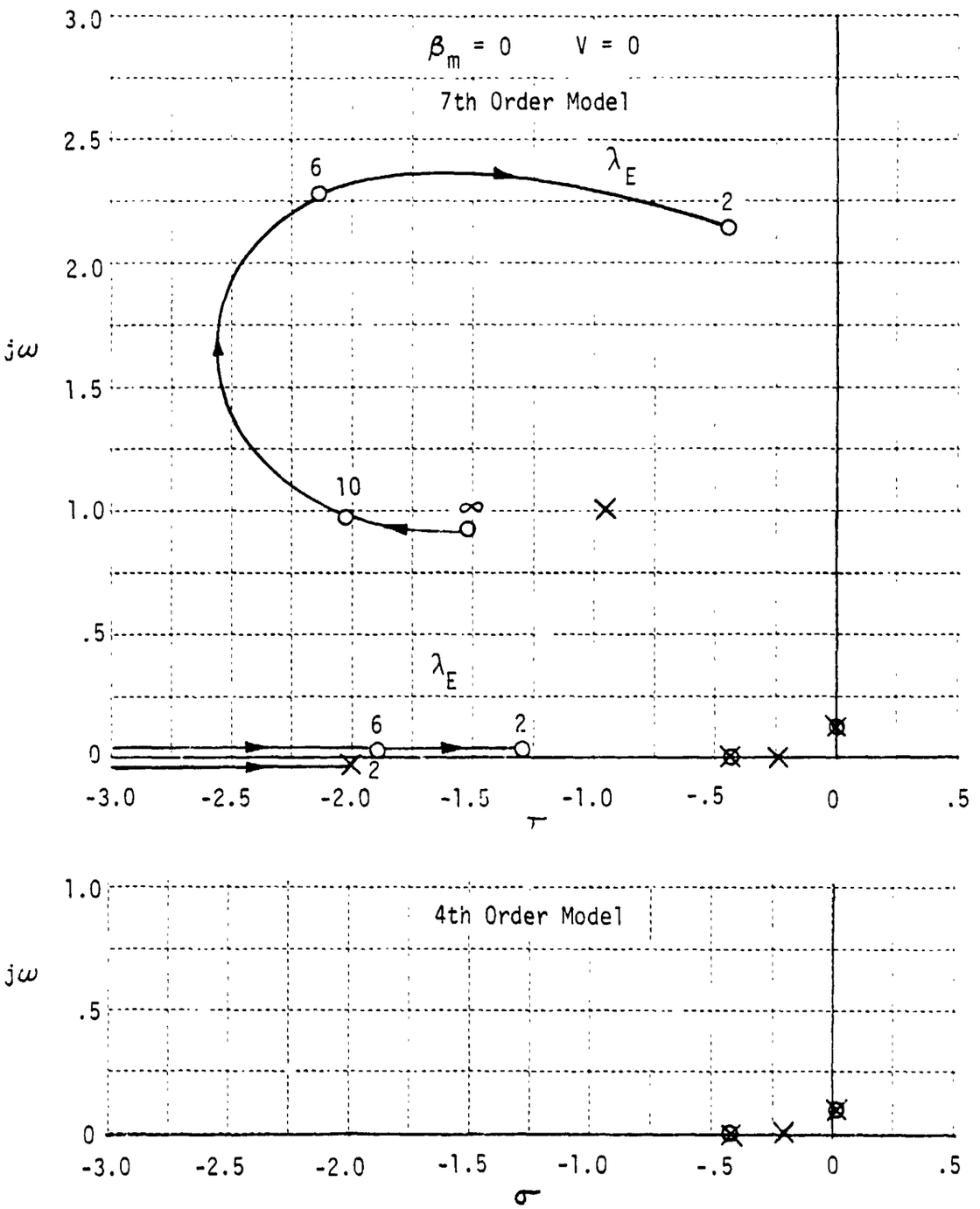

Figure 25 Effects of Engine Power Response on Vertical Velocity to Collective Controller Transfer Functions at 0 Velocity

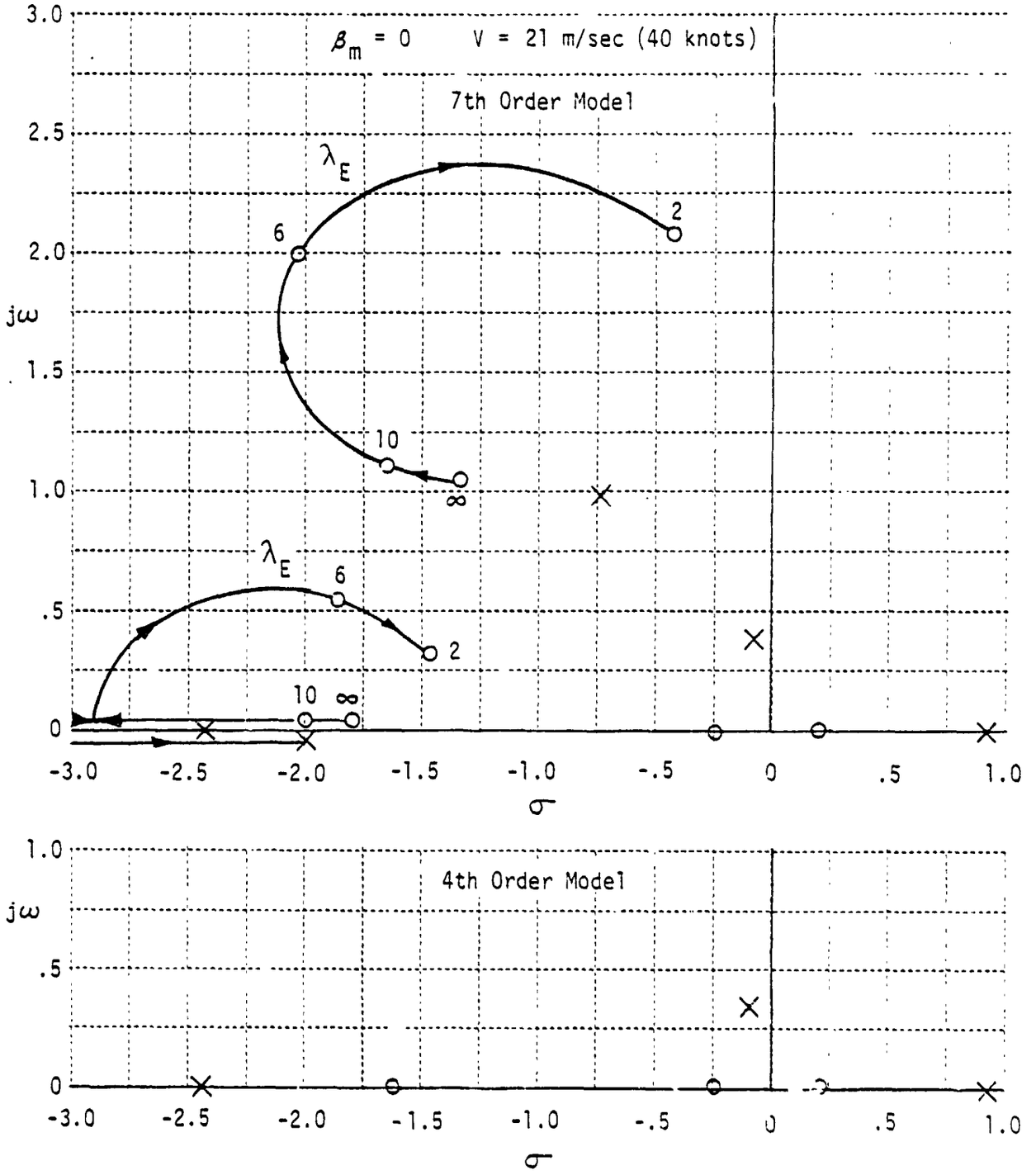

Figure 30 Effects of Engine Power Response on Vertical Velocity to Collective Controller Transfer Functions at 21 m/sec (40 knots)

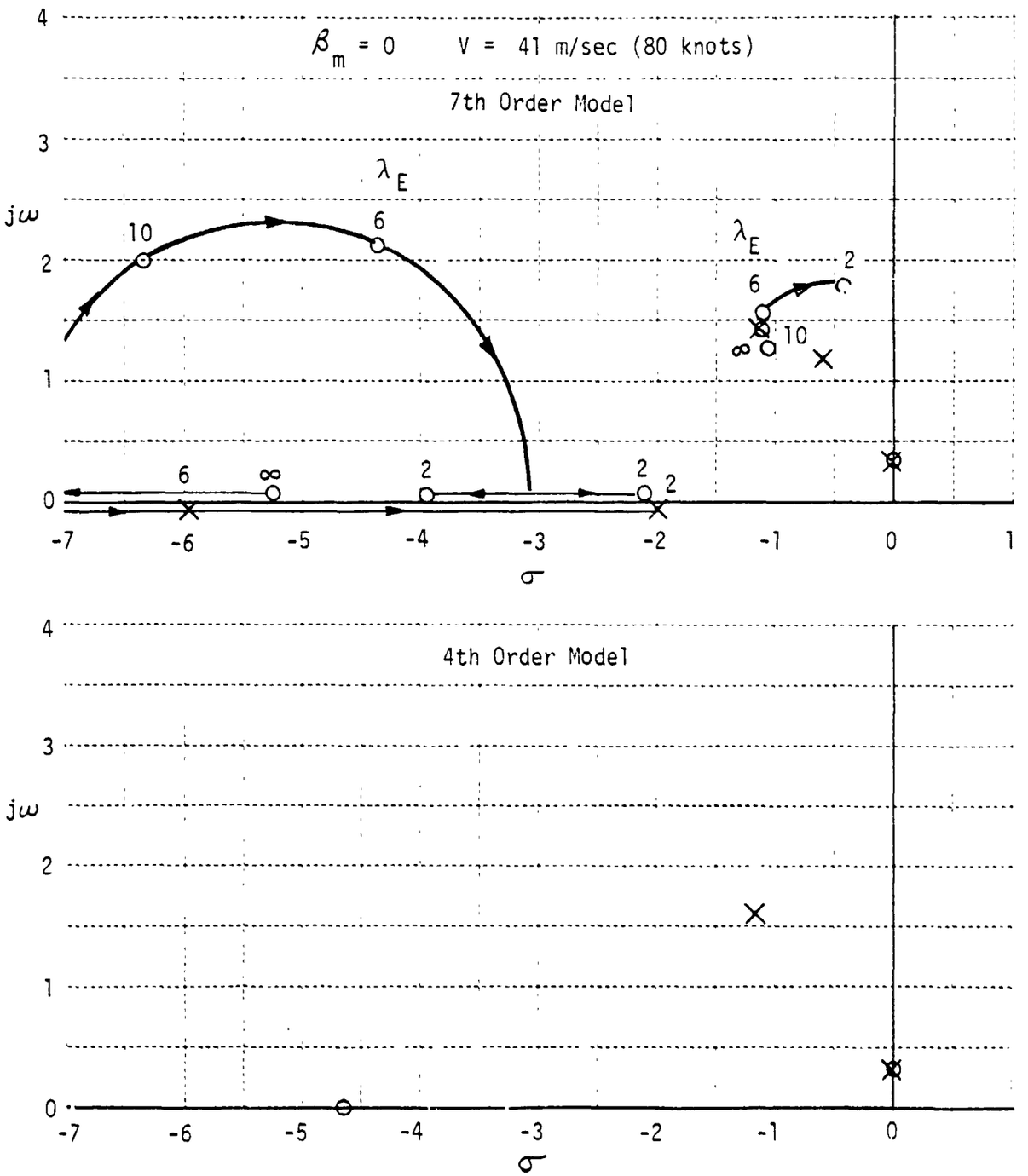

Figure 31 Effects of Engine Power Response on Vertical Velocity to Collective Controller Transfer Functions at 41 m/sec (80 knots)

For finite engine dynamics ($\lambda_\varepsilon < \infty$) it can be seen that as λ_ε is reduced, the governor/RPM mode zero migrates clockwise around the pole. In hover, the engine pole λ_ε and an associated zero migrate toward the origin as λ_ε is reduced. This real pair acts as a lead lag prefilter on the collective control commands and can be observed in time histories of thrust (vertical acceleration) response to cockpit collective commands as a "droop" in thrust following the initial thrust response. Figures 20 to 23 illustrate the sensitivity of this "droop" to λ_ε. Similar root migrations with λ_ε are exhibited at airspeeds of 21 meters/second (40 knots) and 41 meters/second (80 knots) except that for small values of λ_ε, the zero associated with the engine pole tends to couple with a zero associated with the conventional rigid body response of the aircraft.

To illustrate the significance of the governor/RPM mode to the collective transfer functions, Figure 32 compares the vertical velocity and acceleration response predicted by the 7th order model and the 4th order model. For this case, the value of engine time constant (0.1 seconds) produces an almost negligible effect on the thrust response. For the 4th order model the initial acceleration response is proportional to z_{δ_c} followed by an exponential decay to zero acceleration at a rate determined by the aircraft vertical damping z_ω. For the 7th order model, the initial acceleration response is identical. However, this initial response is subsequently augmented as the governor further increases collective pitch to absorb the increased engine power output commanded by the cockpit collective. Finally, as vertical velocity builds up, the vertical damping, z_ω, exponentially reduces the acceleration to zero. With respect to the vertical velocity response, the effect of the governor is reflected primarily as an increase in thrust control power (z_{δ_c}). At this flight condition, the governor adds about 0.5 degrees of collective pitch in the long term for each degree commanded by the cockpit collective lever.

On an overall basis, the governor has the effect of augmenting the thrust control power in the long term. However, since this added thrust is effectively filtered by the governor dynamics, in the short term, the overall thrust response appears sluggish.

Although devising control law strategies for the collective controller which can compensate for the effect of governor dynamics is beyond the scope of this study, some idea of the problems which might be encountered are illustrated in Figure 33. If the longitudinal dynamics of the XV-15 were conventional and it was desired to augment the vertical damping in hover, simple feedback of vertical velocity to the collective controller would achieve the desired result. For the 7th order model, it can be seen that this feedback mechanization results in the desired augmentation of vertical damping but, in addition, causes migration of the governor pole around its associated zero. At infinite gain, the complex poles will close on the zeros but for feedback gains of practical interest, it is likely that a significant residue of the governor mode will be observed in the vertical acceleration and velocity responses.

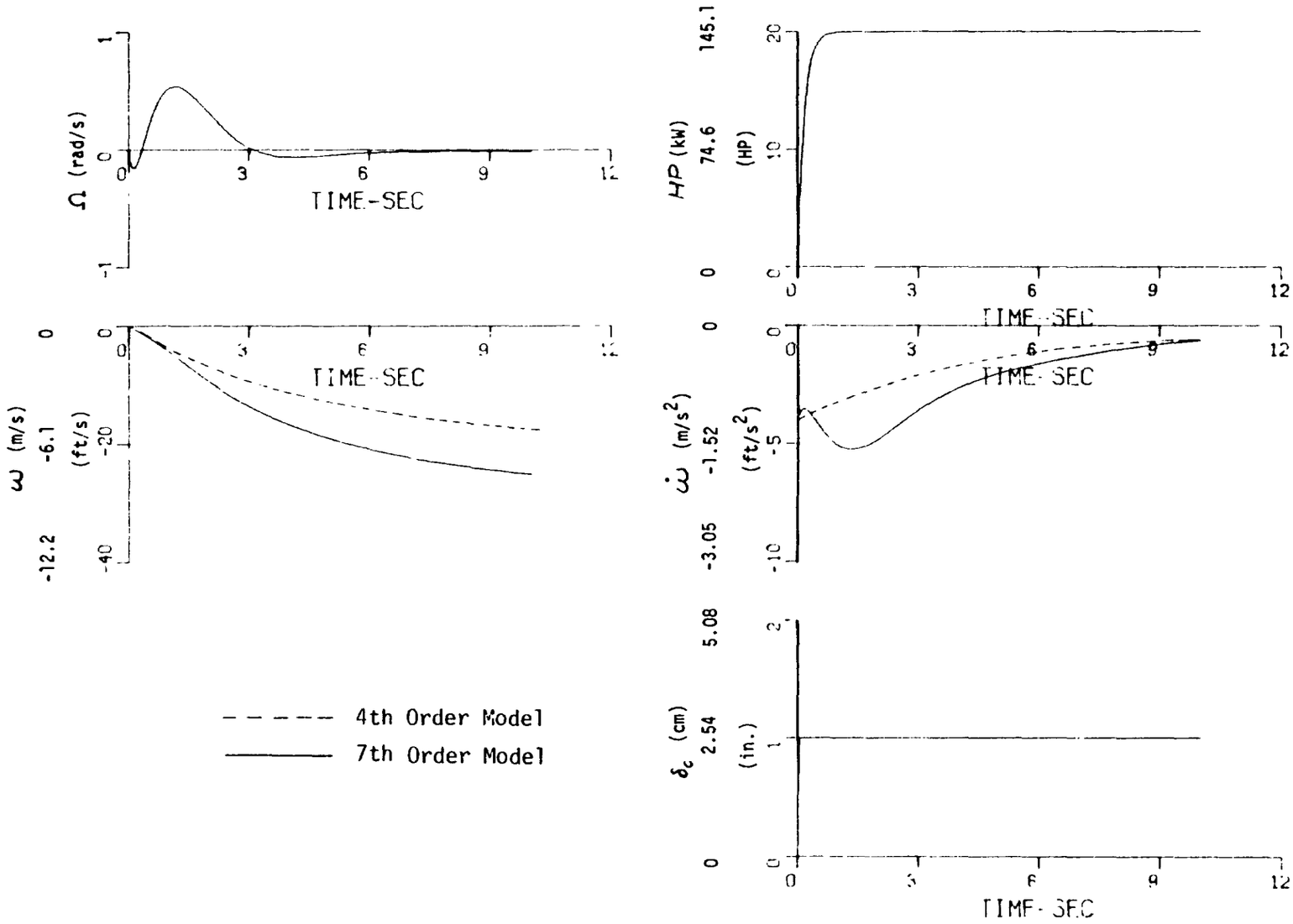

Figure 32 Comparison of Vertical Velocity and Acceleration Response to Collective of 4th and 7th Order Models

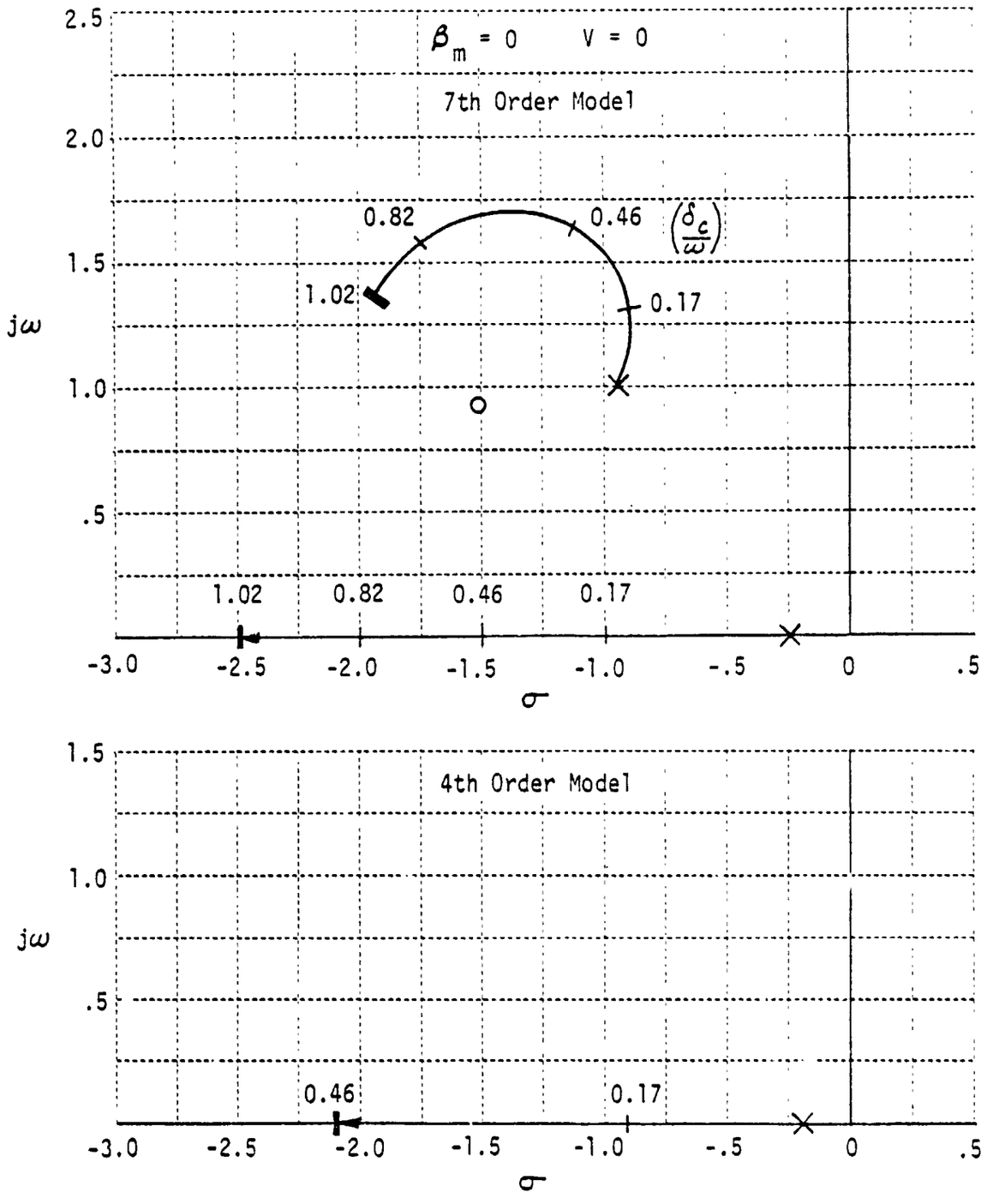

Figure 33 Comparison of Effects of Vertical Velocity to Collective Feedback on 7th Order and 4th Order Models

4.4 Evaluation of Force Feel System and SCAS Actuator Authority Limits on XV-15 Flying Qualities Research Capabilities

The simplest and least expensive integration of the V/STOLAND system with the XV-15 pitch roll and yaw flight control systems for flying qualities research applications is illustrated in the block diagram below. Mechanical control paths are designated by solid lines while electrical paths are dashed.

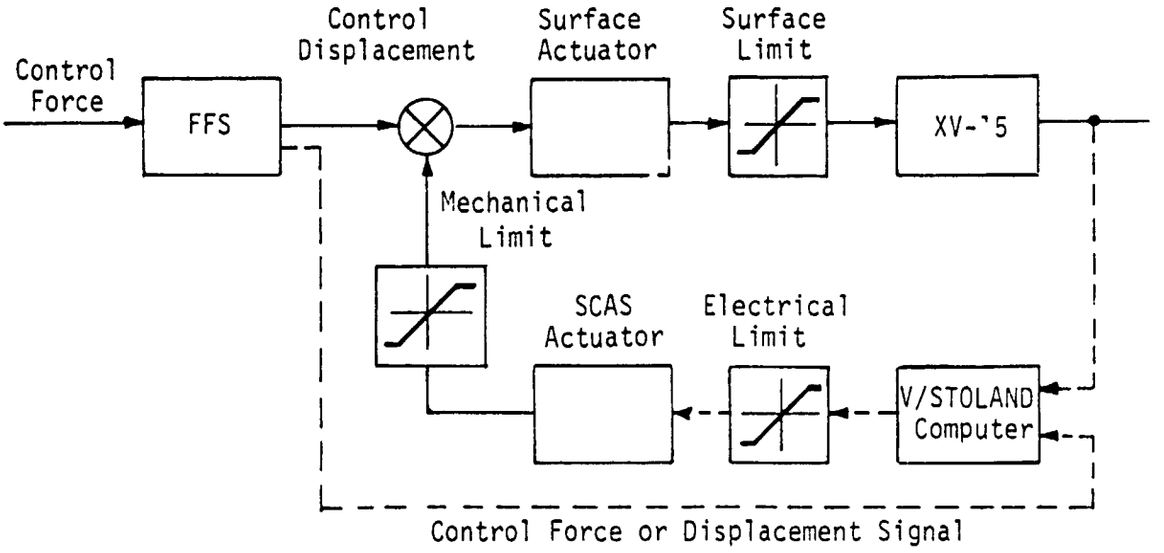

In this configuration, the Force Feel System (FFS) and pilot/copilot cockpit control interconnects would remain intact. The normal XV-15 autopilot and SCAS electronic paths would be interrupted during research operation and the SCAS actuators would be commanded by signals from the V/STOLAND computers. These control commands could be generated in either response feedback or model following control law mechanizations. It would also be possible to command control surface displacement through computer generated signals to the feel system, but this arrangement would not be suitable for flying qualities research because the cockpit controls would try to move in response to these signals.

The major shortcomings of this mechanization are associated with the limited SCAS actuator control authority relative to the total control available to the pilot through the mechanical path and the inflexibility of the feel system. With the existing feel system, it will not be possible to vary the force feel parameters (gradient, frequency, damping) at any given flight condition.

In recognition of these shortcomings, a series of modifications to enhance the flexibility of the force feel system and increase the effective

authority of the SCAS actuator output have been devised. These modifications and details of their electrical and mechanical implementation are described in Section 2.

Obviously, each of these modifications will enhance the research capabilities of the XV-15 but with the attendant penalty of increased implementation cost. The minimum level of feel system sophistication and SCAS actuator authority required by the XV-15 will be directly related to the nature of the research to be conducted. For example, the SCAS actuator displacements during an evaluation flight will be a function of the control laws implemented on the V/STOLAND computers (the simulated aircraft dynamics) and the aggressiveness with which the pilot maneuvers the aircraft (the evaluation task or mission). The situation will be further complicated by the fact that for a given task, the manner in which the pilot flys the aircraft, and, therefore, the SCAS actuator displacements will depend on the augmented vehicle dynamics.

This complex interdependence of SCAS actuator authority, vehicle dynamics and task makes the analytical determination of minimum acceptable SCAS authority extremely difficult. For example, if the approach adapted was to force each augmented configuration to follow a specific time history (e.g. pitch rate, attitude) the SCAS actuator displacements could be easily calculated from the control laws. However, the pilot input would also be determined by the response time history and may, for some dynamic configurations be highly unrealistic from the standpoint of pilot control capability. Therefore, SCAS actuator displacements calculated on this basis would be likewise unrealistic. Similar objections could be raised with respect to the specification of pilot control input time histories, except in these cases, the vehicle responses may be unrealistic.

It is considered that to examine the actuator authority requirements over a broad range of flight conditions and augmented dynamic configurations the only feasible approach is pilot-in-the-loop simulation. Manned simulation would be preferable although for certain specific tasks, analytical pilot models may provide representative results. However, even for the latter approach, the analytical task is complicated by the fact that for each dynamic configuration, at least the pilot gain and possibly other compensation parameters (lead, lag) would have to be adjusted to achieve reasonable closed loop performance. In any case, both of these approaches were considered beyond the scope of this analytical study.

In order to provide at least a limited quantitative basis for examining SCAS actuator authority requirements, specific pitch, roll and yaw dynamic configurations were established for the hover flight condition. The hover flight condition was selected because in addition to its significance for helicopter operations, the dynamic characteristics of the basic aircraft, compared to the augmented configurations, are essentially those of an acceleration system. In other words, the augmented vehicle dynamics are almost entirely a function of the augmentation system gains. In addition, in hover, the trim control surface deflections are approximately at the center of their

travel, therefore, equal control authority is available to the pilot in both directions.

Attitude command systems were implemented in pitch and roll. These control mechanizations were selected as likely candidates for initial control systems studies on the XV-15 and represent a higher order of sophistication than simple rate command systems. In yaw, however, a simple rate command configuration was implemented.

For simplicity, a response feedback control mechanization was assumed and the required feedforward and feedback gains were calculated assuming the V/STOLAND computer could function as a pure analog device. It is recognized that for a digital system, the gains actually employed would have to be compensated for the effects of sample rates and computation intervals. However, these considerations should have little effect on the results of the analysis.

As a measure of the significance of limited SCAS actuator displacement capability, for each dynamic configuration, the maximum step pilot command which could be applied without encountering the limit was estimated and compared to the maximum possible command if the actuator limit was infinite. Whenever an actuator limit is encountered during an evaluation flight, the vehicle reverts to its bare airframe dynamic characteristics during the saturation interval. If the saturation intervals are long or frequent, the simulation, in effect, is destroyed and the aircraft may be considered to be operating beyond its simulation envelope.

Additional simplifying assumptions were to neglect the dynamics of both the SCAS actuators and the control surface actuators. The assumption of a pure step control command is equivalent to neglecting the force feel system dynamics. It is recognized that these assumptions are somewhat unrealistic in that the smoothing introduced by the actuator and feel system dynamics would tend to allow larger control commands when the SCAS actuator limit encounters results from a rapid transient command. Therefore, the results of this analysis should be considered as somewhat conservative. The analysis is presented in detail for the pitch axis. The results of a similar analysis for roll and yaw are summarized.

4.4.1 Pitch SCAS Actuator Limits

To illustrate the effects of actuator limiting, feedback gains were calculated appropriate to three attitude command configurations having the characteristics $\zeta = 0.7$, $\omega_n = 2.0$, 3.0 and 4.0 rad/sec. A block diagram of the system is illustrated below.

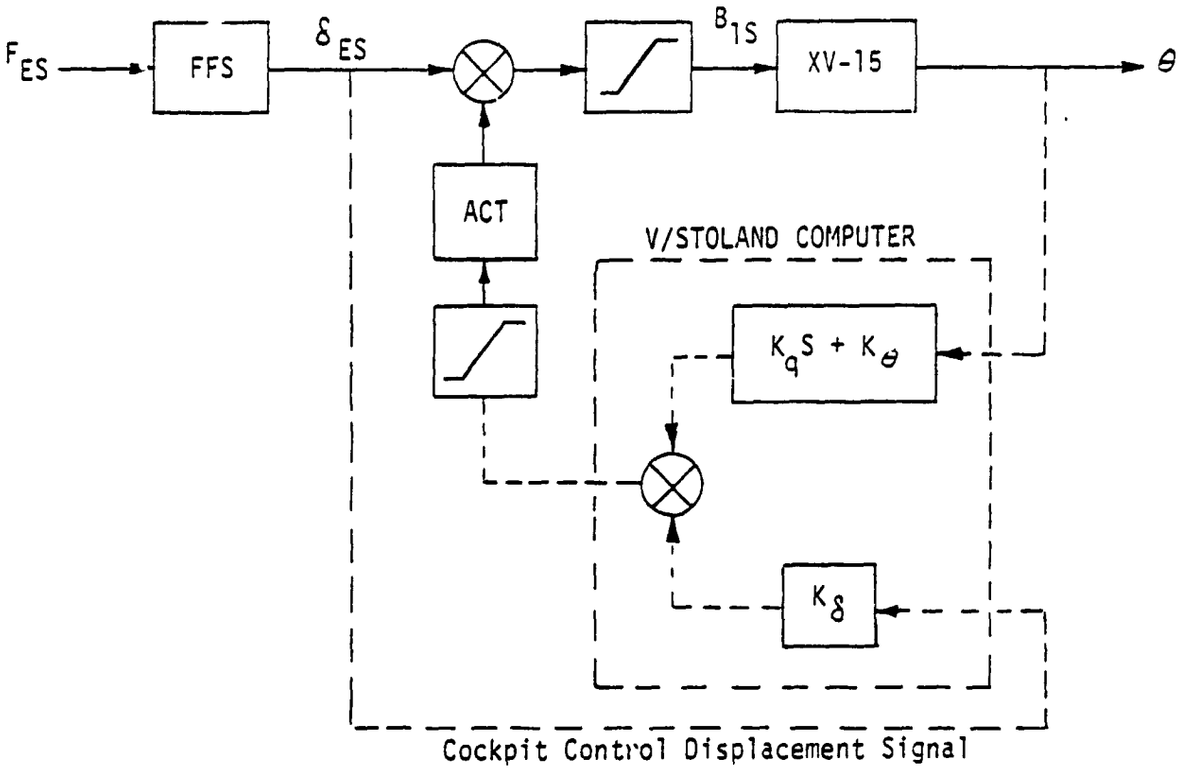

Because of the direct mechanical command path from the pilot to the control surface, control sensitivity variations must be effected within the V/STOLAND computer by adjusting the magnitude and sign of the feedforward gain K_δ. For a given control sensitivity, the attitude to pitch command transfer function is given by

$$\frac{\theta}{\delta_{ES}} = \frac{M_{\delta_{ES}}(1 + K_\delta)}{S^2 + 2\zeta\omega_n S + \omega_n^2} \tag{18}$$

Paragraph 3.2.3.2 of MIL-F-83300 requires that for pitch attitude command systems with $\omega_n > 2$ the Level 1 control sensitivity will be such that in the steady state

$$0.016 < \left(\frac{\theta}{\delta_{ES}}\right)_{SS} < 0.12 \text{ rad/cm} \quad \left(0.04 < \left(\frac{\theta}{\delta_{ES}}\right)_{SS} < 0.3 \text{ rad/in.}\right)$$

Therefore, for each dynamic configuration, control sensitivity was varied to produce this range of steady state response per unit control command.

To realize a given control sensitivity, the feedforward gain K_δ is calculated as follows:

$$\left(\frac{\theta}{\delta_{ES}}\right)_{ss} = \frac{M_{\delta_{ES}}\,(1+K_\delta)}{\omega_n^2} \tag{19}$$

$$K_\delta = \frac{\omega_n^2}{M_{\delta_{ES}}}\left(\frac{\theta}{\delta_{ES}}\right)_{ss} - 1 \tag{19a}$$

It can be seen from this equation, that for high augmented frequencies and steady state attitude response per unit command, the feedforward electrical path gain K_δ, will augment the pilot's command (i.e. $K_\delta > 0$). Conversely at low frequencies and low steady state response per unit command, K_δ will reduce the pilot's command ($K_\delta < 0$).

The transfer function relating the SCAS actuator command signal to the cockpit pitch control displacement is,

$$\frac{\delta_{ES_{SCAS}}}{\delta_{ES}} = K_\delta - (K_q S + K_\theta)\left(\frac{\theta}{\delta_{ES}}\right)$$

$$= K_\delta - (K_q S + K_\theta)\frac{M_{\delta_{ES}}\,(1+K_\delta)}{S^2 + 2\zeta\omega_n S + \omega_n^2} \tag{20}$$

In response to a unit step cockpit control command, the initial SCAS actuator command is K_δ. In the steady state, the actuator command is

$$\left(\delta_{ES_{SCAS}}\right)_{ss} = K_\delta - \frac{K_\theta M_{\delta_{ES}}\,(1+K_\delta)}{\omega_n^2} \tag{21}$$

since $$K_\theta M_{\delta_{ES}} \approx \omega_n^2$$

$$\left(\delta_{ES_{SCAS}}\right)_{ss} = K_\delta - (1+K_\delta) = -1. \tag{22}$$

Depending on the sign of K_δ and the frequency and damping of the augmented pitch dynamics, a time history of the SCAS actuator response to a unit step pitch control command would resemble the sketches below.

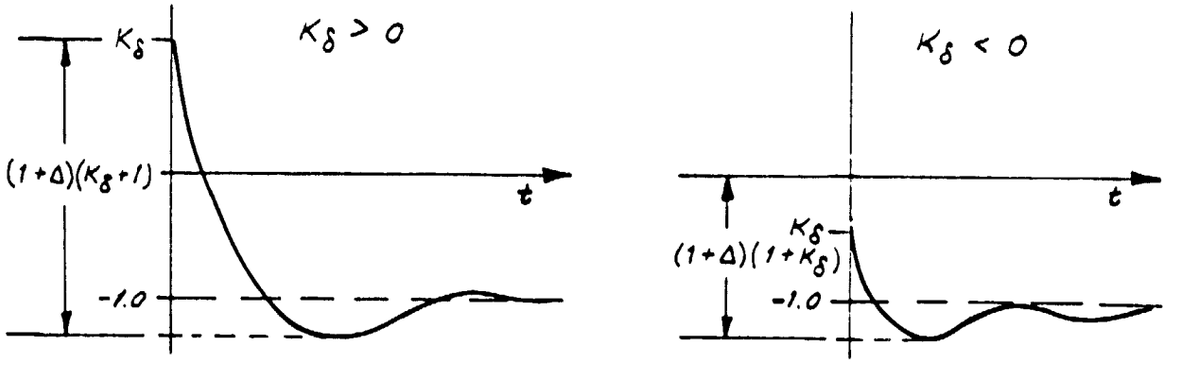

The negative overshoot will be related to the parameter Δ which is a function of the frequency and damping ratio of the augmented configuration. For greater than critical damping, Δ will be zero and no overshoot will be observed.

It can be seen from these time histories that the maximum SCAS actuator signal as a function of the control input magnitude will be given by

$$\left.\begin{aligned} & K_\delta > 0 \\ \left|\delta_{ES_{SCAS}}\right| &= K_\delta \delta_{ES} && K_\delta > 1 + \Delta(1 + K_\delta) \\ &= \left[1 + \Delta(1 + K_\delta)\right]\delta_{ES} && K_\delta < 1 + \Delta(1 + K_\delta) \\ & K_\delta < 0 \\ \left|\delta_{ES_{SCAS}}\right| &= \left[1 + \Delta(1 + K_\delta\right]\delta_{ES} \end{aligned}\right\} \quad (23)$$

Therefore, the maximum step input magnitude which can be commanded without saturating the SCAS actuator limit will be given by

$$\left.\begin{aligned} (\delta_{ES})_{MAX} &= \frac{(\delta_{ES_{SCAS}})_{LIMIT}}{K_\delta} && K_\delta > 1 + \Delta(1 + K_\delta) \\ &= \frac{(\delta_{ES_{SCAS}})_{LIMIT}}{\left[1 + \Delta(1 + K_\delta)\right]} && K_\delta < 1 + \Delta(1 + K_\delta) \end{aligned}\right\} \quad (24)$$

Another factor which may limit the maximum step command input is the control surface deflection. In response to a unit step command, the surface deflection time history resembles the following sketch.

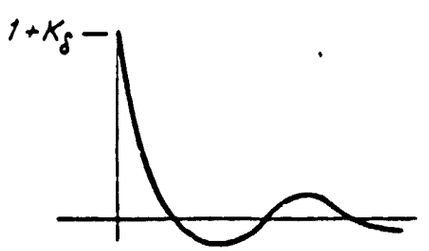

Unless the augmented configuration is very lightly damped, the initial surface deflection will determine the maximum command. In hover, the control surface is initially trimmed very close to the center of its range of travel. Therefore

$$(\delta_{ES})_{MAX} = \frac{(\delta_e)_{LIMIT}}{1 + K_\delta} \quad (25)$$

Figures 34 to 36 summarize the comparisons of the maximum command input as functions of frequency and control sensitivity (steady state attitude per unit command) for the SCAS actuator authority limits of Table 5 In Figure 34 (ω_n = 2.0 rad/sec) for $(\theta/\delta_{ES})_{SS}$ less than about 0.06 rad/cm. (0.16 rad/in), the maximum input size is determined by the negative transient overshoot. For ζ = 0.7, Δ is so small that, in effect, the steady state actuator displacement has determined these boundaries. For (θ/δ_{ES}) greater than 0.06 rad/cm (0.16 rad/in) the limits are determined by the initial feedforward signal causing actuator saturation at $t = 0$.

It can be seen that for the lowest SCAS actuator authority (Condition 1) the maneuvering capability of the aircraft will be severely limited. For example, at $(\theta/\delta_{ES})_{SS}$ = 0.04 rad/cm (0.1 rad/in) the steady state attitude at maximum control displacement is about 0.08 rad (4.6 deg) while for $(\theta/\delta_{ES})_{SS}$ = 0.12 rad/cm (0.3 rad/in.) the limit attitude is reduced to 0.03 rad (1.7 deg). Since attitude controls longitudinal acceleration in the steady state, these maximum attitudes may be interpreted as limiting the maximum acceleration as follows:

$$(\theta/\delta_{ES})_{SS} = 0.04 \text{ rad/cm (0.1 rad/in.)}, \quad \ddot{x}_{MAX} = 0.09g$$

$$(\theta/\delta_{ES})_{SS} = 0.12 \text{ rad/cm (0.3 rad/in.)}, \quad \ddot{x}_{MAX} = 0.03g$$

While attitude excursions of ± 5.0 deg are typical of helicopters in precision tasks near hover, for gross maneuvering such as rapid velocity changes and quick stops or maximum rate transitions to forward flight, 10 deg attitude changes or even higher may be employed by the pilot. Therefore, the data indicates that to assure sufficient capability to simulate helicopter gross maneuvering tasks, it would be necessary to increase the longitudinal SCAS actuator authority limit to at least Condition 3 to assure adequate capability. Even at the Condition 3 limit, however, the maneuvering capability falls far short of the limit imposed by the surface limit at low values of $(\theta/\delta_{ES})_{SS}$.

As frequency is increased (Figures 35 and 36), it can be seen that the boundaries for high $(\theta/\delta_{ES})_{SS}$ shift downward. The boundaries for low $(\theta/\delta_{ES})_{SS}$ are lowered only slightly. Therefore, as augmented frequency is increased, the maneuvering capability of the aircraft would be even further reduced.

4.4.2 Roll SCAS Actuator Limits

Applying the same augmentation schemes to the roll axis, limits similar to those of the pitch axis will be found. Because the authorities for Conditions 1 to 3 are approximately 50 per cent higher for roll than for pitch, the maximum control inputs and therefore the roll attitudes would be correspondingly higher. Therefore, at high $(\phi/\delta_{AS})_{SS}$, the Condition 3 modification would increase the SCAS actuator authority to the extent that the limit control input would now be determined by saturation of the control surface

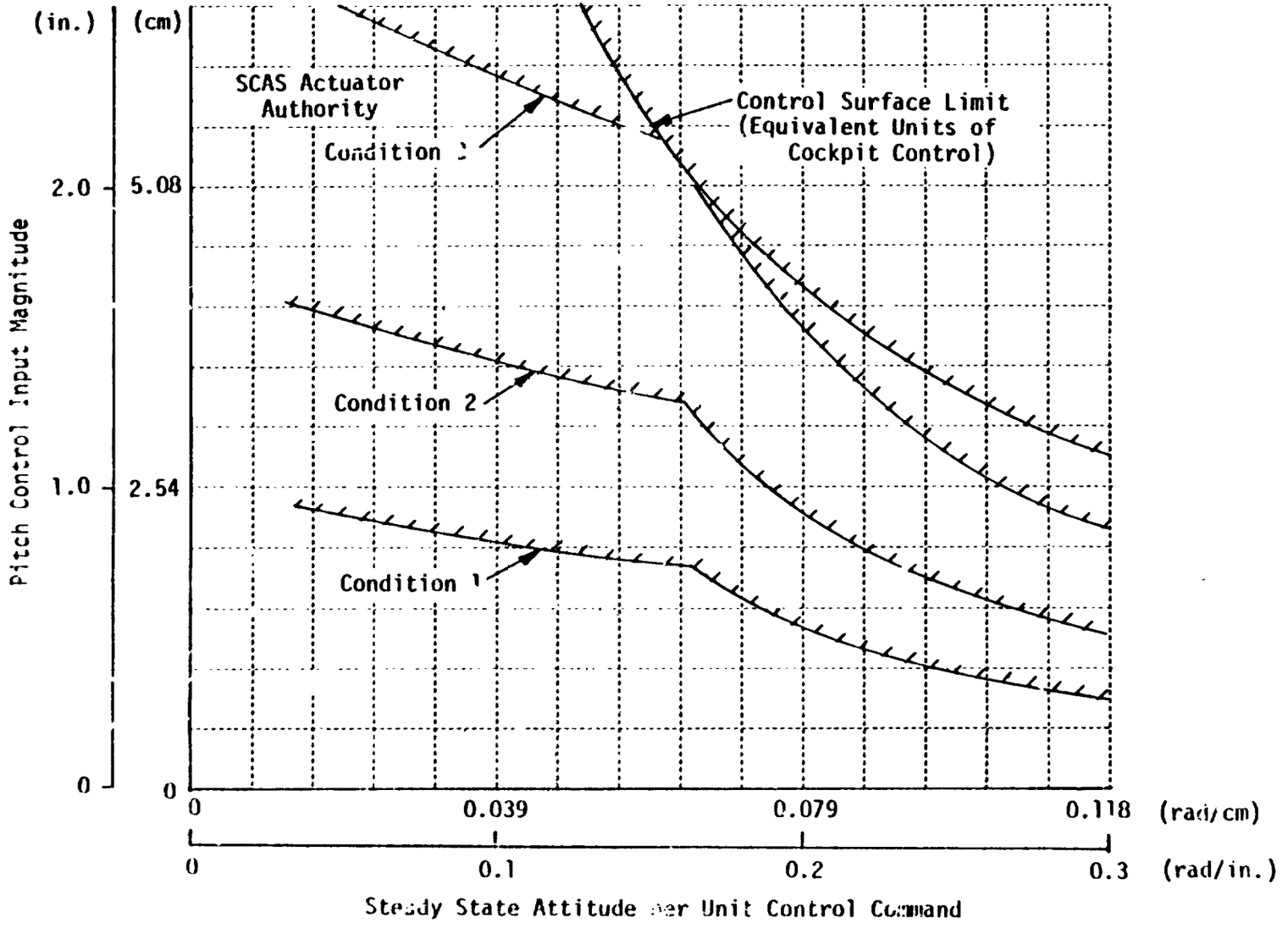

Figure 34 Pitch Control Input Limit as a Function of SCAS Actuator Authority and Control Surface Displacement Limit (ω_n = 2.0 rad/sec, ζ = 0.7)

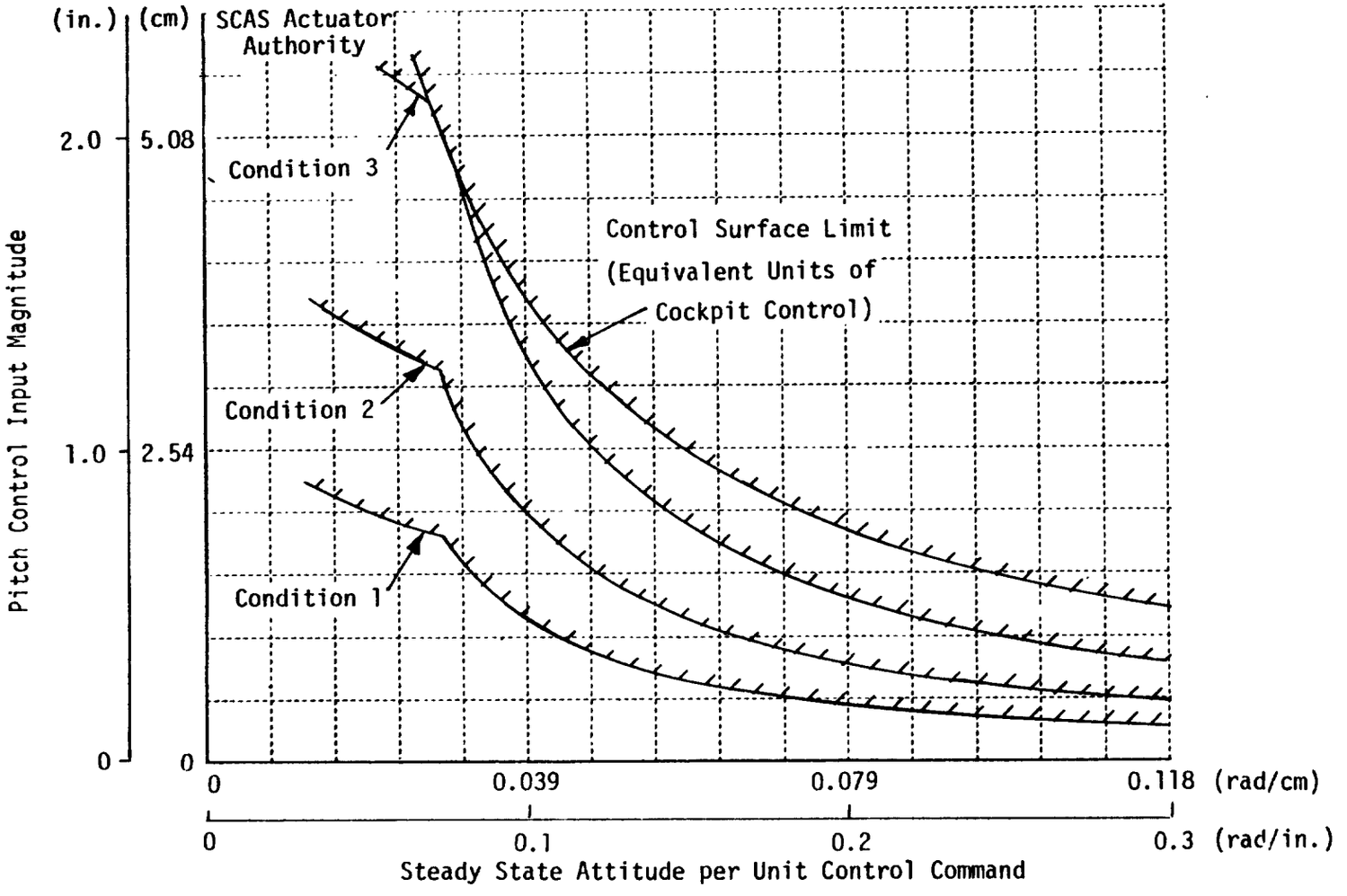

Figure 35 Pitch Control Input Limit as a Function of SCAS Actuator Authority and Control Surface Displacement Limit (ω_n = 3.0 rad/sec, ζ = 0.7)

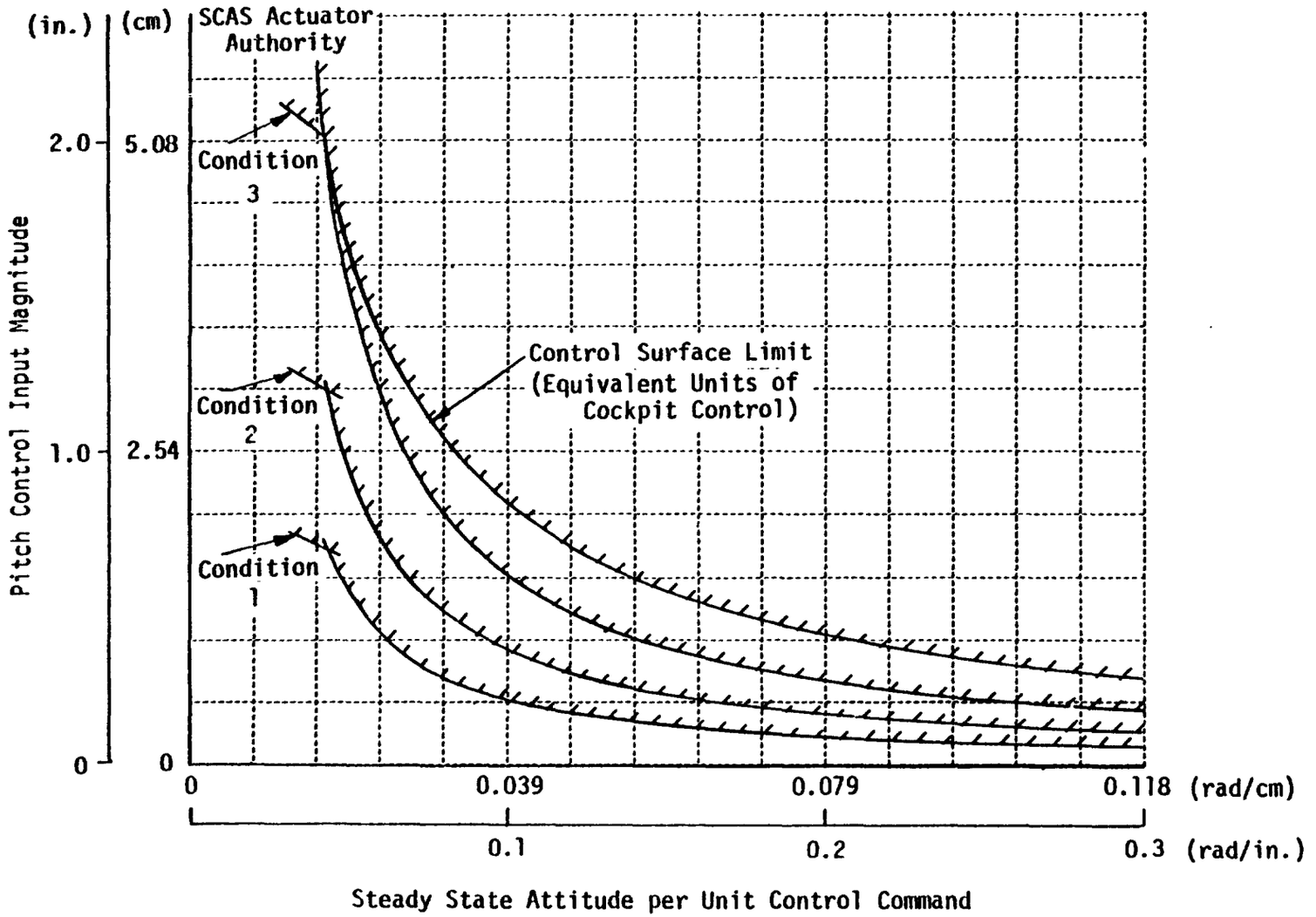

Figure 36 Pitch Control Input Limit as a Function of SCAS Actuator Authority and Control Surface Displacement Limit (ω_n = 4.0 rad/sec, ζ = 0.7)

At low $(\phi/\delta_{AS})_{SS}$, however, the SCAS actuator authority would still determine the maximum control input.

4.4.3 Yaw SCAS Actuator Limits

For the yaw axis, a rate command augmentation system was implemented with effective damping of -3.0 sec^{-1}. The variation in pedal command limit as a function of control sensitivity (steady state yaw rate/unit pedal) for the 3 conditions of SCAS actuator authority is shown in Figure 37. The variation in control sensitivity shown is such that the flying qualities exhibited would vary from Level 3 to Level 1. As can be seen from this figure, the control authority of the basic aircraft (i.e. the surface limit) does not meet the Level 1 requirement of MIL-F-83300. It is likely therefore that the restrictions imposed on control authority even for the Condition 3 SCAS modification will lead to actuator saturation during evaluations.

Similar to the pitch and roll axes, the limits would tend to be even more restrictive at higher levels of augmented angular rate damping.

4.4.4 Force Feel System Configuration 4

To obviate the potential difficulties associated with limited SCAS actuator authority, a modification has been proposed which is illustrated schematically below.

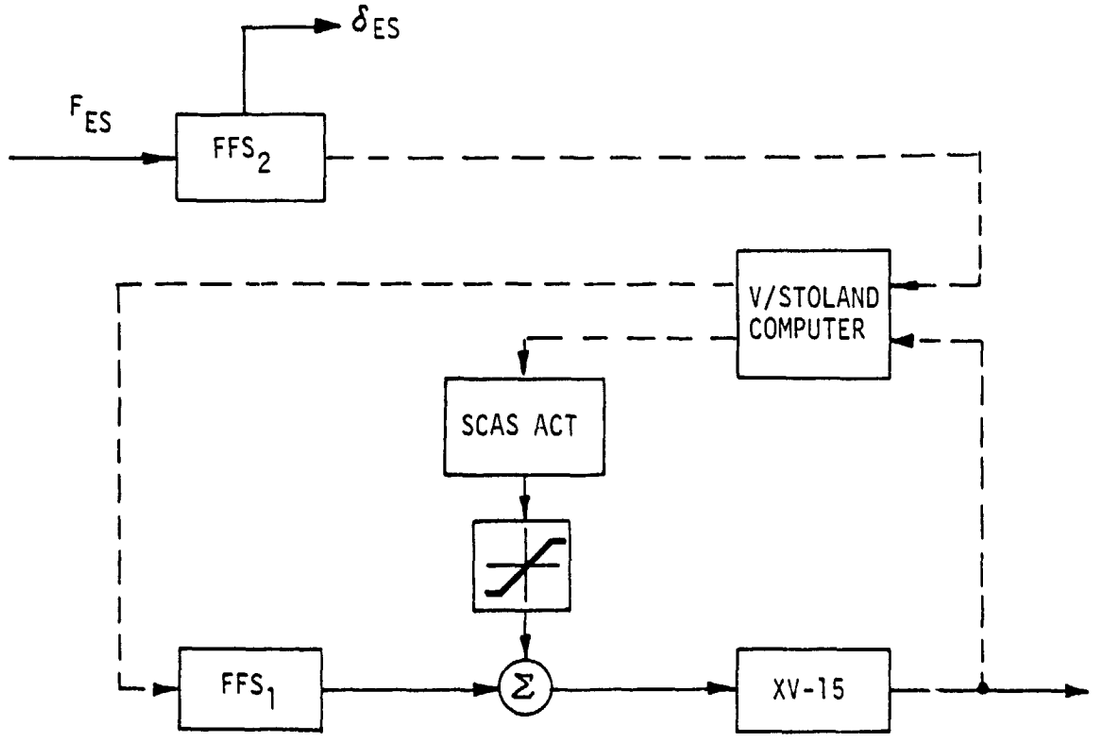

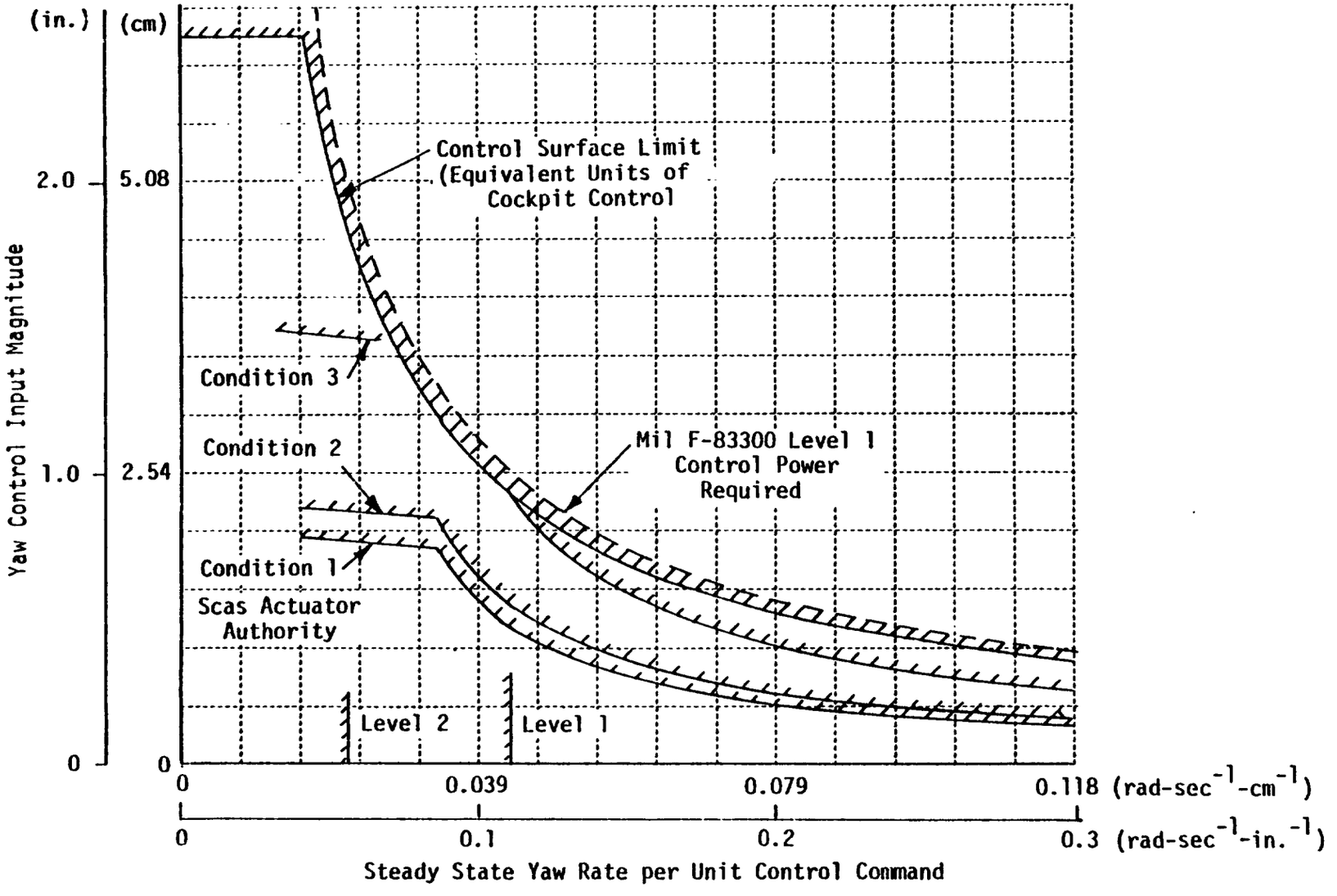

Figure 37 Yaw Control Input Limit as a Function of SCAS Actuator and Control Surface Displacement Limit (Yaw Damping -3.0 sec^{-1})

Implementation of this control system would require separating the pilot and co-pilot pitch roll and yaw controls and installing a second force feel system (FFS_2) for the evaluation pilot's station. With this mechanization, computer control commands could be complimentary filtered so that the control surfaces could be commanded both through the existing force feel system and the SCAS actuator. The evaluation pilot's force feel system would be designed to allow complete flexibility with respect to parameters such as gradient, frequency, damping, and nonlinearities.

Inasmuch as the SCAS actuator is a relatively high bandwidth device compared to the existing force feel system the complimentary filter would likely be configured to drive the SCAS actuator with the high frequency control commands and the force feel system with the low frequency and steady state control commands. However, as the previous analysis indicates, the SCAS actuator will, for many augmentation configurations, tend to saturate because of rapid control commands especially at high control sensitivities. Therefore, from this standpoint, the desired strategy would be to drive the safety pilot's force feel system with the high frequency control commands. If this is the case, a better approach would likely be to modify the safety pilot's force feel system to increase its bandwidth and to eliminate control commands to the SCAS actuator during research operations. Further study of this control mechanization is required.

5. CONCLUSIONS AND RECOMMENDATIONS

This study program has indicated that several deficiencies exist in the present XV-15 system that would limit the application of the aircraft to in-flight research. This section essentially summarizes these system problems and includes recommendations for either system modification or where necessary additional analysis. The results of this study program are the following:

(1) Existing force feel system does not permit controlled variation of feel system characteristics for generalized flying qualities research. System modification is required and several possible modifications with cost estimates are presented in this report.

(2) Levels of augmentation to provide the capability of simulating a significant range of variation in stability and control derivatives require system modification. Studies conducted indicate that while it might be necessary to use both the SCAS and FFS actuators, sufficient authority for many research applications could be achieved by increasing SCAS authority by the following percentages: Longitudinal ~476%; Lateral ~448%; Directional ~ 285%. The directional axis is considered to be the most critical due to basic aircraft control power limitations, therefore increasing SCAS authority could prove to be insufficient. The complex interdependence of control authority requirements with dynamic configuration, task, atmospheric environment and pilot control activity require additional analysis to determine the minimum acceptable SCAS actuator authority limits. This analysis should cover a broader range of dynamic configurations, and include piloted simulations of specific mission-orientated tasks. It is suggested that these piloted simulations be conducted on the FSAA simulator.

(3) Safety-of-flight considerations indicate that it would be desirable for the safety pilot cockpit control positions to reflect control surface motion and position. This would require separation of the force feel systems with extensive modification to the authority and dynamic characteristics of the existing force feel servos. This modification precludes the necessity to modify the existing SCAS authority.

(4) Significant uncertainty exists as to the extent of flight control system lost motion. It is entirely possible that the lost motion that exists could degrade system performance for research to an unacceptable level in one or more axes. Detailed study of the FCS linkage system is required to ascertain the amount of lost motion in the system. This is best obtained from measurement on the aircraft. Further analysis is required to determine the level of lost motion in individual control paths that is acceptable for the research mission. If it is determined that the amount of lost motion is unacceptable, this would impact on suggested FFS and SCAS modifications. Two possible methods, aside from simple mechanical adjustments, for reducing lost motion are:

1. Addition of a limited authority feedforward system in each control path, as required.
2. Conversion of the FCS to a fly-by-wire system with mechanical backup.

If it is determined that the lost motion is intolerable, and an acceptable solution obtained by the addition of a feedforward system, then the cost of implementing the FFS, SCAS and feedforward modifications should be compared to the cost of converting the system to the recommended FBW system. Serious consideration should be given to a FBW mechanization, since greater flexibility and better performance could be achieved with a system that has been developed and dedicated to the research operation of the XV-15 aircraft.

(5) Analysis indicates that the existing XV-15 RPM governor mechanization introduces a stable low frequency mode which couples with the rigid body longitudinal degrees-of-freedom. The governor prefilters collective control commands which slows the thrust response to collective inputs and in addition augments the long term thrust response in proportion to the ratio of engine power output to required rotor power for a collective input. These effects will tend to require additional control law implementation to eliminate or minimize the residue of the RPM mode in the aircraft response to control inputs. The low frequency prefilter effect on collective commands could significantly influence collective feedback gains. It is recommended that additional analysis is required to consider alternate rotor speed governor mechanizations that will not adversely impact on the research operation of the XV-15 for both low speed (powered-lift) and high speed (airplane mode) configurations.

(6) As presently configured, the XV-15 has the potential to function as a three-axis variable stability aircraft (pitch, roll, yaw). The addition of the collective actuator (required by V/STOLAND Specifications) and suitable control system modifications can provide independent control of thrust. The addition of mast angle control would allow limited X, Z- force regulation. Consideration should also be given to the utilization of the lateral cyclic pitch actuators to allow independent control of side force. These additional degrees of freedom are required to faithfully simulate the cockpit acceleration environment and are especially important for the simulation of large VTOL aircraft (e.g., HLH).

(7) In general, the sensors are suitable to provide the range, resolution, accuracy and dynamic response characteristics required for feedback control systems. A major deficiency is the lack of accurate airspeed data in all three body axes near hover. If research use of the system includes precision hovering/low speed tasks then an accurate low speed sensor system is required. Vertical and lateral airspeed information is required for all flight conditions.

(8) The proposed hardware monitor and servo disconnect system is considered to be unacceptable for research application because of the potential for excessive time lags between fault detection and the initiation of corrective action. In addition, there is no indication of the use of operational limits to trip the system. It is recommended that a separate hardware monitor and disconnect system, independent of V/STOLAND computer control, be included for all servos, aircraft states, etc. that could cause a dangerous condition

to develop if not promptly detected and the system disengaged.

(9) The computer system time lags which consist of both sampling process and transport lags from sensor input to surface commands are considered to be excessive and may be unacceptable for computer use in the research mission. Further analysis is required to determine the impact of these lags on closed-loop system stabililty, performance and compensation required to achieve selected simulation configurations.

(10) Some signals (certain control surface motions) are recorded directly while those that are processed through the computer will exhibit a 25 millisecond deterministic skew. It is recommended that all pertinent data be directly recorded through a remote multiplexer/demultiplexer unit in the data adapter to eliminate unnecessary post flight computer processing.

(11) Under software control, the electronic multifunction display unit and the electromechanical attitude director indicator will exhibit sufficient flexibility for general flying qualities control/display research. For certain Army missions, consideration should be given to the installation of a HUD and an electronic ADI capable of intergrating LLTV and FLIR with flight director symbology.

(12) The possibility of introduction of a fly-by-wire system to remedy problems introduced by control system lost motion also introduces the possibility of using the FBW computer as part of an analog-digital hybrid feedback control system. The digital computer could be used to provide low frequency information that is relatively unaffected by the existing system lags, while the high frequency information could be directly provided by an analog computer. The digital and analog information could be blended using complementary filters.

APPENDIX A

ANALYSIS OF I/O TIME LAGS

The I/O arrangement of the V/STOLAND computer system produces two major lags upon data processed through the computer. Sensor and external command data are received via channel 2 input, then processed through the basic and, if required, the research computer and finally the data is transmitted through channel 2 output to the control servos. One source of lag is due to the sampling/desampling process. If the sampled data is held constant within the computer between sampling intervals, this lag can be represented by a zero order hold transfer function. The second lag is a pure time delay or transport lag which is dependent upon the delay introduced to the data measured from the sampling instant to the time data is processed and transmitted as a servo command. Unless eliminated, these lags will impose a restriction upon maximum permissible closed loop gains when control loops are closed through the digital computer. The best approach is to minimize these lags by providing an input/output interface and computation cycle that permits high data throughput rate. A possible alternate method is presented in this appendix to minimize the effect of the transport lag by software within the digital computer. This software program is a predictor function which is essentially an approximation to an inverse time delay and can be mechanized in the computer.

This analysis is concerned mainly with the timing relationship between the analog input and output of computer channel 2. The majority of high frequency content signals are interfaced with channel 2 input and the autopilot servo command signals are transmitted via channel 2 output, Figure A-1. The typical sampling rate of sensor signals and autopilot servo commands is 40 samples per second. The I/O architecture and the software packages designed to accommodate data transfers imposes data time lags. A representation of a typical sampled signal is depicted in Figure A2 with the same signal accompanied by a transport lag which is presented in Figure A3.

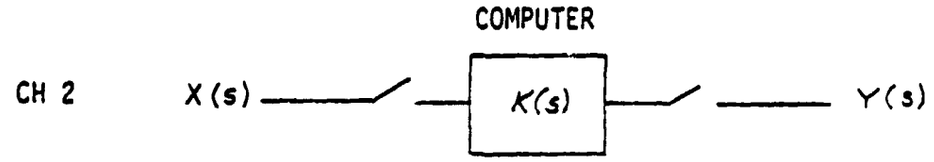

Figure A1 SAMPLING SYSTEM

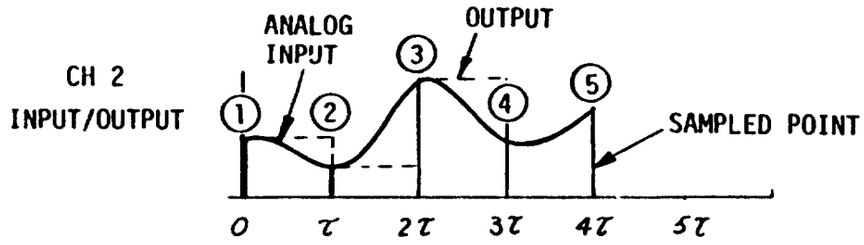

Figure A2 SAMPLED DATA (NO TRANSPORT LAG)

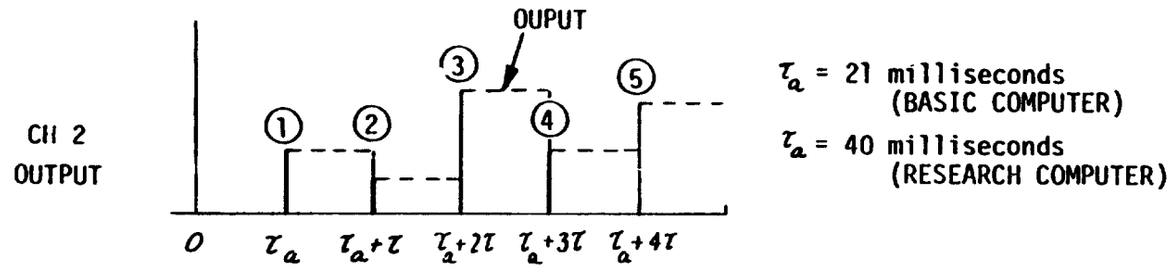

Figure A3 SAMPLED DATA (TRANSPORT LAG = τ_a)

Neglecting transport lags and representing the digital computer transfer function by K(s) where K(s) may be merely a gain schedule, then the relationship between channel 2 input X(s) and channel 2 output Y(s) may be expressed by Equation A1 which demonstrates the effect of the sample and hold process on the data.

$$Y(s) = K(s)\,X(s)\left(\frac{1 - e^{-\tau s}}{s}\right) \qquad (1$$

The sample and hold process is described as a zero order hold and a graphical representation of its effect on the data amplitude and phase as the data frequency content increases is demonstrated in Figures A4 and A5.

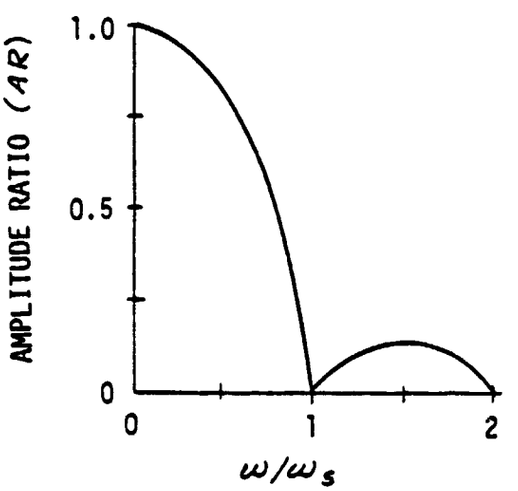

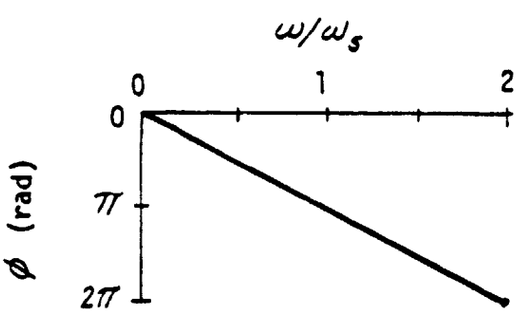

ω = DATA FREQUENCY

$\omega_s = 1/\tau$ = SAMPLING FREQUENCY

$$AR = \frac{2\pi}{\omega_s}\,\frac{|\sin(\pi\omega/\omega_s)|}{\pi\,\omega/\omega_s}$$

$$\phi = \frac{-\pi}{\omega_s}\,\omega \text{ (rad)}$$

Figure A4 ZERO ORDER HOLD AMPLITUDE RATIO

Figure A5 ZERO ORDER HOLD PHASE RESPONSE

If a transport lag, τ_a , is Introduced to the data either because of computation time or I/O structure, the sampled data is effectively delayed in time as represented in Figure A3 and a new relationship between input and output can be determined which is represented by Equation A2 (Reference 18)

$$Y(s) = X(s)\ K(s)\ e^{-\tau_a s}\left(\frac{1 - e^{-\tau s}}{s}\right) \qquad \text{(A2)}$$

The transfer function $e^{-\tau_a s}$ represents the transport lag and is equivalent to multiplying the data by a unity gain function with a phase lag equivalent to $\phi = -\tau_a \omega$ radians. The total phase lag imposed upon the data by the sampling process and the transport lag is represented by Equation A3.

$$\phi = -\omega\left(\tau_a + \frac{\pi}{\omega_s}\right) \qquad \text{(rad)} \qquad \text{(A3)}$$

A method which minimizes the effect of a transport lag, τ_a is presented in Reference 18. This method introduces the inverse transport lag function which is represented by $e^{\tau_a s}$.

A taylor expansion of the transport lag function is expressed by Equation A4.

$$e^{-\tau_a s} = 1 - \tau_a s + \frac{1}{2!}\tau_a^2 s^2 - \frac{1}{3!}\tau_a^3 s^3 + \cdots \qquad \text{(A4)}$$

Since τ_a is small, 20 < τ_a < 40 milliseconds, higher order powers of τ_a may be neglected. The inverse of the transport lag can then be represented by Equation A5.

$$e^{\tau_a s} \approx e^{*\tau_a s} = 1 + \tau_a s \qquad \text{(A5)}$$

$$e^{\tau_a s} \times e^{-\tau_a s} = 1 \qquad \text{(A6)}$$

$$e^{\tau_a s} \times e^{*\tau_a s} = \left(1 - \tau_a s + \frac{1}{2!}\tau_a^2 s^2 - \frac{1}{3}\tau_a^3 s^3\right)(1 + \tau_a s) \qquad \text{(A7)}$$

$$e^{-\tau_a s} \times e^{+\tau_a s} = 1 - \frac{1}{2}\tau_a^2 s^2 + \frac{1}{6}\tau_a^2 s^3 + \cdots \qquad \text{(A8)}$$

Perfect lag cancellation is represented in Equation A6. The effect of neglecting the higher order terms of τ_a is represented in Equation A8. The first order term has been eliminated by using a truncated Taylor series approximation for representing the inverse transport lag. The resultant error is the higher order terms of τ_a in Equation A8. It is evident that functions such as steps or pulses composed of multiple harmonics cannot be completely compensated by the predictor function $e^{+\tau_a s}$. In addition, if the step or pulse functions are asynchronous with respect to the sampling process, additional process errors can be introduced into the data. Because the sampling interval, 25 milliseconds, is small, the previously described process errors probably can be neglected.

Transport lag may be compensated for within the digital computer with a simple backward rectangular integration technique. This integration formula is expressed in Equation A9, Reference 18

$$y_n = y_{n-1} + \tau \frac{dy_n}{dt} \qquad \text{(A9)}$$

Equation A9 can be rearranged and expressed as the first derivative as shown in Equation A10

$$\frac{dy_n}{dt} = \frac{1}{\tau}(y_n - y_{n-1}) \approx sY(s) \qquad \text{(A10)}$$

$$\tau_a s Y(s) \approx \frac{\tau_a}{\tau}(y_n - y_{n-1}) \qquad \text{(A11)}$$

This integration scheme requires that the sampling rate be much greater than the highest frequency content of the data. It also requires storing the digital information from the Previous computation cycle so the data may be employed in calculating the first derivative of the next step. Additional storage and computational burden is imposed on the research computer because τ_a is different for different input/output signal combinations. If indeed the lag problems discussed represent a significant limitation in the research mode, they should be eliminated by hardware modifications first, if possible, and secondly a software compensation technique may be employed to ameliorate their effect.

APPENDIX B

STABILITY AND CONTROL DERIVATIVES FOR ROTOR SPEED DEGREE OF FREEDOM

In order to include the rotor speed degree of freedom in the XV-15 longitudinal equations of motion, it was necessary to derive quantitative estimates for the rotor torque derivatives (Q_u , Q_ω , Q_q , $Q_{B/S}$, Q_{θ_c}) and the rotor to fuselage coupling derivatives (X_Ω , Z_Ω, M_Ω). The derivative calculations are based on the "classical" rotor force and moment equations contained in Reference 19 with the addition of additional terms to account for a linearly twisted rotor blade. For simplicity, the contribution of rotor pitch-flap coupling (δ_3) and the cyclic flapping spring restraint to the rotor forces, moments and torque was neglected. Because of the many simplifying assumptions, these calculated derivatives should be viewed as preliminary estimates pending verification by more sophisticated analytical techniques or test data. Where possible, the derivatives were validated by comparison with trim and stability and control data presented in Reference 15.* This appendix concludes with a brief summary of these comparisons.

Despite these simplifying assumptions, the rotor equations are algebraically complex. Therefore, a digital computer program was written to facilitate the estimation of derivatives. The subsections to follow are a summary of the equations as implemented in the program and are presented, for the most part, without derivation.

Rotor Torque Derivatives

Non-dimensional Derivatives

Non-dimensional torque derivatives with respect to control axis velocities, pitch angular rate and collective pitch are given by

$$Z = A^{-1} X$$

where,

$$Z = \begin{bmatrix} \frac{2}{a\sigma}\frac{\partial C_Q}{\partial \bar{u}} & \frac{2}{a\sigma}\frac{\partial C_Q}{\partial \bar{w}} & \frac{2}{a\sigma}\frac{\partial C_Q}{\partial \theta_c} & \frac{2}{a\sigma}\frac{\partial C_Q}{\partial (q/\Omega)} \\ \frac{2}{a\sigma}\frac{\partial C_T}{\partial \bar{u}} & \frac{2}{a\sigma}\frac{\partial C_T}{\partial \bar{w}} & \frac{2}{a\sigma}\frac{\partial C_T}{\partial \theta_c} & \frac{2}{a\sigma}\frac{\partial C_T}{\partial (q/\Omega)} \\ \frac{\partial \lambda}{\partial \bar{u}} & \frac{\partial \lambda}{\partial \bar{w}} & \frac{\partial \lambda}{\partial \theta_c} & \frac{\partial \lambda}{\partial (q/\Omega)} \\ \frac{\partial a_1}{\partial \bar{u}} & \frac{\partial a_1}{\partial \bar{w}} & \frac{\partial a_1}{\partial \theta_c} & \frac{\partial a_1}{\partial (q/\Omega)} \end{bmatrix} \quad \text{(B1)}$$

*Prior to publication of this report, the data of Reference 15 were superceded by a Bell Helicopter Company letter, dated 10 June 1975, subject: "Model 301 (XV-15) Stability Derivatives for STI Control System Study."

$$A = \begin{bmatrix} 1.0 & 0 & \frac{\theta_c}{3} - \frac{\theta_t}{4} + \lambda + \frac{\bar{u}}{2} a_1 & \frac{a_1}{4}\left(1 + \frac{3\bar{u}^2}{2}\right) + \frac{\bar{u}\lambda}{2} \\ 0 & 1.0 & -\frac{1}{2} & 0 \\ 0 & 1.0 & \frac{2}{a\sigma}\left[2(\lambda^2+\bar{u}^2)^{1/2} - \frac{C_T \lambda}{\lambda^2+\bar{u}^2}\right] & 0 \\ 0 & 0 & -2\bar{u} & 1 - \frac{\bar{u}^2}{2} \end{bmatrix}$$

$$X = \left[\begin{array}{cc:c:c} \left(\frac{\delta}{2a} - \frac{a_o^2}{2} - \frac{3}{8}a_1^2 - \frac{b_1^2}{8}\right)\bar{u} - \frac{\lambda a_1}{2} + \frac{a_o b_1}{3} & 0 & -\frac{\lambda}{3} & 0 \\ \bar{u}\left(\theta_c - \frac{\theta_t}{2}\right) & 0 & \frac{1}{3} + \frac{\bar{u}^2}{2} & 0 \\ \frac{2C_T}{a\sigma} \quad \frac{\bar{u}}{\lambda^2+\bar{u}^2} & \frac{4}{a\sigma}(\lambda^2+\bar{u}^2)^{\frac{1}{2}} & 0 & 0 \\ \frac{8}{3}\left(\theta_c - \frac{3}{4}\theta_t\right) + 2\lambda + a_1\bar{u} & 0 & \frac{8}{3}\bar{u} & -\frac{1}{1-\frac{\bar{u}^2}{2}}\frac{16}{\gamma} \end{array}\right]$$

$$\frac{2}{a\sigma}\frac{\partial C_Q}{\partial B_{1s}} = \bar{w}\left(\frac{2}{a\sigma}\frac{\partial C_Q}{\partial \bar{u}}\right) - \bar{u}\left(\frac{2}{a\sigma}\frac{\partial C_Q}{\partial \bar{w}}\right) \tag{B2}$$

$$\frac{2}{a\sigma}\frac{\partial C_Q}{\partial \Omega} = -\frac{1}{\Omega_o}\left[\bar{u}\left(\frac{2}{a\sigma}\frac{\partial C_Q}{\partial \bar{u}}\right) + \bar{w}\left(\frac{2}{a\sigma}\frac{\partial C_Q}{\partial \bar{w}}\right)\right] \tag{B3}$$

The elements of A and X were calculated as follows:

Resolution of trim thrust from shaft axis system to control axis system.

$$T_c = T_s \cos B_{1s} - H_s \sin B_{1s} \tag{B4}$$

T_s, H_s and B_{1s} are inputs from trim data of Reference 15

$$C_T = \frac{T_c}{\rho \pi R^2 (\Omega_o R)^2} \tag{B5}$$

Rotor inflow ratio

$$\lambda = \bar{w} - \frac{C_T}{2(\lambda^2 + \bar{u}^2)^{\frac{1}{2}}} \tag{B6}$$

where non-dimensional velocities in control axis system are given by,

$$\left.\begin{aligned} \bar{u} &= \frac{V\cos(\alpha - \beta_m - B_{1s})}{\Omega_o R} \\ \bar{w} &= \frac{V\sin(\alpha - \beta_m - B_{1s})}{\Omega_o R} \end{aligned}\right\} \quad \text{(B7)}$$

Trim collective pitch

$$\theta_c = \frac{1}{\frac{1}{3} + \frac{\bar{u}^2}{2}} \left\{ \frac{2C_T}{a\sigma} + \theta_t \frac{(1+\bar{u}^2)}{4} - \frac{\lambda}{2} \right\} \quad \text{(B8)}$$

where blade section lift curve slope is a and total blade twist is θ_t

Rotor coning and flapping

$$\left.\begin{aligned} a_o &= 2.5 \text{ deg (held constant due to blade root constraints)} \\ a_1 &= \frac{\bar{u}}{1 - \frac{1}{2}\bar{u}^2}\left[\frac{8}{3}\left(\theta_c - \frac{3}{4}\theta_t\right) + 2\lambda\right] \\ b_1 &= \frac{\bar{u}}{1 + \frac{1}{2}\bar{u}^2}\left[\frac{4}{3}a_o\right] \end{aligned}\right\} \quad \text{(B9)}$$

Dimensional Derivatives

$$\frac{\partial Q}{\partial u_R} = \frac{a\sigma}{2} K_R \Omega_o \left[\frac{2}{a\sigma}\frac{\partial C_Q}{\partial \bar{u}}\right] \quad \text{lb-sec} \quad \text{(B10)}$$

$$\frac{\partial Q}{\partial \omega_R} = \frac{a\sigma}{2} K_R \Omega_o \left[\frac{2}{a\sigma}\frac{\partial C_Q}{\partial \bar{w}}\right] \quad \text{lb-sec} \quad \text{(B11)}$$

$$\frac{\partial Q}{\partial \theta_c} = \frac{a\sigma}{2} K_R (\Omega_o R)\frac{\pi}{180}\left[\frac{2}{a\sigma}\frac{\partial C_Q}{\partial \theta_c}\right] \quad \text{ft-lb-deg}^{-1} \quad \text{(B12)}$$

$$\frac{\partial Q}{\partial q} = \frac{a\sigma}{2} K_R (\Omega_o R)\left[\frac{2}{a\sigma}\frac{\partial C_Q}{\partial (q/\Omega_o)}\right] \quad \text{ft-lb-sec} \quad \text{(B13)}$$

$$\frac{\partial Q}{\partial B_{1s}} = \frac{a\sigma}{2} K_R (\Omega_o R)\frac{\pi}{180}\left[\frac{2}{a\sigma}\frac{\partial C_Q}{\partial B_{1s}}\right] \quad \text{ft-lb-deg}^{-1} \quad \text{(B14)}$$

where $K = \rho\pi R^4$

and u_R, w_R are the components of the freestream velocity in the rotor control axis system, and $u_R \triangleq \bar{u}(\Omega_o R)$, $w_R \triangleq \bar{w}(\Omega_o R)$.

Since

$$Q = K_R \Omega_o^2 R C_Q$$

$$\frac{\partial Q}{\partial \Omega} = K_R \Omega_o^2 R \frac{\partial C_Q}{\partial \Omega} + 2 K_R \Omega_o R C_Q$$

Thus

$$\frac{\partial Q}{\partial \Omega} = \frac{a\sigma}{2} K_R \Omega_o^2 R \left[\frac{2}{a\sigma} \frac{\partial C_Q}{\partial \Omega}\right] + \frac{2Q}{\Omega_o} \tag{B15}$$

To express torque derivatives in terms of state perturbations at aircraft c.g.

$$\begin{bmatrix} \frac{\partial Q}{\partial u} \\ \\ \frac{\partial Q}{\partial w} \end{bmatrix} = \begin{bmatrix} \cos(\beta_m + B_{1s}) & -\sin(\beta_m + B_{1s}) \\ \\ \sin(\beta_m + B_{1s}) & \cos(\beta_m + B_{1s}) \end{bmatrix} \begin{bmatrix} \frac{\partial Q}{\partial u_R} \\ \\ \frac{\partial Q}{\partial w_R} \end{bmatrix} \tag{B16}$$

(B17)

and,

$$\frac{\partial Q}{\partial q} = \frac{\partial Q}{\partial q_R} - \ell_x \frac{\partial Q}{\partial w} - \ell_z \frac{\partial Q}{\partial u}$$

where ℓ_x, ℓ_z are the distances of the rotor center ahead of and above the c.g. respectively.

The derivative expressions developed to this point are the rate of change of power required with respect to state and control changes. In terms of rotor acceleration, positive changes in power required cause negative rotor acceleration. That is

$$I_R \dot{\Omega} = -\frac{\partial Q}{\partial u} u - \frac{\partial Q}{\partial w} w \ldots\ldots$$

where I_R is the moment of inertia of one rotor.

Therefore, by definition

$$\left.\begin{aligned} Q_u &= -\frac{1}{I_R}\frac{\partial Q}{\partial u} \\ Q_w &= -\frac{1}{I_R}\frac{\partial Q}{\partial w} \qquad \text{etc.} \\ &\vdots \end{aligned}\right\} \quad \text{(B18)}$$

where Q_u, Q_w, etc, are the rates of change in rotor acceleration associated with state perturbations. The control derivatives are

$$\left.\begin{aligned} Q_{\delta_{es}} &= -\left(\frac{B_{1s}}{\delta_{es}}\right)\frac{1}{I_R}\frac{\partial Q}{\partial B_{1s}} \\ Q_{\delta_c} &= -\left(\frac{\theta_c}{\delta_c}\right)\frac{1}{I_R}\frac{\partial Q}{\partial \theta_c} \end{aligned}\right\} \quad \text{(B19)}$$

Force and Moment Derivatives with Respect to RPM

By analogy to the rotor angular speed damping derivative

$$\frac{\partial X}{\partial \Omega} = \frac{1}{\Omega_o}\left[2X - u_R\frac{\partial X}{\partial u_R} - w_R\frac{\partial X}{\partial w_R}\right]$$

$$\frac{\partial Z}{\partial \Omega} = \frac{1}{\Omega_o}\left[2Z - u_R\frac{\partial Z}{\partial u_R} - w_R\frac{\partial Z}{\partial w_R}\right]$$

Since the rotor control axis velocities u_R, w_R are orthogonal to the aircraft body axis velocities u, w these derivatives can also be expressed as

$$\frac{\partial X}{\partial \Omega} = \frac{1}{\Omega_o}\left[2X - u\frac{\partial X}{\partial u} - w\frac{\partial X}{\partial w}\right]$$

$$\frac{\partial Z}{\partial \Omega} = \frac{1}{\Omega_o}\left[2Z - u\frac{\partial Z}{\partial u} - w\frac{\partial Z}{\partial w}\right]$$

X and Z can be expressed in terms of the rotor trim thrust and horizontal force as follows:

$$X = 2\left[T_s \sin\beta_m - H_s \cos\beta_m\right]$$

$$Z = -2\left[T_s \cos\beta_m + H_s \sin\beta_m\right]$$

Thus,

$$\left.\begin{aligned} X_\Omega &= \frac{4}{m\Omega_o}\left(T_s \sin\beta_m - H_s \cos\beta_m\right) - \frac{u}{\Omega_o}(X_u)_R - \frac{w}{\Omega_o}(X_w)_R \\ Z_\Omega &= -\frac{4}{m\Omega_o}\left(T_s \cos\beta_m + H_s \sin\beta_m\right) - \frac{u}{\Omega_o}(Z_u)_R - \frac{w}{\Omega_o}(Z_w)_R \end{aligned}\right\} \text{(B20)}$$

where the notation $(\quad)_R$ denotes the contribution of the two rotors to the total aircraft derivative, e.g. $(X_u)_R = 2\,\partial X/\partial u$.

Since the XV-15 rotor has zero effective flap hinge offset, no moments can be generated through shear forces at the flap hinge. However, because of the cyclic flapping spring restraint there are moments developed proportional to the longitudinal flapping. Thus, the moment at the rotor hub for a 3 bladed rotor is

$$M = \frac{3}{2} K_\beta a_1$$

and

$$\frac{\partial M}{\partial \Omega} = \frac{3}{2} K_\beta \frac{\partial a_1}{\partial \Omega}$$

where K_β is the flapping spring constant.

By analogy to the expressions derived for rotor torque,

$$\frac{\partial a_1}{\partial \Omega} = -\frac{\bar{u}}{\Omega_o}\frac{\partial a_1}{\partial \bar{u}} - \frac{\bar{w}}{\Omega_o}\frac{\partial a_1}{\partial \bar{w}}$$

Since the rotor is offset from the c.g. the total moment derivative with R.P.M. for two rotors is

$$M_\Omega = \frac{1}{I_{YY}} \left[3 K_\beta \frac{\partial a_1}{\partial \Omega} - \ell_x m Z_\Omega - \ell_z m X_\Omega \right] \qquad \text{(B21)}$$

The table below summarizes the physical properties of the rotor and airframe utilized in the quantitative derivative estimates

Coefficient	Numerical Value	Units
a	$5.2 + 8\bar{u} - 30\bar{u}^2$	rad^{-1}
θ_t	$\pi/4$	rad
a_o	.044 (2.5)	rad (deg)
Ω_o	59.2 (helicopter mode)	$rad\text{-}s^{-1}$
	48.0 (airplane mode)	$rad\text{-}s^{-1}$
R	12.5	ft
σ	.089	-
I_R	412	$slug\text{-}ft^2$
δ	.0206	-
m	403.7	slug
K_β	225.	ft-lb/deg

Table B1 summarizes the estimated stability and control coefficients over a range of airspeed and rotor mast angle conditions.

TABLE B1 ESTIMATED ROTOR DERIVATIVES

TRIM COND.		Q_u	Q_w	Q_q	Q_Ω	$Q_{\delta_{ES}}$	Q_{δ_c}	Q_{θ_c}	X_Ω	Z_Ω	$M_{\dot{w}}$
V(Kt)	β_m (deg)	$ft^{-1}\text{-}s^{-1}$	$ft^{-1}\text{-}s^{-1}$	s^{-1}	s^{-1}	$rad\text{-}s^{-2}\text{-}in.^{-1}$	$rad\text{-}s^{-2}\text{-}in.^{-1}$	$rad\text{-}s^{-2}\text{-}deg^{-1}$	$ft\text{-}s^{-1}$	$ft\text{-}s^{-1}$	s^{-1}
0	0	$-3.16(10^{-4})$	$2.08(10^{-2})$	$5.55(10^{-5})$	$-6.60(10^{-1})$	0	-2.83	-2.05	$11.72(10^{-2})$	-1.14	$-3.02(10^{-3})$
40		$2.46(10^{-2})$	$5.26(10^{-2})$	-2.38	$-4.69(10^{-1})$	$-1.32(10^{-1})$	-2.16	-1.57	$2.82(10^{-3})$	-1.03	$-2.29(10^{-3})$
80		$1.44(10^{-2})$	$7.02(10^{-2})$	-4.33	$-3.98(10^{-1})$	$-3.54(10^{-1})$	-1.68	-1.21	$-2.98(10^{-2})$	$-9.92(10^{-1})$	$2.35(10^{-3})$
40	15	$1.14(10^{-2})$	$5.04(10^{-2})$	-2.23	$-4.35(10^{-1})$	$-1.16(10^{-1})$	-1.85	-2.23	$1.91(10^{-1})$	$-9.48(10^{-1})$	$-1.98(10^{-3})$
80		$-1.75(10^{-3})$	$6.76(10^{-3})$	-3.12	$-3.45(10^{-1})$	$-3.32(10^{-2})$	-1.60	-1.29	$1.62(10^{-1})$	$-7.31(10^{-1})$	$-4.90(10^{-3})$
120		$3.72(10^{-2})$	$-1.48(10^{-1})$	-3.65	$-6.55(10^{-1})$	1.05	-3.06	-2.47	$1.46(10^{-1})$	$-7.19(10^{-1})$	$-2.94(10^{-3})$
80	30	$2.23(10^{-2})$	$-5.89(10^{-2})$	-2.26	$-3.68(10^{-1})$	$2.65(10^{-1})$	-1.58	-1.58	$2.49(10^{-1})$	$-5.27(10^{-1})$	$-6.22(10^{-3})$
120		$1.49(10^{-1})$	$-2.79(10^{-1})$	-2.02	$-9.61(10^{-1})$	1.78	-3.54	-3.54	$1.89(10^{-1})$	$-4.83(10^{-1})$	$5.87(10^{-4})$
120	60	$4.96(10^{-1})$	$-3.4(10^{-1})$	$-6.87(10^{-1})$	-2.03	1.261	-2.51	-5.57	$1.86(10^{-1})$	$-2.13(10^{-1})$	$3.25(10^{-3})$
120	90	$6.77(10^{-1})$	$-1.05(10^{-2})$	$-1.38(10^{-1})$	-2.70	0	0	-6.19	$1.49(10^{-1})$	$-2.04(10^{-2})$	$-4.27(10^{-3})$

Validation of Estimated Stability and Control Derivatives

To validate the rotor stability and control derivatives estimated with the simple rotor model, coefficients were compared with data published in Reference 15.

The tables below compare selected rotor $\dot{z}$-force stability and control derivatives for helicopter mode operation at low airspeed. Inasmuch as the purpose of this table is to demonstrate the confidence level associated with the estimated derivatives by comparison with existing data, the data has been left in U.S. Customary Units.

TRIM COND'N		$\partial \dot{z}/\partial u$ lb-s-ft^{-1}		$\partial \dot{z}/\partial w$ lb-s-ft^{-1}	
V(Kt)	(deg)	Ref 15	Rotor Model	Ref 15	Rotor Model
0	0	- 7.7	0	- 82.1	- 71.6
40	0	-55.1	-56.8	-112.5	-120.0
80	0	-32.0	-41.8	-149.1	-158.9

TRIM COND'N		$\partial \dot{z}/\partial \theta_c$ lb-deg^{-1}		$\partial \dot{z}/\partial B_{ls}$ lb-deg^{-1}	
V(Kt)	(deg)	Ref 15	Rotor Model	Ref 15	Rotor Model
0	0	-1263.	-1234.	- 4.2	0
40	0	-1237.	-1270.	-146.9	-145.7
80	0	-1433.	-1488.	-336.2	-282.1

Since no rotor torque derivatives were published in Reference 15 no direct comparisons of these coefficients were possible. However, it was possible to compare total torque changes for small changes in trim flight conditions with predictions from linearized stability derivatives. Several representative comparisons are presented below.

Comparing the torque required from an initial level flight trim with $\beta_m = 15$ deg $V = 80$ knots to a 500 ft/min rate of descent at the same airspeed, the data of Reference 15 indicates a change in torque per rotor of -1031.6 ft-lb.

From the rotor model linearized coefficients,

$$\Delta Q = \frac{\partial Q}{\partial u}\Delta u + \frac{\partial Q}{\partial w}\Delta w + \frac{\partial Q}{\partial B_{1s}}\Delta B_{1s} + \frac{\partial Q}{\partial \theta_c}\Delta\theta_c$$

$$= 0.71(-0.854) + (-2.76)(8.59) + 6.60(0.05) + 531.2(-1.66)$$

$$= -905.8 \quad \text{ft-lb}$$

It can be seen that the change in torque is dominated by the contribution of the collective pitch term. Therefore, this comparison is primarily a check on the derivative Q_{θ_c}. It can be seen that the total torque change is predicted by the linearized coefficients to within about 10 percent.

A similar comparison starting from an initial level flight trim with β_m = 60 deg, V = 100 knots is as follows:

ΔQ = -825 ft-lb (Reference 15 data)

ΔQ = -812 ft-lb (linearized coefficient model)

At this flight condition, the linearized model differs from the Reference 15 data by only 2 percent.

Finally, Figure B1 is a comparison of the total torque per rotor as a function of trim airspeed at several rotor mast angles. It can be seen that up to airspeeds of the order of 100 to 120 knots, the simple model predicts torque with reasonable accuracy. Based on these trim and stability derivative comparisons, it was concluded that despite the many simplifying assumptions, the simple rotor model could provide reasonable estimates of the required rotor derivatives up to airspeeds of the order of 120 knots.

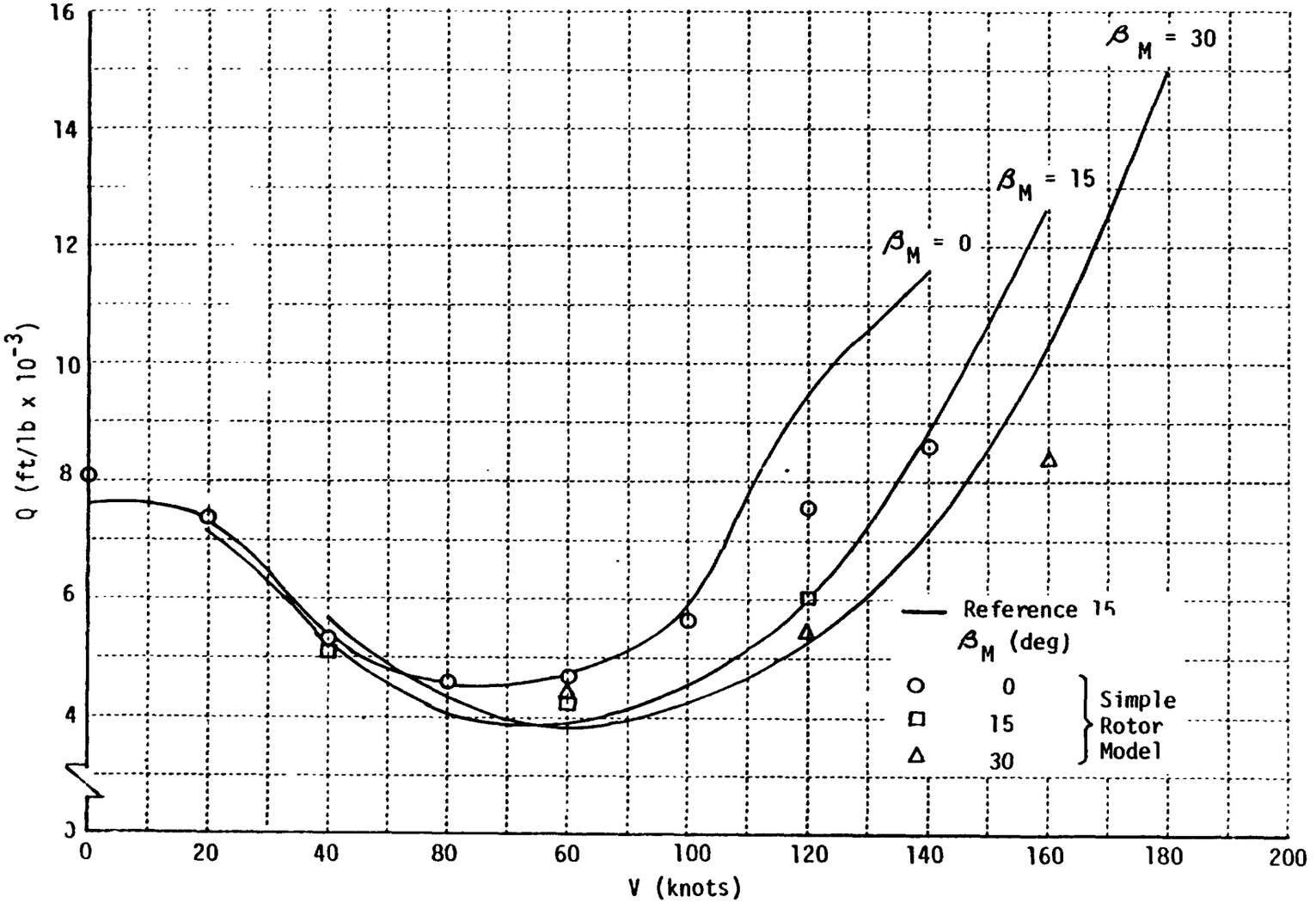

Figure B1 ROTOR TORQUE REQUIRED AS A FUNCTION OF AIRSPEED AND ROTOR MAST ANGLE

APPENDIX C

XV-15 EQUATIONS OF MOTION

Longitudinal

The longitudinal state equations for the XV-15 including the rotor angular speed degree of freedom (ungoverned) have the form:

$$\dot{x} = Fx + Gu \tag{C1}$$

where

$$x = [u, w, q, \theta, \Omega]^T$$

$$u = [\delta_{es}, \theta_c, Q_E]^T$$

$$F = \begin{bmatrix} X_u & X_w & X_q - w_o & -g\cos\theta_o & X_\Omega \\ Z_u & Z_w & Z_q + u_o & -g\sin\theta_o & Z_\Omega \\ M_u & M_w & M_q & 0 & M_\Omega \\ 0 & 0 & 1.0 & 0 & 0 \\ Q_u & Q_w & Q_q & 0 & Q_\Omega \end{bmatrix}$$

$$G = \begin{bmatrix} X_{\delta_{ES}} & X_{\theta_c} & 0 \\ Z_{\delta_{ES}} & Z_{\theta_c} & 0 \\ M_{\delta_{ES}} & M_{\theta_c} & 0 \\ 0 & 0 & 0 \\ Q_{\delta_{ES}} & Q_{\theta_c} & 1.0 \end{bmatrix}$$

The control vector u is related to the cockpit pitch and collective control inputs, the governor collective and the engine torque output as follows,

$$u = A u_p + B\theta_G + C Q_E \tag{C2}$$

where

$$A = \begin{bmatrix} 1.0 & 0 \\ 0 & \left(\frac{\theta_c}{\delta_c}\right) \\ 0 & 0 \end{bmatrix}$$

$$B = [\,0, \quad 10, \quad 0\,]^T$$

$$C = [\,0, \quad 0, \quad 1.0\,]^T$$

and

$$u_p = [\,\delta_{ES}, \quad \delta_c\,]^T$$

Neglecting the governor actuator dynamics, the governor collective pitch is related to the rotor speed error by the following equations.

$$\dot{\theta}_G = K_G K_1 \dot{\Omega} + K_G \Omega$$

The dummy variable y is defined as

$$y = \theta_G - K_G K_1 \Omega$$

Thus, the governor dynamics can be written,

$$\dot{y} = Dx \tag{C3}$$

where

$$D = [0, 0, 0, 0, K_G]$$

and

$$\theta_G = y + Ex \tag{C4}$$

where

$$E = [0, 0, 0, 0, K_G K_1]$$

Since horsepower is proportional to the product of torque and rotational speed, an increment in engine power output can be reflected at the rotor as accelerating torque or rotational speed. That is

$$HP = \left(\frac{Q_{E_0}}{550}\Omega + \frac{\Omega_0}{550} Q_E\right) I_R$$

where torque is expressed in units of rad/sec^2

I_R is the rotor angular moment of inertia,

HP has units of shaft horsepower,

subscript 0 denotes trim or initial value.

Thus
$$Q_E = \frac{550}{\Omega_o \dot{I}_R} HP - Hx \qquad (C5)$$

where
$$H = \left[0, 0, 0, 0, \frac{Q_{E_o}}{\Omega_o}\right]$$

A linear first order model for the engine power response dynamics is assumed

$$\dot{HP} = -\lambda_E HP + K u_p \qquad (C6)$$

where
$$K = \left[0, \ \lambda_E HP_{\delta_c}\right]$$

From Equations (1) to (6) the state equations can be expressed as follows:

$$\left.\begin{aligned} \dot{x}' &= F'x' + G'u' \\ u' &= A'u_p + K'x' \end{aligned}\right\} \qquad (C7)$$

where

$$x' = \left[u \ w \ q \ \theta \ \Omega \ y \ HP\right]^T$$

$$u' = \left[u^T, u_p^T\right]^T$$

$$F' = \begin{bmatrix} F & 0 & 0 \\ \mathcal{D} & 0 & 0 \\ 0 & 0 & -\lambda_E \end{bmatrix}$$

$$= \begin{bmatrix} X_u & X_w & X_q - w_o & -g\cos\theta_o & X_\Omega & 0 & 0 \\ Z_u & Z_w & Z_q + u_o & -g\sin\theta_o & Z_\Omega & 0 & 0 \\ M_u & M_w & M_q & 0 & M_\Omega & 0 & 0 \\ 0 & 0 & 1.0 & 0 & 0 & 0 & 0 \\ Q_u & Q_w & Q_q & 0 & Q_\Omega & 0 & 0 \\ 0 & 0 & 0 & 0 & K_\Omega & 0 & 0 \\ 0 & 0 & 0 & 0 & 0 & 0 & -\lambda_E \end{bmatrix}$$

$$G' = \begin{bmatrix} G & 0 \\ 0 & 0 \\ 0 & K \end{bmatrix}$$

$$= \begin{bmatrix} X_{\delta_{ES}} & X_{\theta_c} & 0 & 0 & 0 \\ Z_{\delta_{ES}} & Z_{\theta_c} & 0 & 0 & 0 \\ M_{\delta_{ES}} & M_{\theta_c} & 0 & 0 & 0 \\ 0 & 0 & 0 & 0 & 0 \\ Q_{\delta_{ES}} & Q_{\theta_c} & 1.0 & 0 & 0 \\ 0 & 0 & 0 & 0 & 0 \\ 0 & 0 & 0 & 0 & \lambda_E HP_{\delta_c} \end{bmatrix}$$

$$A' = \begin{bmatrix} A \\ \\ I_2 \end{bmatrix}$$

$$= \begin{bmatrix} 1.0 & 0 \\ 0 & \left(\frac{\theta_c}{\delta_c}\right) \\ 0 & 0 \\ 1.0 & 0 \\ 0 & 1.0 \end{bmatrix}$$

$$K' = \begin{bmatrix} BE - CH & B & \frac{550}{\Omega_o I_R} C \\ 0 & 0 & 0 \\ 0 & 0 & 0 \end{bmatrix}$$

$$= \begin{bmatrix} 0 & 0 & 0 & 0 & 0 & 0 & 0 \\ 0 & 0 & 0 & 0 & K_G K_1 & 10 & 0 \\ 0 & 0 & 0 & 0 & -\frac{Q_{E_o}}{\Omega_o} & 0 & \frac{550}{\Omega_o I_R} \\ 0 & 0 & 0 & 0 & 0 & 0 & 0 \\ 0 & 0 & 0 & 0 & 0 & 0 & 0 \end{bmatrix}$$

Lateral-Directional

For lateral-directional motions, the torque disturbances on the two rotors will be, for the most part, antisymmetric. That is, an increase in power required by one rotor will be accompanied by a decrease in power required by the other rotor. Since the rotors are cross-shafted, the net power change will be zero and no governor activity will be excited. Therefore, the linearized lateral-directional equations are a conventional 4th order set of form

$$\begin{bmatrix} \dot{v} \\ \dot{r} \\ \dot{p} \\ \dot{\phi} \end{bmatrix} = \begin{bmatrix} Y_v & Y_r - u_o & Y_p + w_o & g\cos\theta_o \\ N'_v & N'_r & N'_p & 0 \\ L'_v & L'_r & L'_p & 0 \\ 0 & \tan\theta_o & 0 & 0 \end{bmatrix} \begin{bmatrix} v \\ r \\ p \\ \phi \end{bmatrix}$$

$$+ \begin{bmatrix} Y_{\delta_{AS}} & Y_{\delta_{RP}} \\ N'_{\delta_{AS}} & N'_{\delta_{RP}} \\ L'_{\delta_{AS}} & L'_{\delta_{RP}} \\ 0 & 0 \end{bmatrix} \begin{bmatrix} \delta_{AS} \\ \delta_{RP} \end{bmatrix} \qquad \text{(C8)}$$

Primed derivatives are derived from unprimed derivatives by the transformation

$$\begin{bmatrix} L'_{(x)} \\ N'_{(x)} \end{bmatrix} = \frac{1}{1 - \frac{I_{xz}^2}{I_{xx} I_{zz}}} \begin{bmatrix} 1.0 & \frac{I_{xz}}{I_{xx}} \\ \frac{I_{xz}}{I_{zz}} & 1.0 \end{bmatrix} \begin{bmatrix} L_{(x)} \\ N_{(x)} \end{bmatrix} \qquad \text{(C9)}$$

APPENDIX D

ENGINE POWER RESPONSE MODEL

Response To Discrete Power Commands

In the XV-15, engine power is commanded by the position of the cockpit collective lever which is connected to the engine throttles through a lever and cam arrangement. The steady state power output per engine as a function of collective position is shown in Figure D1 which was plotted from trim data contained in Reference 15. It can be seen for this data that, provided the collective position is greater than about 2.5 inches, the relationship is essentially linear with a gradient of about 58.7 kilowatts/cm. (200 shaft horsepower/inch).

The response of engine power to rapid step changes in power commands is nonlinear characterized by an initial constant rate increase followed by an exponential capture of the commanded power. The magnitude of the initial rate of power increase is a function of the trim power setting as illustrated in the time histories of Figure D2. At a given trim power setting, the rate of power change is invarient with the magnitude of the commanded power change. Therefore, the time to reach the commanded power is a function of the magnitude of the power command.

For the purposes of the analysis performed in this study, it was desired to model the engine power response dynamics as simply as possible. Figure D2 illustrates the transient power characteristic displayed by a first order lag model, compared to the actual power time history. It can be seen that adjusting the filter time constant to match the rise time (time to 66 percent of steady state response) will overestimate the initial rate response. Matching the initial rate will, in turn, result in considerable error in the rise time. It would be possible to employ higher order filters to improve the transient response matching but even with more sophisticated models, the characteristics of any linear filter would have to be tailored specifically for each trim power setting and the magnitude of the discrete power command. Because of these considerations, for discrete power commands the engine was modeled as a simple first order linear filter with a static gain of 5817 kilowatts per cm (200 shaft horsepower per inch) of collective.

Response To Continuous Power Commands

In the general case, to model the engine power response to continuous power commands, a nonlinear model will likely have to be employed because large amplitude, high frequency power commands will tend to saturate the engine power rate limit resulting in large phase shift and higher harmonics in the power output. This situation will arise, for example, in pilot in the loop analysis or in the determination of augmented vehicle dynamics when the collective controller is used in a response feedback or model following mechanization to modify the vehicle's stability and control characteristics.

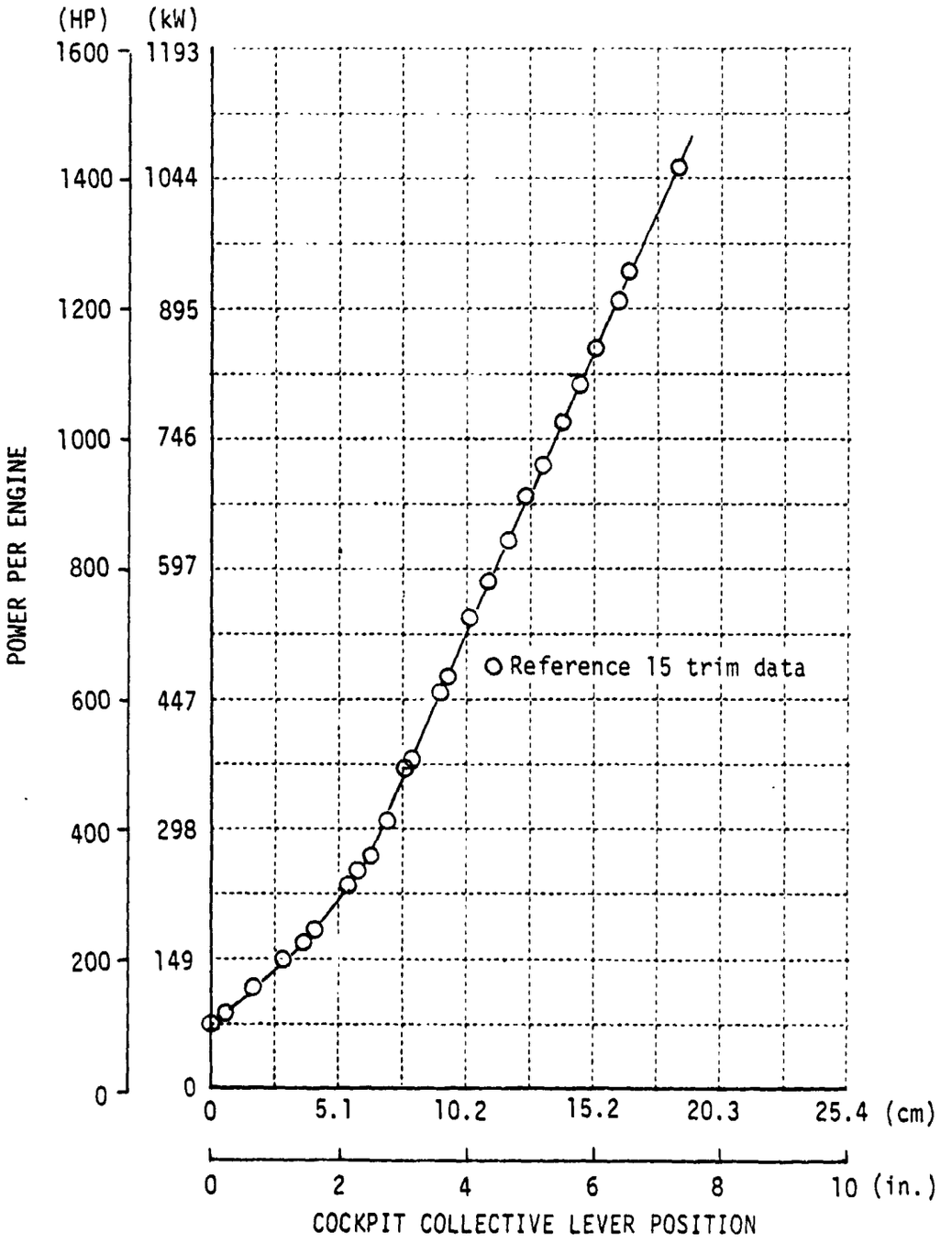

Figure D1 Trim Power as a Function of Cockpit Collective Position

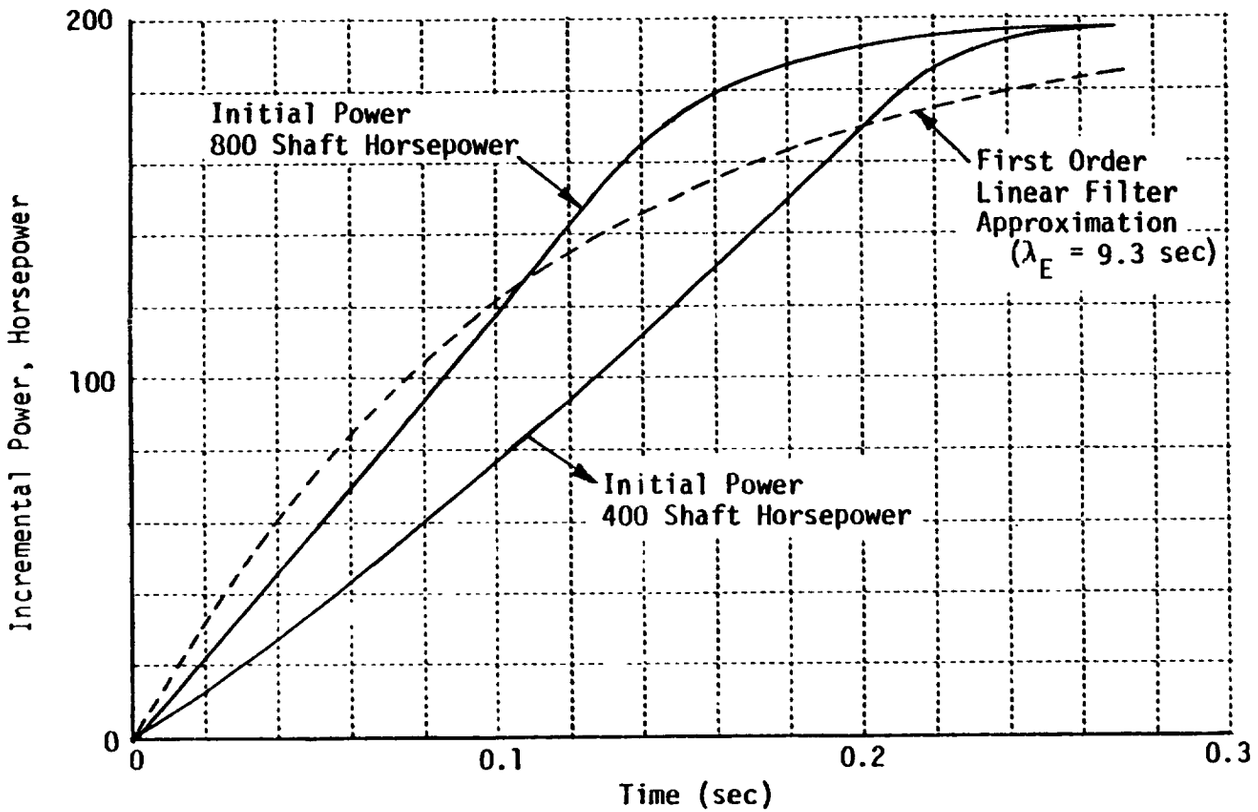

Figure D2 Variation of Engine Power Response to Power Commands as a Function of Initial Power Setting

It is possible however, that under conditions of limited bandwidth and amplitude of power commands it may be possible to neglect the engine dynamics with little error. These limiting conditions can be determined approximately as follows. Consider, for example, that the collective controller is being forced sinusoidally with amplitude $|\delta_c|$. Then the maximum rate of change of power commanded is $\omega|\delta_c|HP_{\delta_c}$ where HP_{δ_c} is the static power gain of the engine. Provided $\omega|\delta_c|HP_{\delta_c}$ is less than the engine power rate limit, then engine power output should follow the power commands with little or no phase shift or attenuation. These limiting conditions on collective magnitude and frequency are illustrated for the rate limits corresponding to trim power settings of 298. and 596. kilowatts (400 and 800 shaft horsepower) in Figure D3.

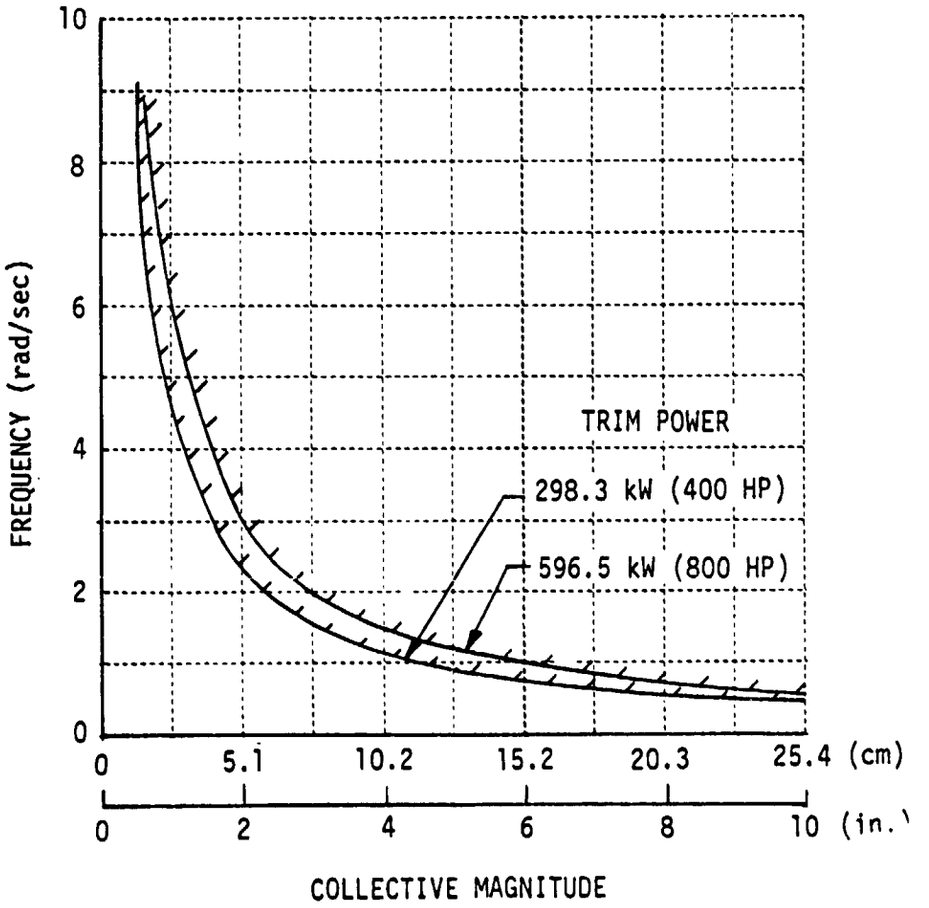

Figure D3 Collective Control Magnitude and Frequency Limits for Continuous Power Commands

REFERENCES

1. Siracuse, R.J. and Schelhorn, A.E.: XV-15 Force Feel System Current Capability and Proposed Revisions for Flight Research Application. Memo No. 369-05, Calspan Corporation, October 1975.

2. Huber, R., Schelhorn, A.E. and Siracuse, R.: Operation and Maintenance Instructions, XV-15 Tilt Rotor Aircraft, Automatic Flight Control System, Volume I, II and III. XV-15 TM No. 41, Calspan Corporation, July 1975.

3. Close, W.: Modifying SCAS Authority. Memo No. 369-06, Calspan Corporation, October 10, 1975.

4. Siracuse, R. and Close, W.: XV-15 Research Augmentation System, Authority Limits and Proposed Modifications. Memo No. 369-08, Calspan Corporation, October 27, 1975.

5. Ringland, R.F. and Craig, S.J.: Flight Control System Linkage Study for the XV-15 Tilt Rotor Aircraft. Working Paper No. 1048-5, Systems Technology Inc., December 1974.

6. Beilman, J.L.: Results of Test to Evaluate Several Techniques to Obtain Satisfactory VSS Performance with the Present X-22A Flight Control System. X-22A TM No. 47, Calspan Corporation, March 20, 1967.

7. Parrag, M.: Static Calibration of the Elevon Control System With Feedforward System Operating. X-22A TM No. 50, Calspan Corporation, November 22, 1968.

8. Parrag, M.: Static Calibration of the Propeller Pitch Control System With Feedforward System Operating. X-22A TM No. 58, Calspan Corporation, January 15, 1968.

9. Anon.: Requirements for Avionics for Terminal Area Navigation, Guidance, and Control System for XV-15 Tilt Rotor Aircraft (V/STOLAND). Specification, NASA Ames Research Center, July 1, 1975.

10. Anon.: V/STOLAND Tilt Rotor Interface Documents MQP Section XI. Sperry Flight Systems, July 1, 1975.

11. Till, R.D.: XV-15 V/STOLAND Design Review. Memo No. 369-07, Calspan Corporation, October 24, 1975.

12. Montgomery, R.C.: Analytic Design of Digital Flight Controllers to Realize Aircraft Flying Quality Specifications. AIAA Paper No. 71-955, August 1971.

13. Lebacqz, J.V. and Aiken, E.W.: A Flight Investigation of Control Display and Guidance Requirements for Decelerating Descending VTOL Instrument Transitions Using the X-22A Variable Stability Aircraft Volumes I and II. Report No. AK-5336-F-1, Calspan Corporation, September, 1975.

14. Anon.: V/STOLAND Failure Modes and Effects Analysis. Report No. 5440-0888-G20 Revision A, Sperry Flight Systems, January 1974.

15. Anon.: V/STOL Tilt Rotor Research Aircraft, Volume 2, Stability and Control and Handling Qualities Analysis. Report No. 301-199-002, Bell Helicopter Company.

16. Marr, R.L.: XV-15 Simulation Period No. 1. Final Report, Bell Helicopter Company, February 13, 1974.

17. Marr, R.L.: XV-15 Simulation Period No. 2. Final Report, Bell Helicopter Company, August 30, 1974.

18. Bekey, G.A. and Karplus, W.J.: Hybrid Computation. John Wiley and Sons, Inc., 1968.

19. Gessow, A. and Meyers, C.M. Jr.: Aerodynamics of the Helicopter. Third Printing, Frederick Ungar Publishing Company, 1962.